SPECTROSCOPIC STUDY OF Eu^{3+} IN $LiYF_4$ SINGLE CRYSTAL

by

BIPIN BIHARI

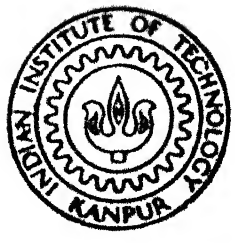

DEPARTMENT OF PHYSICS
INDIAN INSTITUTE OF TECHNOLOGY, KANPUR

OCTOBER, 1988

SPECTROSCOPIC STUDY OF Eu^{3+} IN $LiYF_4$ SINGLE CRYSTAL

A Thesis Submitted
In Partial Fulfilment of the Requirements
for the Degree of
DOCTOR OF PHILOSOPHY

by

BIPIN BIHARI

to the

DEPARTMENT OF PHYSICS
INDIAN INSTITUTE OF TECHNOLOGY, KANPUR
OCTOBER, 1988

माँ !

समर्पण शक्य नहीं। जो मैं हूँ, जो मेरा है, बस तुमसे है। तुम्हारे प्रतिबद्ध हाथों से मेरी ऊँगलियाँ ग्रसमय ही टूट गयीं, फिर भी तुम्हारी प्रेरणा की दाँह संघर्षों की कड़ी धूप में हमेशा मेरे साथ रही है। तुम जहाँ भी हो, तुमसे माँगता हूँ – स्नेहसिक्त ग्राकलन, कि मै तुम्हारी प्रतिबद्धता, प्रेरणा ग्रौर विश्वास के साथ कितना न्याय कर सका हूँ !

CERTIFICATE

Certified that the work presented in this thesis entitled 'SPECTROSCOPIC STUDY OF Eu^{3+} IN $LiYF_4$ SINGLE CRYSTAL' has been carried out by Mr Bipin Bihari under my supervision and that the same has not been submitted elsewhere for a degree.

Thesis Supervisor

KK Sharma 18/10/8

(K K Sharma)
Professor
Dept of Physics
IIT Kanpur

October, 1988

ACKNOWLEDGMENT

I am grateful to my thesis supervisor Professor K K Sharm for his competent guidance, constant encouragement and interest in my general well-being during the course of this research. I express my sincere gratitude to my teachers for their guidance and help at various stages. Thanks are due to Professor L E Erickson of NRC, Ottawa, Canada for providir the crystal used in this work. I am thankful to Dr I S Minha Dr B P Singh and Dr K Ram with whom I had many useful discussions at the initial stages of this work.

My colleagues and friends; Mr G Ravindra Kumar and Mr A N Thakur deserve to be thanked for their multidimensional support; Mr K Diwakar, Mr Anil Dubey and Mr M P Singh for proof reading parts of the thesis and all members of the Ligh Talk group for help and pleasant company.

I wish to thank:

Mr Jagir Singh and Mr Joseph John of the A C E S for help in equipment servicing. Mr Kuldeep Singh for his assistance in all sorts of technical problems; Mr J S Sharma, Mr Ram Singh Mr V K Bajpai, Mr S D Sharma and other employees of the Physics and CELT Workshops for providing help at various stages; Employees of the Electronic Shop, Liquid Nitrogen Plant, Glass Blowing Shop, Physics and CELT Offices for their 'ever-ready to help' approach.

Mr S L Yadav is thanked for typing this thesis at a short notice.

I acknowledge all my friends particularly Mr Sudhir Kumar Dwivedi and Mr Atul Kumar for their company and helpful attitude. A special word of thanks to Mrs Tripta Sharma, Shikha, Sheema, Atul and Anjali for their affection. I also acknowledge my family members specially my wife Rita, daughter Kritika and sister Sumitra, who always inspired me and kept me cheerful even at times of distress by their gentle and hilarious temperaments.

Finally I bow my head to my father.

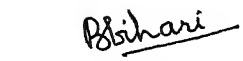

BIPIN BIHARI
Department of Physics
IIT Kanpur

TABLE OF CONTENTS

LIST OF TABLES

LIST OF FIGURES

SYNOPSIS

The results of an investigation undertaken to record and interpret the absorption and fluorescence spectra of Eu^{3+} doped in $LiYF_4$ single crystal are presented in this thesis. The host crystal $LiYF_4$ belongs to the tetragonal scheelite family. The Eu^{3+} ion substitutes for Y^{3+} at a site of S_4 point symmetry.

A sample of $LiYF_4:Eu^{3+}$, of dimensions 3.8 mm x 3.1 mm x 2.1 mm with $\bar{c}$-axis along the 3.1 mm edge was obtained from Dr L.E. Erickson (NRC, Ottawa, Canada). A glass dewar employing cold finger was fabricated for the low temperature spectroscopic measurements. The absorption spectrum was obtained using a water cooled 1000W tungsten-halogen lamp as a white light source and the fluorescence spectra were recorded using a Coherent Ar^+ Laser and a Coherent ring dye laser (with R 6G dye). The signals transmitted or emitted by the sample were detected by a PMT attached to a double grating monochromator and then amplified by a lock-in-amplifier. These amplified signals were recorded on an x-t recorder. The excitation spectrum was obtained by monitoring the ^5D_o (Γ_1)-$^7F_1$(Γ_1) fluorescence and scanning the dye laser within the spectral range of R 6G dye. The fluorescence and absorption spectra were obtained in π, σ and axial modes at liquid nitrogen temperature. None of the Ar^+ laser lines is in resonance with any of the Eu^{3+} absorption transitions, but $LiYF_4:Eu^{3+}$ exhibits

fluorescence when excited with any of the Ar^+ laser lines. The 457.9 nm and 514.5 nm lines produce fairly strong fluorescence in this sample. The selective excitation of the ^5D_o level was obtained using the dye laser lasing at 16938 cm^{-1} (which corresponds to the wavenumber interval for the $^7F_1(\Gamma_3) - {}^5D_o(\Gamma_1)$ transition) and at 17630 cm^{-1} (excitation through a phonon assisted process). The excitation spectrum was helpful in ascertaining the position of the ^5D_o level and also in identifying some of the interfering Raman and vibronic lines. Initial assignment to the crystal field levels within a given multiplet was made on the basis of symmetry considerations and the observed polarizations in the absorption and fluorescence spectra. This assignment was later found to be consistent with our calculations. All the crystal field energy levels belonging to the ^5F_J(J=0,1,2,3,4) and ^5D_J (J=0,1,2) multiplets were identified, while the structure of the $^7F_5$ and $^5L_6$ multiplets could be established only partially. Experimental free ion level positions were obtained by taking the centres of gravity of the crystal field levels belonging to a given multiplet.

A detailed computational analysis of the data has been attempted. The free ion energy matrices were constructed and diagonalized to obtain the free ion energy levels and the wavefunctions in the intermediate coupling scheme. The angular parts of the matrix elements were calculated exactly

and the radial quantities were treated as adjustable parameters. The crystal field calculations were carried out with and without J-mixing effects using intermediate coupling wavefunctions as zero-order wavefunctions. Here again radial parts were parametrized in an attempt to match the experimental and theoretical results. The best possible set of parameters obtained within the computational constraints are presented.

Chapter I of the thesis contains a brief introduction to the crystal spectra of rare earth ions and a summary of the proposed work on $LiYF_4:Eu^{3+}$ system. The over-all approach adopted to interpret the observed data has been briefly outlined. Chapter II contains the theoretical background relevant to the present problem. Information on the crystal structure of $LiYF_4$ and experimental detail relevant to the work are given in Chapter III. The experimental results are tabulated in this chapter. A detailed analysis of the experimental data is presented in chapter IV. A summary of the results and their significance is discussed in the fifth and the final chapter.

Some comments on the computer programming and calculation procedures are given in the appendices.

CHAPTER I

INTRODUCTION

Lanthanides form a group of chemically similar elements, which have a partially filled 4f shell in common. Neutral atoms of lanthanide group have Xenon like core of 54 electrons ($1s^2$, $2s^2$ $2p^6$, $3s^2$ $3p^6$ $3d^{10}$, $4s^2$ $4p^6$ $4d^{10}$, $5s^2$ $5p^6$), 'N' 4f electrons and two or three loosely bound outer electrons. The '3+' oxidation state for rare earths is the most stable, although the '2+' oxidation state is also encountered for some of them. In the optical spectra of rare earth doped crystals, one is primarily concerned with ionized rare earths, having only $4f^N$ electrons besides the Xe core.

The existence of sharp bands in the absorption spectra of crystalline lanthanides was known from the work of Becquerel [1]. Further, they were known to show considerable Zeeman splittings [2]. However, it was Bethe [3], who first proposed a highly successful crystal field theory to account for these observations. The absorption data of the aqueous solution of all rare earths (except Pm^{3+}) were obtained as early as 1934 [4]. The interpretation of the complex spectra

of rare earths became possible only after Racah developed his powerful tensor operator techniques [5]. He introduced the concepts of tensor-operators, recoupling coefficients, seniority and coefficients of fractional parentage. Stevens [6] developed the equivalent operator technique for the theoretical interpretation of the spectra of complex systems. Satten for the first time applied these techniques to the $4f^3$ spectra of Nd^{3+} in $Nd(BrO_3).9H_2O$. He, however, used Russell Saunders coupling [7]. It was subsequently realized that Intermediate coupling is more appropriate for these systems [8,9]. Since then considerable progress has been made in the interpretation of the spectra of lanthanide spectra [10,11,12].

The 4f electrons, responsible for the spectroscopic properties of the lanthanides, are not the outermost electrons. They are shielded by $5s^2$, $5p^6$ electrons with larger spatial extension. As a result they interact rather weakly with the surrounding ions. This fact is responsible for the 'atomic like' spectra observed for rare-earth ions embedded in solids. The spectra of rare-earth ions in crystalline environment consist essentially of well separated groups of sharp lines. Each such group corresponds to the crystal field-split structure of the so called 'free ion levels'. Free ion levels of rare earths do not change much from one host to another, indicating the localized nature

of the 4f electrons. The observed spectra of trivalent lanthanides originate from the transitions within the $4f^N$ manifold.

Spectroscopic study of rare earths is an interesting topic of research in itself. Lanthanides have proved to be good probes for the study of the crystalline field. Moreover, the use of rare earth doped materials [13] as gain media in lasers, has made this type of study more relevant.

Tripositive europium (Eu^{3+}), with six equivalent electrons in its 4f shell, is unique in the lanthanide series in the sense that it has the ground term ^7F_o with total angular momentum J = 0. This imposes special restrictions on transitions involving the ground term. Further, the nuclear magnetic moment of Eu^{3+} is quenched to such an extent that no NMR signal has been observed in any host by conventional NMR methods [14]. Laser action has been observed in Eu^{3+} doped Y_2O_3 and YVO_4 crystals [15,16,13].

Laser action has been observed in the $LiYF_4$ host when doped with Ce^{3+}, Pr^{3+}, Nd^{3+}, Tb^{3+}, Ho^{3+}, Er^{3+}, Tm^{3+} etc [13]. In $LiYF_4$, rare earth ions substitute for Y^{3+} with site symmetry D_{2d} somewhat distorted to S_4. There is strong evidence for the appearance of several magnetic dipole transitions in this system. This is somewhat unusual because magnetic dipole transitions, generally weak, are seldom observed.

In this thesis, we have undertaken the task of an in-depth study of the absorption and fluorescence spectra of $Eu^{3+}:LiYF_4$. We have basically followed the procedure described by Wybourne [11] and Hüfner [13]. We obtained polarized absorption and fluorescence spectra at liquid nitrogen temperature in the visible spectral region. The absorption spectrum was obtained using a 1000W tungsten-halogen lamp, while for fluorescence studies, a Coherent Ar^+ laser and a Coherent ring dye laser with R 6G dye were used. Further, excitation spectrum covering the spectral range of R 6G dye was recorded to ascertain the position of the ^5D_o level of Eu^{3+}. The results have been analyzed in the framework of intermediate coupling scheme and crystal field theory.

Weak interaction of rare earth ions with surroundings permits one to treat the crystal field effects as a small perturbation over the free ion Hamiltonian. In the theoretical treatment of free ions, the non-central electrostatic, the spin-orbit and the configuration interactions are treated as perturbations to the central field Hamiltonian. Matrices, consisting of the sum of the matrix elements of the three interactions, calculated in LS basis states, are diagonalized to obtain the free ion energies and the intermediate coupling wave functions. The basis states $|WUSLJ\rangle$, used to calculate individual matrix elements involve composite

orbital (L), spin (S) and total (J) angular momentum quantum numbers. U and W are additional quantum numbers introduced by Racah for a complete classification of the states of the $4f^N$ configurations. The angular parts of the matrix elements can be calculated exactly, while radial parts are treated as adjustable parameters in an effort to match experimental and calculated energy positions of 'free ion' levels.

The free ion levels are (2J+1) fold degenerate. This degeneracy is wholly or partially lifted by the crystal field depending upon the symmetry of the field. Matrix elements of the crystal field are calculated using free ion wave functions as zero order wave functions. Basis states chosen are the linear combinations $|\alpha\ JJz\rangle$, denoted by $|\alpha\ JJz\ \Gamma i\rangle$ where α stands for the rest of the quantum numbers and Γi is the i^{th} irreducible representation of the point group under consideration. Again, radial parts of the matrix elements are treated as adjustable parameters. We adopted this approach and used computer programmes to minimize the r.m.s. deviations between the theoretical and experimental positions of the energy levels and obtained the free ion and crystal field parameters for the system $Eu^{3+}:LiYF_4$ in the intermediate coupling scheme. Subsequently the J-mixing terms were included in the calculations.

REFERENCES

[1] J Becquerel; Radium 4 328 (1907).

[2] J Becquerel and H K Onnes; Radium 5 227 (1908).

[3] H Bethe; Ann Physik 3 133 (1929).

[4] W Prandtl and K Sheiner; Z Anorg Alge Chem 220 107 (1937).

[5] G Racah; Phys Rev 62 438 (1942).

[6] K W H Stevens; Proc Phys Soc (London) A65 209 (1952).

[7] R A Satten; J Chem Phys 21 637 (1953).

[8] G H Dieke; Advances in Quantum Electronics, Columbia Univ Press, NY (1961).

[9] G H Dieke and H M Cross-White; Appl Opt 2 675 (1963).

[10] B G Wybourne; Spectroscopic properties of rare earths, Wiley New York (1965).

[11] G H Dieke; Spectra and energy levels of rare earths ions in crystals, John Wiley and Sons N Y (1968).

[12] S Hüfner; Optical spectra of transparent rare earth compounds, Academic Press N Y (1978).

[13] A A Kaminskii; Laser Crystals, Springer Verlag Berlin (1981).

[14] K K Sharma and L E Erickson; J Phys C:Solid State Phys 18 2935 (1985).

[15] N C Chang; J Appl Phys 34 3500 (1963).

[16] J R O'Conner; Trans Metl Soc AIME 239 362 (1967).

CHAPTER II

THEORY OF CRYSTAL SPECTRA OF RARE EARTH IONS

1. INTRODUCTION

Trivalent lanthanides possess electronic configurations of the type (Pd core)^{46} $4f^N$, $5s^2$ $5p^6$, where $1 \leq N \leq 13$. With the increase in the atomic number within the lanthanide series, the nuclear charge and the number of electrons in 4f shell increase. Due to imperfect shielding [1,2] among 4f electrons, this leads to an increased nuclear attraction for the f-electrons. This potential well near the nucleus reduces the spatial extension of the 4f wavefunction to such an extent that its peak lies well within the spatial extension of the 5s and 5p wavefunctions. This reduction in the spatial extension of the 4f wavefunction is named 'lanthanide contraction' [2]. Figure (2.1) gives the radial distribution functions of the 4f, 5s, 5p and 6s electrons for Gd^+ as obtained from Hartree-Fock calculations of Freeman and Watson [3]. Thus 4f electrons are substantially screened from outside influences by the $6s^2$ and $5p^6$ electrons. This screening effect makes 4f electrons less sensitive to ligands in molecular and solid

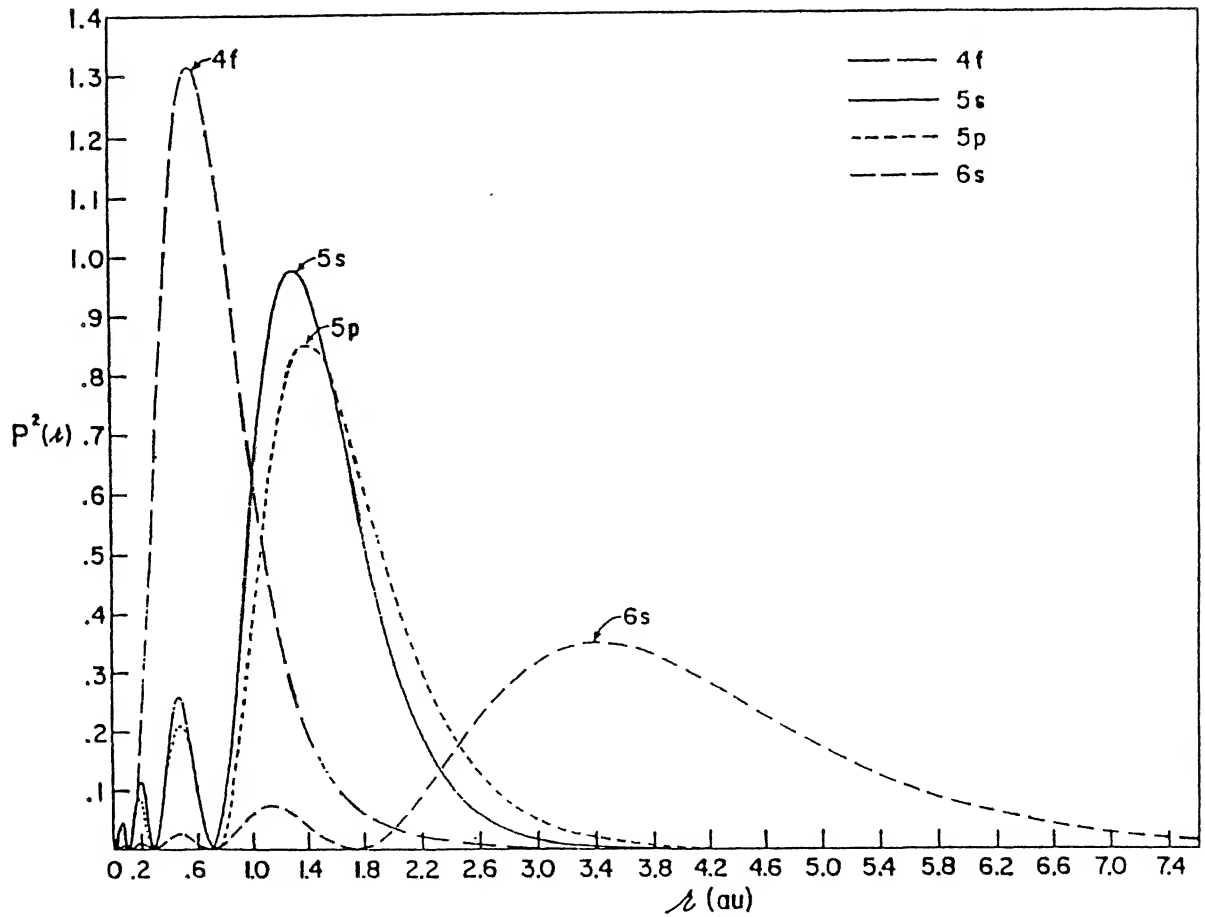

FIG.2.1 : RADIAL CHARGE DISTRIBUTION $P^2(r)$ AS A FUNCTION OF r FOR THE 4f, 5s, 5p and 6s ORBITALS [11].

complexes. In fact the spin-orbit and the residual Coulomb interactions for trivalent lanthanides are usually much larger than the ion-ligand interactions. These circumstances allow the crystal field to be treated as a perturbation over the 'free ion' interactions.

2. FREE ION HAMILTONIAN

With the assumption that all the electronic shells except the 4f shell are complete and therefore do not contribute to the relative positions of the 4f energy levels, one can write the free ion Hamiltonian involving only the 4f electrons.

$$H = -\frac{\hbar^2}{2m}\sum_{i=1}^{N}\nabla_i^2 - \sum_{i=1}^{N}\frac{Z^* e^2}{r_i} + \sum_{i<j}^{N}\frac{e^2}{r_{ij}} + \sum_{i=1}^{N}\xi(r_i)(s_i \cdot l_i) \qquad \ldots\ldots 1$$

Here $Z^* e$ is the screened nuclear charge, r_i is the coordinate of the i^{th} electron w.r.t. the nucleus, r_{ij} is the distance between i^{th} and j^{th} electrons and $\xi(r_i)$ is the spin-orbit coupling function defined as

$$\xi(r_i) = \frac{\hbar^2}{2m^2c^2}\frac{dU(r_i)}{dr_i} \qquad \ldots\ldots 2$$

where $U(r_i)$ is the spherical potential experienced by the i^{th} electron. Remaining quantities have their usual meaning.

The first term in the Hamiltonian 1 represents the kinetic energy of the electrons, the second represents their

Coulomb interaction with the nucleus, and the third and fourth terms respectively represent the mutual Coulomb repulsion among the electrons and the spin-orbit interaction. The last two terms are responsible for the energy level structure of the $4f^N$ configuration.

It is impossible to solve the Schrodinger equation exactly for atoms containing more than one electron, analytically or numerically. Therefore one has to use some approximate models. The most commonly used approximation for solving the Schrodinger equation for complex atoms is the central field approximation [4].

2.1 CENTRAL FIELD APPROXIMATION

In the central field approximation, it is assumed that individual electrons of the atom move independently in a spherically symmetric central field $(-\frac{U(r_i)}{e})$ created by the remaining electrons and the nucleus. Under the above approximation the Hamiltonian 1 takes the form,

$$H = \sum_{i=1}^{N} \left[-\frac{\hbar^2}{2m} \nabla_i^2 + U(r_i)\right] + \left[\sum_{i=1}^{N} \frac{Z^* e^2}{r_i} - U(r_i) + \sum_{i<j}^{N} \frac{e^2}{r_{ij}}\right] + \sum_{i=1}^{N} \xi_i(r_i)\,(s_i \cdot l_i)$$

$$= H_{C\,F} + H'_{Coul} + H'_{S-O} \qquad \ldots\ldots 3$$

The non-central residual Coulomb interaction H'_{Coul} and the

spin-orbit interaction H'_{S-O} are smaller than the central field $H_{C.F}$ by at least a few orders of magnitude and in the theory of atomic spectra they are treated as perturbations over the central field Hamiltonian.

The time independent Schrodinger equation for the central field Hamiltonian

$$H_{CF}\ \Psi_{CF} = E_{CF}\ \Psi_{CF} \qquad .....4$$

can be solved in the single electron approximation by writing the wavefunction Ψ_{CF} and energy E_{CF} in the form

$$\Psi_{CF} = \prod_{i=1}^{N} \Phi_i(k_i).\sigma_i = \prod_{i=1}^{N} \Phi_i\ (\alpha^i) \qquad .....5A$$

$$E_{CF} = \sum_{i=1}^{N} E_i \qquad .....5B$$

Here σ_i is the spin wavefunction. k and α represent the set of quantum numbers $(n\ell m_\ell)$ and $(n\ \ell\ m_\ell\ m_s)$. $\Phi(k)$ for each electron satisfies

$$[-\frac{\hbar^2}{2m}\ \nabla^2 + U(r)]\ \Phi(k) = E\ \Phi(k) \qquad .....6$$

The equation 6 is similar to the Schrodinger equation for the hydrogen atom except for the replacement of the Coulomb potential $-e^2/r$ by the central field potential U(r). This can be solved by the introduction of polar coordinates (r, θ, ϕ) and separating the one electron eigenfunctions into their radial and angular parts. The normalized bound state solutions for equation 6 can be written in the form

$$\Phi(k) = r^{-1}.\ R_{n\ell}(r).\ Y_\ell^{m_\ell}\ (\theta, \phi) \qquad .....7$$

where $R_{n\ell}(r)$ is the radial function and depends on the central field potential energy function $U(r)$. $R_{n\ell}(r)$ satisfies the equation

$$\frac{1}{r^2}\frac{d}{dr}\left(r^2\frac{dR_{n\ell}(r)}{dr}\right) - \frac{\ell(\ell+1)}{r^2}R_{n\ell}(r) + \frac{2m}{\hbar^2}[E-U(r)]R_{n\ell}(r) = 0 \qquad .....8$$

whereas spherical harmonics $Y_\ell^{m_\ell}(\theta, \phi)$ are defined by

$$Y_\ell^{m_\ell}(\theta, \phi) = (-1)^{m_\ell}\left[\frac{(2\ell+1)(\ell-|m_\ell|)!}{4\pi(\ell+|m_\ell|)!}\right]^{1/2} P_\ell^{m_\ell}(\cos\theta) \times e^{im_\ell\phi} \qquad .....9$$

and

$$P_\ell^{m_\ell}(x) = \frac{(1-x^2)^{m_\ell/2}}{2^\ell.\ell!}\frac{d^{m_\ell+1}}{dx^{m_\ell+1}}(x^2-1)^\ell \qquad .....10$$

The angular part of the one electron eigenfunction (Eqn.7) is identical to that of the hydrogenic eigenfunction and can be evaluated exactly. Radial part can be evaluated only approximately in the absence of the knowledge of the potential function $U(r_i)$. Therefore it is customary to treat radial parts as adjustable parameters to fit the experimental data.

The normalized antisymmetric solution of central field can be written in the determinantal form as

$$\Psi_{CF} = \frac{1}{\sqrt{N!}} \begin{vmatrix} \Phi_1(\alpha^1) & \Phi_2(\alpha^1) & - - - & \Phi_N(\alpha^1) \\ \Phi_1(\alpha^2) & \Phi_2(\alpha^2) & - - - & \Phi_N(\alpha^2) \\ \vdots & & & \\ \Phi_1(\alpha^N) & \Phi_2(\alpha^N) & - - - & \Phi_N(\alpha^N) \end{vmatrix} \quad .....11$$

These wavefunctions will serve as zero order wavefunctions. The eigen values of the central field wave equation are degenerate in quantum numbers m_ℓ and m_s and can be characterized by a sequence of quantum numbers $(n_1\ \ell_1)$ $(n_2\ \ell_2)$ - - - $(n_N\ \ell_N)$ which defines an electronic configuration.

Once the zeroth-order wavefunctions are known one can use them as basis states to calculate matrix elements of residual electrostatic (H'_{Coul}) and spin-orbit (H'_{S-O}) perturbations. The closed shells do not affect the relative splittings in a configuration, but shift the whole configuration. So the optical spectra of rare-earth ions can be explained by considering electrons in 4f shell only. Even with this simplification, the direct method of calculating the effect of the perturbation ($H' = H'_{Coul} + H'_{S-O}$), using determinantal product states as basis functions is tedious, except for very simple configurations. For example the configuration $4f^6(Eu^{3+})$, in which we are interested, has 295 free ion terms with total degeneracy 3003. This requires the evaluation of 295x295 = 87025 matrix elements and diagonalization

of a secular determinant of order 295x295. Moreover this method does not provide any physical insight into the structure of the configuration. The calculations are simplified if group theoretical and tensorial techniques are used.

2.2 CLASSIFICATION OF THE STATES

In the LS coupling scheme L and S define a Term. In complex atomic configurations, one frequently encounters more than one Term with same L and S values. Additional quantum numbers are then needed to label such Terms uniquely. Racah [5,6] developed a group theoretical approach to classify the states of ℓ^N type configurations systematically. In his method the complete set of states of the f^N configuration can be classified by their properties under certain groups of transformations. The irreducible representations of the group can then serve as suitable labels to classify the states. Complete classification of f^N configurations can be achieved using the unitary transformation group U_7 and its sub groups R_7, R_3 and G_2 such that

$$U_7 \supset R_7 \supset R_3 \supset G_2$$

The infinitesimal operators of the seven dimensional unitary group U_7 are the tensor operators $V_q^{(k)}$ where $-k \leq q \leq k$ and $0 \leq k \leq 6$. $V_q^{(k)}$ commute with spin s. The totality of the states of the configuration ℓ^N forms a

basis for a single irreducible representation of $U_{2\ell+1}$. Since the representation does not depend on m_s, the labeling of states by specifying $(2\ell+1)$ integers $(\lambda_1, \lambda_2 \ldots \lambda_{2\ell+1})$ is equivalent to specifying the total spin S. The three dimensional rotation group R_3 (a sub group of U_7) has tensor operators $V_q^{(k)}$ of odd rank as its elements. Its irreducible representation D_L transforms as total orbital angular momentum L. This implies that the labeling of states with D_L is equivalent to specifying L. Thus labeling by λ and D_L is equivalent to Russell-Saunders labeling. The L-S labeling is preferred over λ and D_L, as it has more direct physical meaning.

Further classification is obtained according to the seven dimensional rotation group R_7 and its sub group G_2. The irreducible representations of R_7 are labelled by three integers $(\omega_1\ \omega_2\ \omega_3) = W$, such that $2 \geq \omega_1 \geq \omega_2 \geq \omega_3 \geq 0$ and that of G_2 by two integers $(u_1\ u_2) = U$ such that $2 \geq u_1 \geq u_2 \geq 0$. Using these labels as additional quantum numbers, the states of f^N configuration can be uniquely defined with the exception of a few of the states with U = (31) and U = (40), where some doubly occurring LS states remain unseparated. These unseparated states are distinguished arbitrarily by giving an additional label τ to these pairs of states. Thus the states of configuration f^N can be completely specified by writing them as $|f^N\ \tau\ \text{WUSL}\rangle$.

Racah also introduced the concept of seniority numbers [6] which give an alternate way to classify the states of f^N configurations and are convenient for the calculation of matrix elements of certain operators. In this approach the terms $|SLJM_J\rangle$ of a configuration ℓ^N can be divided into two types. The first type of terms can be obtained by the addition of a pair of electrons in the ℓ^{N-2} configuration, the other type can not be obtained in this manner. The second type of terms can be considered to appear for the first time. A unique number 'v' called seniority number, can be assigned to the term appearing for the first time in a configuration, starting from the configuration ℓ^{N-N}. The term S=0, L=0 will have v = 0. Classification of terms using seniority number is equivalent to specifying 'W'. Thus the states denoted as $|f^N\ \tau\ WUSL\rangle$ can be equivalently written as $|f^N\ \tau\ vUSL\rangle$. The complete classification of the terms of the $4f^6$ configuration is given in appendix-I.

2.3 CHOICE OF BASIS STATES

The matrix elements of the perturbation Hamiltonian (equation 3) can be calculated by choosing a complete set of basis states in any well defined coupling scheme. The Russell-Saunders(L-S)coupling is applicable when $H'_{Coul} >> H'_{S-O}$ and the j-j coupling scheme works when $H'_{Coul} << H'_{S-O}$. For the rare earth ions $H'_{S-O} \leq H'_{Coul}$ and therefore neither of the coupling schemes are appropriate. The coupling

scheme commonly used for calculating the energy levels of rare earth ions is called the intermediate coupling scheme. The matrix elements of the perturbation Hamiltonian are usually calculated using the L-S basis states and the secular equation of the composite Hamiltonian $(H'_{Coul} + H'_{S-O})$ is then solved. Since H'_{Coul} is diagonal in $|SL\rangle$ representation and independent of J and J_z, while H'_{S-O} is diagonal in J and independent of J_z, we calculate the matrix elements with $|SLJ\rangle$ bases. This choice breaks up the secular equation into smaller secular equations, one for each J value. Now the secular equation for a specified J takes the form

$$\begin{vmatrix} \langle 1|H'|1\rangle - \lambda & \langle 1|H'|2\rangle & \cdots & \langle 1|H'|n\rangle \\ \langle 2|H'|1\rangle & \langle 2|H'|2\rangle - \lambda & \cdots & \langle 2|H'|n\rangle \\ \langle i|H'|1\rangle & \langle i|H'|2\rangle & \cdots & \langle i|H'|n\rangle \\ \vdots & & & \\ \langle n|H'|1\rangle & \langle n|H'|2\rangle & \cdots & \langle n|H'|n\rangle - \lambda \end{vmatrix} = 0 \quad \ldots 12$$

where $\langle i| = \langle S_i L_i J|$ and $|j\rangle = |S_j L_j J\rangle$

and $H' = H'_{Coul} + H'_{S-O}$

The roots of this equation $\epsilon_1, \epsilon_2 \ldots\ldots \epsilon_n$ give the required energy correction. Once the secular equations are solved eigen functions ψ_J can be determined.

The problem now reduces to the calculation of the matrix elements $\langle S_i\ L_i\ J\ J_z|\ H'_{Coul} + H'_{S-O}|\ S_j\ L_j\ J\ J_z\rangle$. Since both the perturbation Hamiltonians H'_{Coul} and H'_{S-O}

are the functions of the coordinates of individual electrons and the states $|S\ L\ J\ J_z\rangle$ are of composite nature, this require the calculation of the matrix elements to be carried out in determinantal product states. This will be a difficult task for complex configurations. Tensor operator techniques developed by Racah [6,7] make these calculations practically simpler. Using these techniques calculations are done directly in composite states by an appropriate transformation of the Hamiltonian and using the concept of fractional parentage coefficients [6].

2.4 TENSOR OPERATORS [6]

Spherical tensor operator $T^{(k)}$ of rank k is a set of (2k+1) operators $T_q^{(k)}$ (q = -k, -k+1,. . .k) having transformational properties similar to those of spherical harmonics $Y_q^{(k)}$. This means $T_q^{(k)}$ will satisfy the same commutation relations as those of $Y_q^{(k)}$ with the total angular momentum J.

$$[(J_x \pm J_y),\ T_q^{(k)}\ ] = [(k \mp q)(k \pm q+1)]^{1/2}\ T_{q\pm1}^{(k)} \quad .....13$$

and

$$[J_z,\ T_q^{(k)}] = q\ T_q^{(k)}$$

In the JJ_z representation, the J_z dependence of the matrix elements of tensor operators can be obtained by Wigner-Eckart theorem.

$$\langle \gamma\ JJ_z|T_q^{(k)}|\gamma'J'J_z'\rangle = (-1)^{J-J_z} \langle \gamma J\ ||T^{(k)}||\gamma'J'\rangle \begin{pmatrix} J & k & J' \\ -J_z & q & J_z' \end{pmatrix} \quad .....14$$

The quantity, $\langle \gamma\ J||T^{(k)}||\gamma'\ J'\rangle$, which is independent of J_z, J'_z and q, is called the reduced matrix element, $\begin{pmatrix} J & k & J' \\ -J_z & q & J'_z \end{pmatrix}$ is a 3-J symbol and γ stands for the rest of the quantum numbers on which $T^{(k)}_q$ does not act.

The reduced matrix elements $\langle \gamma\ J||T^{(k)}||\gamma' J'\rangle$ can be evaluated if the J values and the nature of $T^{(k)}$ are known.

Another tensor operator, called 'product tensor operator' is encountered in the calculation of the matrix elements of H'_{Coul} and H'_{S-O}. A spherical product tensor operator $X^{(k)}_Q$ is defined as the product of two spherical tensor operators $T^{(k_1)}_{q_1}$ and $U^{(k_2)}_{q_2}$

$$X^{(K)}_Q = \sum_{q_1 q_2} T^{(k_1)}_{q_1}\ U^{(k_2)}_{q_2}\ (2K+1)\ (-1)^{k_1-k_2+Q} \begin{pmatrix} k_1 & k_2 & K \\ q_1 & q_2 & -Q \end{pmatrix}$$

$$= \left\{ T^{(k_1)} \cdot U^{(k_2)} \right\}^{(K)}_Q \qquad \ldots\ldots 15$$

$X^{(K)}_Q$ satisfies the same commutation relations as $T^{(k)}_q$'s.

If $k_1=k_2=k$, the scalar product of two tensors can be defined as

$$(T^{(k)} \cdot U^{(k)}) = \sum_q (-1)^q T^{(k)}_q\ U^{(k)}_{-q}$$

or

$$(T^{(k)} \cdot U^{(k)}) = (-1)^k\ (2k+1)^{1/2} \left\{ T^{(k)} \cdot U^{(k)} \right\}^0_0 \qquad \ldots\ldots 16$$

Again Q dependence of the matrix elements of $X^{(k)}_Q$ can be given by Wigner-Eckart theorem.

$$(\tau j_1 j_2\ JJ_z|X_Q^{(K)}|\tau'\ j_1'\ j_2'\ J'J_z'>$$

$$= (-1)^{J-J_z}\begin{pmatrix} J & K & J' \\ -J_z & Q & J_z' \end{pmatrix}(\tau j_1 j_2\ J||X^{(K)}||\tau'\ j_1'\ j_2'\ J') \quad ....17$$

The reduced matrix element can be expressed in terms of the product of two reduced matrix elements in the following way (If $T^{(k_1)}$ and $U^{(k_2)}$ operate on two different parts 1 and 2 of the system respectively).

$$<\tau j_1 j_2\ J||X^{(K)}||\tau' j_1' j_2'\ J> = \Sigma_{''}(\tau j_1||T^{(k_1)}||\tau''\ j_1'>\cdot$$

$$<\tau''\ j_2'||U^{(k_2)}||\tau' j_2'>\cdot\sqrt{[(2J+1)(2K+1)(2J'+1)]}\begin{Bmatrix} j_1 & j_1' & k_1 \\ j_2 & j_2' & k_2 \\ J & J' & K \end{Bmatrix} ..18$$

where the last factor is a 9-J symbol.

For the case $k_1 = k_2 = k$, $K = 0$. Using the definition of scalar product of two spherical tensors we have

$$<\tau\ j_1 j_2\ JJ_z|(T^k.U^k)|\tau'\ j_1'\ j_2' J'J_z'>$$

$$= (-1)^{j_1'+j_2+J}\cdot\delta_{JJ'}\,\delta_{J_zJ'_z}\cdot\begin{Bmatrix} j_1' & j_2' & J \\ j_2 & j_1 & k \end{Bmatrix}$$

$$X\ \sum_{\tau''}<\tau j_1||T^{(k)}||\tau''\ j_1'><\tau''\ j_2||U^{(k)}||\tau'\ j_2'> \quad ....19$$

where the factor in curly brackets is a 6-J symbol.

The 3-J and 6-J symbols are tabulated by Rotenburg et al [8].

2.5 MATRIX ELEMENTS FOR COULOMB INTERACTION

In equation 3 for the free ion Hamiltonian, we have defined the non-central part of the Coulomb interaction as

$$H'_{Coul} = \sum_{i=1}^{N} \left[- \frac{Z^* e^2}{r_i} - U(r_i) \right] + \sum_{i<j}^{N} \frac{e^2}{r_{ij}} \qquad \ldots\ldots 20$$

The terms in the bracket are purely radial and centrally symmetric. They shift the configuration as a whole and do not participate in the relative splittings of the terms in a given configuration. They can be ignored for the present problem. The term $\sum_{i<j} e^2/r_{ij}$ removes the degeneracy of the terms partially. The tensor operators corresponding to the last term can be obtained by transforming it in such a way as to separate the radial and angular variables. The factor $1/r_{ij}$ can be expanded in a series of Legendre polynomials

$$\frac{1}{r_{ij}} = \frac{1}{|\bar{r}_i - \bar{r}_j|} = (\bar{r}_i^2 + \bar{r}_j^2 - 2\, \bar{r}_i . \bar{r}_j \, \mathrm{Cos}\ \omega)^{-1/2}$$

$$= \sum_{k=0} \frac{r_<^k}{r_>^{k+1}} P_k\ (\mathrm{Cos}\ \omega) \qquad \ldots\ldots 21$$

Here $r_<$ and $r_>$ denote the smaller and greater of the magnitudes of the vectors $\bar{r}_i$ and $\bar{r}_j$, and ω is the angle between the vectors $\bar{r}_i$ and $\bar{r}_j$. Using the theorem of addition of spherical functions, $P_k(\omega)$ can be written in terms of spherical harmonics $Y_q^{(k)}(\theta_i \phi_i)$ and $Y_q^{(k)}(\theta_j \phi_j)$. Let us also define a single particle tensor operator $C_q^{(k)}(i)$ as,

$$C_q^{(k)}(i) = \left(\frac{4\pi}{2k+1}\right)^{1/2} Y_q^{(k)}(i) \qquad \ldots\ldots 22$$

Thus the expression for e^2/r_{ij} becomes

$$e^2/r_{ij} = e^2 \sum_k \frac{4\pi}{2k+1} \frac{r_<^k}{r_>^{k+1}} \sum_{q=-k}^{k} Y_q^{(k)}(\theta_i \phi_i) . Y_q^{(k)}(\theta_j \phi_j)$$

$$= e^2 \sum_k \frac{r_<^k}{r_>^{k+1}} \cdot \sum_{q=-k}^{k} C_q^{(k)}(i)\, C_q^{(k)}(j)$$

$$= e^2 \sum_k \frac{r_<^k}{r_>^{k+1}} \sum_{q=-k}^{k} (-1)^q\, C_q^{(k)}(i)\, C_{-q}^{(k)}(j)$$

$$= e^2 \sum_k \frac{r_<^k}{r_>^{k+1}} (C_i^{(k)} \cdot C_j^{(k)}) \qquad \text{.....23}$$

The matrix elements for the residual Coulomb interaction can be evaluated by using equation 19 for the scalar product of two tensor operators.

Using $|\tau SL\rangle$ basis states (where τ stands for the rest of the quantum numbers) the matrix elements can be written as

$$\langle nf^N \tau SL | \sum_{i<J} \frac{e^2}{r_{ij}} | nf^N \tau' S' L' \rangle$$

$$= \langle n\, f^N \tau\, S\, L |\, e^2 \sum_{i<J} \sum_k \frac{r_<^k}{r_>^{k+1}} (C_i^{(k)} \cdot C_j^{(k)}) | n\, f^N \tau'\, S' L' \rangle$$

$$= \sum_k f_k \langle nf^N \tau SL,\ nf^N \tau' S' L' \rangle \cdot F^k(nf,nf) \qquad \text{.....24}$$

Here angular parts f_k of the matrix elements are defined as

$$f_k = \langle nf^N \cdot \tau SL | \sum_{i<j} C_i^{(k)} \cdot C_j^{(k)} | nf^N \tau' S' L' \rangle$$

$$= \delta_{SS'}\, \delta_{LL'} (-1)^L \begin{Bmatrix} 3 & 3 & K \\ 3 & 3 & L \end{Bmatrix} (\langle 3 || c^{(k)} || 3 \rangle)^2 \qquad \text{.....25}$$

and Slater's radial integrals F^k are defined as

$$F^k = F^k(nf,nf) = e^2 \int_0^\infty \int_0^\infty \frac{r_<^k}{r_>^{k+1}} [R_{nf}(r_i) \cdot R_{nf}(r_j)]^2\, dr_i\, dr_j \qquad \text{..26}$$

The reduced matrix elements $\langle 3||C^{(k)}||3\rangle$ can be calculated using the expression

$$\langle l||C^{(k)}||l'\rangle = (-1)^{l} \times\sqrt{(2l+1)(2l'+1)}\ \begin{pmatrix} l & k & l \\ 0 & 0 & 0 \end{pmatrix}$$

Thus

$$\langle 3||C^{(k)}||3\rangle = -\sqrt{87} \times \begin{pmatrix} 3 & k & 3 \\ 0 & 0 & 0 \end{pmatrix} \qquad \ldots\ldots 27$$

The triangular condition and the condition $k+l+l' = 2g$ (g -integer) for non zero values of 3-J symbols restrict the values of k for non-zero matrix elements to 0,2,4 and 6.

To avoid the occurrence of large fractional coefficients for F^k in the evaluation of matrix elements, Condon and Shortley redefined f^k and F^k as

$$f_k = \frac{f^k}{D_k} \quad \text{and} \quad F_k = \frac{F^k}{D_k} \qquad \ldots\ldots 28$$

Where D_k are the denominators listed in the Table 1^6 and 2^6 of reference [4].

The operator $(C_i^{(k)} \cdot C_j^{(k)})$ does not have the transformational properties of groups R_7 and G_2, used to classify the states of the configuration, though it is a scalar with respect to the group R_3. This makes the calculation of matrix elements difficult for systems having more than two equivalent f electrons. To overcome this problem Racah defined a new set of parameters e_k and E^k, which are linear combinations of the parameters f^k and F_k. The matrix elements in terms of Racah's parameters can be expressed as

$$E = \sum_{k=0}^{3} e_k\, E^k \qquad \ldots\ldots 29$$

Where e_k, the angular parts are related with the old parameters f_k by the expressions:

$$e_o = f^o = N(N-1)$$

$$e_1 = (9/7)\, f^o + (1/42)\, f^2 + (1/77)\, f^4 + (1/462)\, f^6$$

$$e_2 = (143/42)\, f^2 - (130/77)\, f^4 + (35/462)\, f^6$$

$$e_3 = (11/42)\, f^2 + (4/77)\, f^4 - (7/462)\, f^6 \qquad .....30$$

and the new radial parameters E^k are related to F_k's as

$$E^o = F_o - 10F_2 - 33F_4 - 286F_6$$

$$E^1 = \tfrac{1}{9}(70F_2 + 231F_4 + 2002F_6)$$

$$E^2 = \tfrac{1}{9}(F_2 - 3F_4 + 7F_6)$$

$$E^3 = \tfrac{1}{3}(5F_2 + 6F_4 - 91F_6) \qquad .....31$$

Nelson and Koster [8], have calculated and tabulated the angular parts e_k for all ℓ^N configurations. The radial quantities E^k are treated as adjustable parameters in the interpretation of experimental results.

2.6 SPIN-ORBIT INTERACTION

The spin-orbit Hamiltonian defined in equation 3 as

$$H'_{S-O} = \sum_{i=1}^{N} \zeta_i(r_i)(s_i \cdot \ell_i) \qquad .....32$$

is a simple example of the product tensor operator of two tensors of rank one; one operating only on the spin and the other operating only on the spatial coordinates. H'_{S-O} commutes with J^2 and J_z but not with L^2 and S^2. As a

result the matrix elements are independent of J_z and diagonal in J but mix the states of different L and S values.

The matrix elements of H'_{S-O} in the basis functions $|f^N \tau SLJJ_z\rangle$ can be obtained as

$$\langle f^N \tau SLJJ_z | H'_{S-O} | f^N \tau' S'L'J'J'_z\rangle$$

$$= \delta_{JJ'} \delta_{J_z J'_z} \zeta_{nf} \cdot (-1)^{J+L+S'} \begin{Bmatrix} L & L' & 1 \\ S' & S & J \end{Bmatrix}$$

$$\times \langle f^N \tau SL \,|\, \sum_{i=1}^{N} (s_i \cdot \ell_i) | f^N \tau' S'L' \rangle \quad .....33$$

Here, the spin-orbit radial factor ζ_{nf} is defined as

$$\zeta_{nf} = \int_0^\infty R_{nf}^2(r) \cdot \xi_i(r)\, dr \quad .....34$$

The last factor can be further evaluated as

$$\langle f^N \tau SL | \sum_{i=1}^{N} (s_i \cdot \ell_i) | f^N \tau' S'L' \rangle = [3(3+1)(2\times3+1)]^{1/2}$$

$$\cdot \langle f^N \tau SL || V^{(11)} || f^N \tau' S'L' \rangle$$

$$= \sqrt{84} \cdot \langle f^N \tau SL || V^{(11)} || f^N \tau' S'L' \rangle \,..35$$

The reduced matrix element $\langle || V^{(11)} || \rangle$ can be evaluated using coefficients of fractional parentage[6]; the results can be written as

$$\langle f^N \tau SL || V^{(11)} || f^N \tau' S'L' \rangle = 3N[(2S+1)(2S'+1)(2L+1)(2L'+1)]^{1/2}$$

$$\times (-1)^{1/2 + 3 + S + L} \cdot \sum_{\bar{\Psi}} (\Psi\xi|\bar{\Psi})\, (\Psi\xi|\bar{\Psi}) (-1)^{\bar{S}+\bar{L}}$$

$$\cdot \begin{Bmatrix} S & 1 & S' \\ 1/2 & S & 1/2 \end{Bmatrix} \cdot \begin{Bmatrix} L & 1 & L' \\ 3 & L & 3' \end{Bmatrix} .....36$$

$(\Psi\xi|\bar{\Psi})$ are coefficients of fractional parentage. The reduced

matrix elements of $V^{(11)}$ for all p^N, d^N and f^N configurations are calculated and tabulated by Nielson and Koster [8]. The triangular conditions for the 6-J symbols restrict the non-zero matrix elements to those with

$$\Delta S = 0, \pm 1 \text{ and } \Delta L = 0, \pm 1 \qquad .....37$$

2.7 CONFIGURATION INTERACTION

Free ion calculations carried out within a single configuration approximation usually leads to a disagreement (of the order of hundreds of wave numbers) between calculated and experimentally estimated free ion energy levels, even if the radial integrals are treated as parameters. To consider the complete configuration interaction, one has to take into account very large number of configurations including those in the continuum. This will require handling unmanageably large size matrices. Therefore the commonly adopted method to treat this type of interaction is to incorporate the most dominant effects of the interaction within the states of the ground configuration. The most dominant type of configuration interaction is via the Coulomb interaction. For the ℓ^N configurations, this effect has been theoretically studied by Rajnak and Wybourne [9] and also by Racah

and Stein [10]. Following are the most likely configurations which can perturb an ℓ^N configuration.

(1) $\ell^{N-1}\ \ell'$

(2) $\ell^{N-2}\ \ell'^2$ and $\ell^{N-2}\ \ell'\ \ell''$

(3) $\ell'^{4\ell'+1}\ \ell^{N+1}$

(4) $\ell'^{4\ell'+1}\ \ell^{N+1}$

(5) $\ell'^{4\ell'}\ \ell^{N+2}$ and $\ell'^{4\ell'+1}\ \ell''^{4\ell''+1}\ \ell^{N+2}$

The last three configurations correspond to core excitations and their effect is to shift the centre of gravity of the perturbed configuration as a whole. They do not contribute to its structure, hence these can be neglected from the present discussion.

Rajnak and Wybourne [9] showed that the configuration interaction through the Coulomb field adds a correction term

$$C(\Psi\Psi') = \Sigma \frac{\langle \ell^N \Psi | G | m_\tau \rangle \langle m_\tau | G | \ell^N \Psi' \rangle}{E_\tau} \qquad \ldots\ldots 38$$

to each of the matrix elements of the perturbed configuration. Here m_τ represents perturbing configuration states which are separated by an energy E_τ from the perturbed configuration and G is an operator representing the Coulomb energy of repulsion, $\Sigma_{i<j} e^2/r_{ij}$. They were able to show by using tensor algebra and tedious summations, that the above term can be expressed in terms of the matrix elements of the

tensor operators $U^{(k)}$

$$C(\Psi\Psi') = \sum_{k=0}^{2l} P^k (f^N \Psi | \sum_{i<j}^{N} (U_i^{(k)} . U_j^{(k)}) | f^N \Psi') \quad .....39$$

Here P^k contains radial integrals and excitation energies.

For even k the angular part of the equation (39) is having exactly the same form as the coefficients of F^k in the matrix elements of H'_{Coul}. Hence treating the radial integrals of the matrix elements of H'_{Coul} as adjustable parameters automatically includes this part of the configuration interaction.

The terms with k odd, are not taken into account even when the Slater integrals are treated as adjustable parameters. These can be included only by introducing additional parameters. Rajnak and Wybourne used properties of Casimirs operators [6] to replace these terms with an equivalent expression.

$$\delta(\Psi\Psi') \; [\alpha . L(L+1) + \beta \; G(G_2) + \gamma \; G(R_7)] \quad .....40$$

Where $G(G_2)$ and $G(R_7)$ are the eigenvalues of Casimir's operators for the groups G_2 and R_7 used to classify the states of the f^N configuration. These are tabulated in Tables 2.6 and 2.7 of reference (11).

α, β and γ are associated parameters corresponding to a particular linear combination of the P^k (odd) parameters and are to be treated as adjustable parameters in order to improve upon the agreement between theoretical and experimental

results. Wybourne [12] has generalized the configuration interaction to higher orders of perturbation, but this needs introduction of additional parameters and in the absence of sufficient experimental data, it is not possible to consider these types of effects. Rajnak and Wybourne [13] have also examined configuration interaction via spin-orbit interaction. This simply screens the spin-orbit coupling radial integral and is taken care of by parameterization of spin-orbit interaction.

2.8 OTHER INTERACTIONS

Though the normal Coulomb, spin-orbit and configuration interactions take care of the major contribution to the energy of the states of the configurations encountered in the rare earths, some other interactions are also present; for example, orbit-orbit, spin-spin and spin- other orbit etc. Most of these magnetic interactions do not make any substantial change in the energy contribution while their consideration increases the complexity of the calculations. It may however be pointed out that the parameterization technique already discussed does take care of some of these effects.

3. CRYSTAL FIELD INTERACTION

In an ionic crystal the electrons occupy orbitals that are highly localized about the ions in such a way that any electron can still be associated with a particular ion. Each electron, however, feels the influence of the electrons belonging to the other ions (a repulsion) and of the nuclei belonging to the other ions (an attraction). We can take this influence into account by considering that the electrons of the individual ions are subjected to the action of a 'crystalline field'.

The 4f shell of rare earths is incomplete and therefore has an aspherical charge distribution. The crystal field is completely external to the ion and has a definite symmetry, invariant under time reversal. The crystal field experienced by the ions distorts the closed shells of the RE ions and removes, to a certain extent, the (2J+1) degeneracy of the free ion levels. In the case of an even electron system the degeneracy can be completely lifted by an electric field (crystal field) of low enough symmetry. For an odd electron system, at least a two fold degeneracy remains, irrespective of the symmetry of the field. This is known as Kramers' degeneracy [13]. This degeneracy may be lifted only by magnetic interactions. It is possible to predict the extent to which the degeneracy of the energy levels can be lifted and also the transformation properties of the eigen functions,

if the symmetry of the crystal field is known. The actual evaluation of the crystal field splittings, however, requires the solution of the crystal field Hamiltonian. The Hamiltonian for an ion in a crystal can be written as

$$H = H_F + H'_{cry}. \qquad \ldots.41$$

Where H_F is the free ion Hamiltonian already considered and H'_{cry} represents the interaction of the free ion with its environment and is given as

$$H'_{cry} = -\sum_i \int \frac{e_i \rho(\bar{R})}{|\bar{R} - \bar{r}_i|} d\tau \qquad \ldots.42$$

Here $\rho(\bar{R})$ is charge distribution which interacts with a given electron, $\bar{r}_i$ is the position vector of the i^{th} electron with respect to the nucleus.

The Hamiltonian H'_{cry} can be expanded in terms of the spherical harmonics in a fashion similar to the H'_{Coul} term of the free ion Hamiltonian

$$\text{Thus } H'_{cry} = -\sum_i \int \frac{e_i \rho(\bar{R})}{|\bar{R} - \bar{r}_i|} d\tau$$

$$= -\sum_{ik} e_i \int \rho(\bar{R})\, P_k\,(\mathrm{Cos}(\bar{R},\bar{r}_i))\, \frac{r_<^k}{r_>^{k+1}}\, d\tau$$

$$= \sum_{ikq} e_i \int \rho(\bar{R})\, \frac{4\pi}{2K+1}(-1)^q\, Y_q^{(k)}(\theta_i,\phi_i)\, Y_{-q}^{(k)}(\theta,\phi)\, \frac{r_<^k}{r_>^{k+1}}\, d\tau$$

$$= -\sum_{ikq} e_i \int \rho(\bar{R})(-1)^q\, C_q^{(k)}(\theta_i,\phi_i)\, C_{-q}^{(k)}(\theta,\phi)\, \frac{r_<^k}{r_>^{k+1}}\, d\tau$$

$$= \sum_{kqi} B_q^k \, C_q^{(k)}(\theta_i, \phi_i) \qquad \ldots\ldots 43$$

Where the crystal field parameter B_q^k to be treated as an adjustable parameter is defined as

$$B_q^k = -e\int (-1)^q \rho(\bar{R}) \, C_{-q}^{(k)}(\theta,\phi) \, \frac{r_<^k}{r_>^{k+1}} \, d\tau \qquad \ldots\ldots 44$$

3.1 NUMBER OF TERMS OCCURRING IN THE EXPANSION OF H'_{cry}

The allowed values of k and q in equation 43 depend on the site symmetry of the ion under consideration. The crystal potential must possess the symmetry of the lattice under consideration, that is, it must be invariant under the operation of the point group. In the case of $LiYF_4:Eu^{3+}$: Eu^{3+} has site symmetry of S_4. This means that the potential function in this case must be invariant under the operations of the group S_4. The symmetry operation S_4 can be expressed by the transformation

$$\begin{pmatrix} x \\ y \\ z \end{pmatrix} \xrightarrow{S_4} \begin{pmatrix} y \\ -x \\ -z \end{pmatrix} \qquad \ldots\ldots 45$$

Using the cartesian representation of spherical harmonics and the above transformation, the H'_{cry} for 4f electrons can be obtained.

$$H'_{cry}(S_4) = B_o^o \, C_o^{(o)} + B_o^2 \, C_o^{(2)} + B_o^4 \, C_o^{(4)} + B_o^6 \, C_o^{(6)}$$

$$+ \sum_{k=4,6} [B_4^k (C_4^{(k)} + C_{-4}^{(k)}) + i \, B_4'^k (C_4^{(k)} - C_{-4}^{(k)})] \qquad \ldots\ldots 46$$

Here the restriction $k \leq 6$ applies because we are considering 4f electrons. The odd terms are neglected because their matrix elements within the states of the same parity are identically zero. In writing Eqn.46 we have made sure that H'_{cry} is Hermitian. This requires

$$B_q^k = (-1)^q \, B_{-q}^{k*} \qquad \ldots\ldots 47$$

From the properties of spherical harmonics, operators $(C_4^{(k)} + C_{-4}^{(k)})$ are real and hence coefficients B_4^k will also be real. The operators $(C_4^{(k)} - C_{-4}^{(k)})$ are imaginary, therefore, to make H'_{cry} hermitian and B_4^k real, 'i' has been introduced explicitly.

The first term in the expansion with $k = q = 0$ is spherically symmetric. It does not contribute to the splitting of the free ion terms and may, therefore, be omitted in the calculations. However, if the precise configuration interaction is to be considered, it can not be neglected.

Once the H'_{cry} has been obtained in tensorial form, its matrix elements can be calculated by selecting a suitable set of basis states.

3.2 CHOICE OF BASIS STATES

The S_4 point group involves a 90^o rotation followed by a reflection in a plane perpendicular to the rotation axis. It is characterized by four irreducible representations for the single group, two of which are degenerate.

The relevant character table of the point group S_4 is shown in Table 2.1. In this table a(b) under the column time reversal indicates that the basis functions for the representation in question are real(complex). Tables 2.2 and 2.3 list the relevant portion of the multiplication table and the full rotation compatibility table respectively. We note that the representations Γ_3 and Γ_4 are degenerate and for the purpose of calculating the crystal field splittings, we need to consider only one of them.

H'_{cry} does not commute with J and J_z, so it mixes the states with different J and J_z values and hence J and J_z are no more good quantum numbers. However, the matrix elements of the crystal field interaction, between wavefunctions belonging to different irreducible representations are zero. Thus the irreducible representations of the point group act as good quantum numbers. It is always possible to find some linear combinations of $|f^N\ J\ J_z\rangle$ states having transformation properties like those of the irreducible representations of the point group under consideration. These irreducible representations can be used to label the basis states $|f^N\ J\ J_z\ \Gamma_i\rangle$ where Γ_i is the irreducible representation. The appropriate J_z-linear combinations can be obtained through the use of the projection operators $P_k^{(i)}$[14]. The projection operator $P_k^{(i)}$ for a group G, when operated on a set of functions $|JJ_z\rangle$, selects those

TABLE 2.1

CHARACTER TABLE FOR GROUP S_4 [15]

S_4	E	$\bar{E}$	S_4^{-1}	$\bar{S}_4^{-1}$	C_2	$\bar{C}_2$	S_4	$\bar{S}_4$	Time Inversion	Bases
Γ_1	1	1	1	1	1	1	1	1	a	S_z
Γ_2	1	1	-1	-1	1	1	-1	-1	a	Z or XY
Γ_3	1	1	i	i	-1	-1	-i	-i	b	$-(S_X + iS_Y)$ or $i(X - iY)$
Γ_4	1	1	-i	-i	-1	-1	i	i	b	$(S_X - iS_Y)$ or $-i(X + iY)$

TABLE 2.2

MULTIPLICATION TABLE FOR S_4 [15]

	Γ_1	Γ_2	Γ_3	Γ_4	
	Γ_1	Γ_2	Γ_3	Γ_4	Γ_1
		Γ_1	Γ_4	Γ_3	Γ_2
			Γ_2	Γ_1	Γ_3
				Γ_2	Γ_4

TABLE 2.3

FULL ROTATION GROUP COMPATIBILITY TABLE FOR THE GROUP S_4: CONFIGURATION $4f^6$ [15]

D_0^+	Γ_1
D_1^+	$\Gamma_1 + (\Gamma_3 + \Gamma_4)$
D_2^+	$\Gamma_1 + 2\Gamma_2 + (\Gamma_3 + \Gamma_4)$
D_3^+	$\Gamma_1 + 2\Gamma_2 + 2(\Gamma_3 + \Gamma_4)$
D_4^+	$3\Gamma_1 + 2\Gamma_2 + 2(\Gamma_3 + \Gamma_4)$
D_5^+	$3\Gamma_1 + 2\Gamma_2 + 3(\Gamma_3 + \Gamma_4)$
D_6^+	$3\Gamma_1 + 4\Gamma_2 + 3(\Gamma_3 + \Gamma_4)$
D_7^+	$3\Gamma_1 + 4\Gamma_2 + 4(\Gamma_3 + \Gamma_4)$
D_8^+	$5\Gamma_1 + 4\Gamma_2 + 4(\Gamma_3 + \Gamma_4)$
D_9^+	$5\Gamma_1 + 4\Gamma_2 + 5(\Gamma_3 + \Gamma_4)$
D_{10}^+	$5\Gamma_1 + 6\Gamma_2 + 5(\Gamma_3 + \Gamma_4)$
D_{11}^+	$5\Gamma_1 + 6\Gamma_2 + 5(\Gamma_3 + \Gamma_4)$
D_{12}^+	$7\Gamma_1 + 6\Gamma_2 + 5(\Gamma_3 + \Gamma_4)$

functions which transform according to the k^{th} row of the i^{th} irreducible representation of the group G. For a point group of type S_{2n}

$$P_k^{(i)} \, |\sigma \; J \; J_z\rangle = |\sigma \; J \; J_z\rangle . \; \delta(J_z, \; \mu(i,k) + n\sigma + 2np) \quad .....48$$

Where $\sigma = 1$ for even parity configurations

$= 0$ for odd parity configurations

$p = 0, \pm 1, \pm 2, \pm 3, \ldots$

For S_4, $n = 2$ and

$k = 1$ for all irreducible representations of S_4.

$\mu(i,1) = 0$ and 2 for $i = 1$ and 2 respectively

$= \pm 1$ for $i = 3$ and 4.

Table 2.4 shows the basis functions for the irreducible representations of S_4 for the $4f^6$ configuration. Numbers under the column $N(\Gamma_i)$ represent the number of times the i^{th} representation appears when D_J^+ is broken into Γ_i's.

TABLE 2.4

THE J_z-BASES FOR THE IRREDUCIBLE REPRESENTATIONS OF THE POINT GROUP S_4 APPLICABLE TO Eu^{3+}

J	Γ_1		Γ_2		Γ_3		No. of Stark Components $=\sum_i N(\Gamma_i)$
	J_z	$N(\Gamma_1)$	J_z	$N(\Gamma_2)$	J_z	$N(\Gamma_3)$	
0	0	1					1
1	0	1			1	1	2
2	0	1	± 2	2	1	1	4
3	0	1	± 2	2	1,-3	2	5
4	$0,\pm 4$	3	± 2	2	1,-3	2	7
5	$0,\pm 4$	3	± 2	2	0,-3,5	3	8
6	$0,\pm 4$	3	$\pm 2,\pm 6$	4	1,-3,5	3	10
7	$0,\pm 4$	3	$\pm 2,\pm 6$	4	1,-3,5,-7	4	11
8	$0,\pm 4,\pm 8$	5	$\pm 2,\pm 6$	4	1,-3,5,-7	4	13
9	$0,\pm 4,\pm 8$	5	$\pm 2,\pm 6$	4	1,-3,5,-7,9	5	14
10	$0,\pm 4,\pm 8$	5	$\pm 2,\pm 6,\pm 10$	6	1,-3,5,-7,9	5	16
11	$0,\pm 4,\pm 8$	5	$\pm 2,\pm 6,\pm 10$	6	1,-3,5,-7,9,-11	6	17
12	$0,\pm 4,\pm 8,\pm 12$	7	$\pm 2,\pm 6,\pm 10$	6	1,-3,5,-7,9,-11	6	19

3.3 MATRIX ELEMENTS FOR H'_{cry}

Matrix elements of H'_{cry} can be calculated by tensorial methods. A typical matrix element will be given by

$$\langle f^N\ SLJJ_z|H'_{cry}|f^N\ S'L'J'J'_z\rangle = \sum_{kq} B_q^k \langle f^N\ SLJJ_z|U_q^{(k)}|f^N\ SL'J'J'_z\rangle$$

$$x\ \langle f||C^{(k)}||f\rangle \qquad \ldots.49$$

Further J_z dependence of the matrix element of the tensor operator can be obtained using the Wigner-Eckart theorem.

$$\langle f^N\ SLJJ_z|U_q^{(k)}|f^N\ SL'J'J'_z\rangle = (-1)^{J-J_z} \begin{pmatrix} J & k & J' \\ -J_z & q & J_z \end{pmatrix} x$$

$$\langle f^N\ SLJ||U^{(k)}||f^N\ SL'J'\rangle \qquad \ldots.50$$

Where

$$\langle f^N\ SLJ||U^{(k)}||f^N\ SL'J'\rangle = (-1)^{S+L'+J+K} \sqrt{[(2J+1)(2J'+1)]}$$

$$x \begin{Bmatrix} J & J' & k \\ L' & L & S \end{Bmatrix} \quad x\ \langle f^N\ SL||U^{(k)}||f^N\ SL'\rangle \ldots.51$$

The doubly reduced matrix elements $\langle f^N\ SL||U^{(k)}||f^N\ SL'\rangle$ are calculated and tabulated by Nielson and Koster [8]. These expressions can be used to calculate matrix elements of the crystal field Hamiltonian within a multiplet or between multiplets.

In equation 49, the terms with q = 0, $(U_o^{(k)})$ are axial terms and give the non zero matrix elements for a given J_z,

whereas the terms $U_q^{(k)}$ mix states for which $J'_z - J_z = q$. Because of this mixing, J and J_z are no more good quantum numbers. The odd terms in H'_{cry} do not contribute to the crystal field splittings. They are, however, responsible for the appearance of electric dipole transitions in the spectra of trivalent rare earth ions by mixing configurations of opposite parity.

4. SELECTION RULES

4.1 FREE ION SELECTION RULES

The electric dipole transitions among the levels of a $4f^N$ configuration are forbidden by the parity rule. The magnetic dipole transitions though allowed, are usually weak. For an ion placed in a crystal lacking a centre of inversion, mixing of configurations of opposite parity can take place due to the presence of odd terms of the crystal field Hamiltonian. The resulting electric dipole transitions are called 'forced electric dipole transitions'. Judd [16] and Ofelt [17] have independently developed the theory of forced electric dipole transitions. They have obtained the following selection rules for the magnetic dipole and for the forced electric dipole transitions.

For electric dipole transitions: $\Delta J \leq 6$

For transitions involving J=0 state, the following additional selection rules also hold.

(i) $J = 0 \longrightarrow J' = 0$ forbidden

(ii) $J = 0 \longrightarrow J'$ odd weak

(iii) $J = 0 \longrightarrow J' = 2,4,6$ allowed

For magnetic dipole transitions

(i) $\Delta J = 0, \pm 1$

(ii) $J = 0 \longrightarrow J' = 0$ forbidden

J - mixing by the crystal field can relax these selection rules.

4.2 CRYSTAL FIELD SELECTION RULES

The selection rules mentioned in the earlier section need to be supplemented due to the additional constraints imposed by site symmetry considerations. The character table for the point group S_4 (Table 2.1) shows that the operator z and $(x \pm iy)$ transform according to Γ_2 and $\Gamma_{3,4}$ representations respectively. An electric dipole transition between levels characterized by the irreducible representations Γ_i and Γ_j will be allowed in $\pi(\sigma)$ polarization provided the product $\Gamma_i \Gamma_2 (\Gamma_{3,4}) \Gamma_j$ contains the symmetric representation Γ_1. For example the product $\Gamma_1 \Gamma_2 \Gamma_2$ contain Γ_1 and therefore $\Gamma_1 \longrightarrow \Gamma_2$ transitions is allowed in π-polarization but the product $\Gamma_1 \Gamma_3 \Gamma_2$ does not contain Γ_1 and hence $\Gamma_1 \longrightarrow \Gamma_2$ is not allowed in σ-polarization. Using these considerations, the E.D. and M.D. rules listed in Table 2.5 can be obtained.

TABLE 2.5

FORCED ELECTRIC DIPOLE AND MAGNETIC DIPOLE SELECTION RULES FOR $LiYF_4:Eu^{3+}$

E.D.	Γ_1	Γ_2	$\Gamma_{3,4}$
Γ_1	-	π	σ
Γ_2	π	-	σ
$\Gamma_{3,4}$	σ	σ	π

M.D.	Γ_1	Γ_2	$\Gamma_{3,4}$
Γ_1	σ	-	π
Γ_2	-	σ	π
$\Gamma_{3,4}$	π	π	σ

The Γ_3 and Γ_4 representations are degenerate.

-x-

REFERENCES

[1] M G Mayer; Phys Rev 60 184 (1941).

[2] C M Jørgensen; J Inorg Nuclear Chem 1 301 (1955).

[3] A J Freeman and R E Watson; Phy Rev 127 2058 (1962).

[4] E U Condon and G H Shortley; The Theory of Atomic Spectra, Cambridge Univ Press, Cambridge (1935).

[5] G Racah; Phy Rev 76 1352 (1949).

[6] B R Judd; Operator Techniques in Atomic Spectroscopy, McGraw-Hill book company N Y (1963).

[7] G Racah; Phys Rev 62 438 (1942).

[8] C W Nielson and G F Koster; Spectroscopic Coefficients for the p^n, d^n and f^n Configurations, The MIT Press (1963).

[9] K Rajnak and B G Wybourne; Phys Rev 132 280 (1963)

[10] G Racah and J Stein; Phy Rev 156 58 (1967).

[11] B G Wybourne; Spectroscopic Properties of Rare Earths, Interscience Publications, Wiley, N Y (1965).

[12] S Hüfner; Optical Spectra of Transparent Rare Earth Compounds, Acad Press N Y (1978).

[13] H A Kramers; Proc Amsterdam Acad 33 959 (1930).

[14] Donald S McClure et al; Electronic Spectra of Transition Metal Ions in Crystals, RCA Labs Project 5621, Task 5611 (1961).

[15] G F Koster et al; Properties of the Thirtvtwo Point Groups (MIT Press 1963).

[16] B R Judd; Phys Rev 127 750 (1962).

[17] G S Ofelt; J Chem Phys 37 511 (1962)

-x-

CHAPTER III

EXPERIMENTAL DETAILS

1. GENERAL

This thesis deals with the observation and interpretation of the absorption and fluorescence spectra of Eu^{3+} doped in $LiYF_4$ single crystal. The single crystal used in this work was obtained from Dr L.E. Erickson of the National Research Council, Ottawa (Canada). The dimensions of the oriented and polished sample were 3.8 mmx 3.1 mm x 2.1 mm with the $\bar{c}$ axis parallel to the 3.1 mm edge. Eu^{3+} concentration in the sample is approximately 1%.

2. CRYSTAL STRUCTURE [1]

$LiYF_4$ belongs to the tetragonal scheelite ($CaWO_4$) type family of crystals with

$$a = b \neq c$$

$$\alpha = \beta = \gamma = 90^{\circ}$$

The scheelites have space group C_{4h}^6 ($I4_1/a$). In the isomorphism between $LiYF_4$ and $CaWO_4$, Li^+ corresponds to W^{6+}, Y^{3+} corresponds to Ca^{2+} and F^- to O^{2-}. The unit cell contains four molecules. The positions of the atoms in the unit cell are [2]

L : (0,0,0); (0,1/2,1/4); (1/2,1/2,1/2); (1/2,0,3/4)

Y : (0,0,1/2);(1/2,0,1/4); (1/2,1/2,0);(0,1/2,3/4)

F : (x,y,z); $(\bar{x},\bar{y},z)$; $(\bar{y},x,\bar{z})$; $(y,\bar{x},\bar{z})$

$(x,y+1/2,1/4-z)$; $(\bar{x}, 1/2-y, 1/4-z)$; $(\bar{y}, x+1/2,z+1/4)$; $(y,1/2-x, z+1/4)$ + BCC.

Where x = 0.25, y = 0.15 and z = 0.075. Crystallographic information on some of the scheelites is listed in Table 3.1. Figure 3.1 shows the positions of Li and Y ions in the unit cell of $LiYF_4$. The fluorine ions have not been shown in the figure. If we consider the site (1/2,1/2,1/2) in Figure 3.1, we notice that the Yttrium ion there is surrounded by 8 Li ions: 4 at the corner of a square with a Y-Li distance of 3.72 A^o, and 4 others at the corners of a tetrahedron with a Y-Li distance of 3.79 A^o. These are marked 1 to 8 in Figure 3.1. The four fluorine ions surrounding a Li site lie on the vertices of a somewhat distorted tetrahedron. One fluorine ion from each of the 8 $(LiF_4)^{3-}$ tetrahedra contribute to the eight fluorine neighbours of a Y ion, which is nearly a dodecahedron. Fig 3.2 shows the projected positions of the fluorine neighbours of a Y ion. The position coordinates of the first nearest neighbours and the second nearest neighbours are listed in Table 3.2. Table 3.3 gives the radii of Li^+, Y^{3+}, Eu^{3+} and F^- ions.

TABLE 3.1

LATTICE PARAMETERS OF $LiYF_4$ AND SOME OTHER SCHEELITES [3]

S.No.	Crystal	C(A^o)	a(A^o)	c/a
1.	$LiYF_4$*	10.94	5.26	2.08
2.	$LiYF_4$**	10.85	5.16	2.10
3.	$CaMoO_4$	11.194	5.1554	2.171
4.	$CaWO_4$	11.376	5.243	2.170
5.	$PbMoO_4$	12.0165	5.0165	2.121

TABLE 3.2

POSITION COORDINATES OF FLUORINE IONS IN THE UNDISTORTED CRYSTAL

$R_1(A^o)$	θ_1	ϕ_1	$R_2(A^o)$	θ_2	ϕ_2
2.246	$67^o05'$	$-33^o00'$	2.293	$142^o03'$	$-36^o59'$

(R_1 θ_1 ϕ_1) and (R_2 θ_2 ϕ_2) are the position coordinates of the first and the second nearest neighbours.

* Reference [1]

** Reference [4]

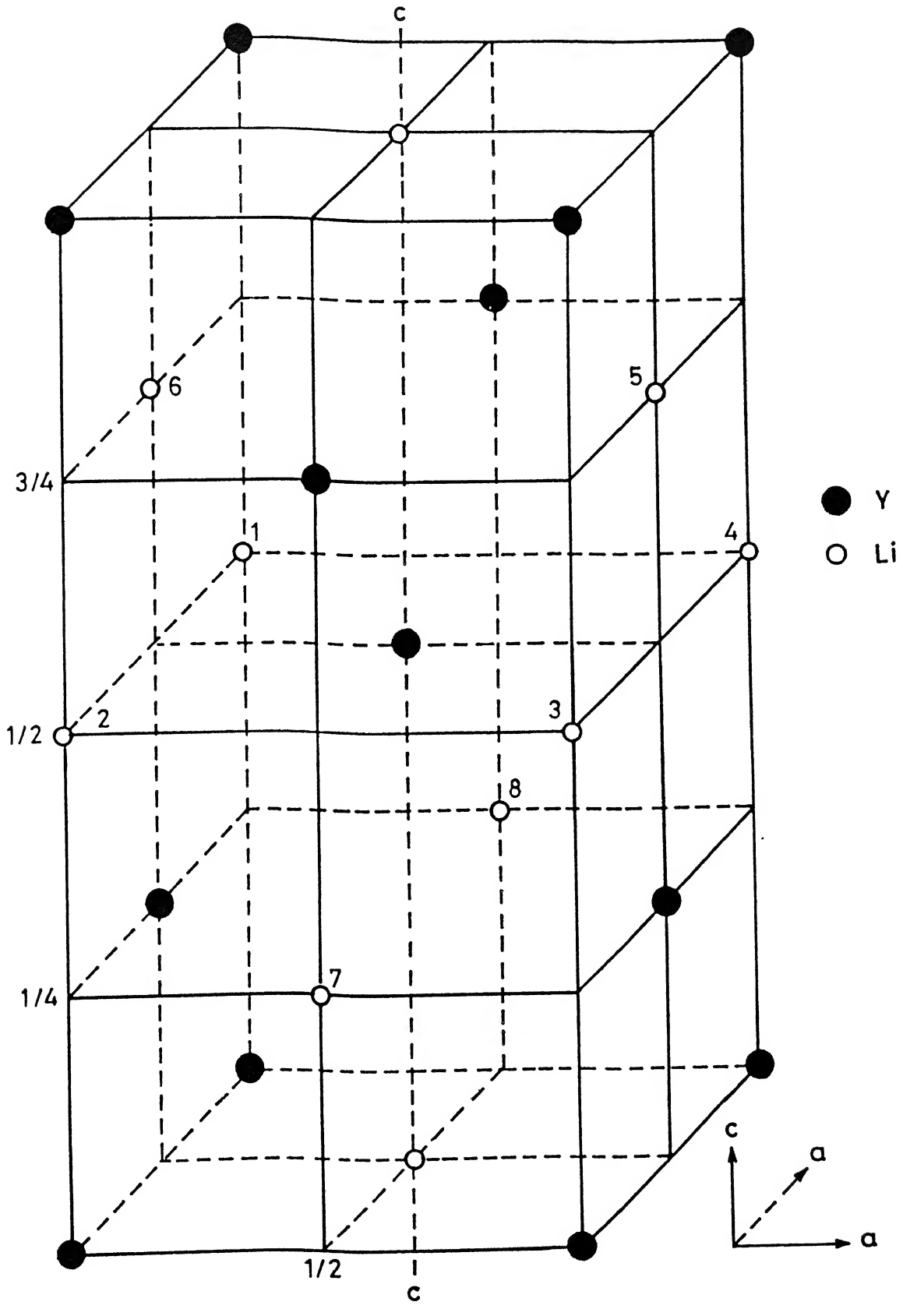

FIG.3.1 : Y AND Li SITES IN THE UNIT CELL OF $LiYF_4$ SINGLE CRYSTAL.

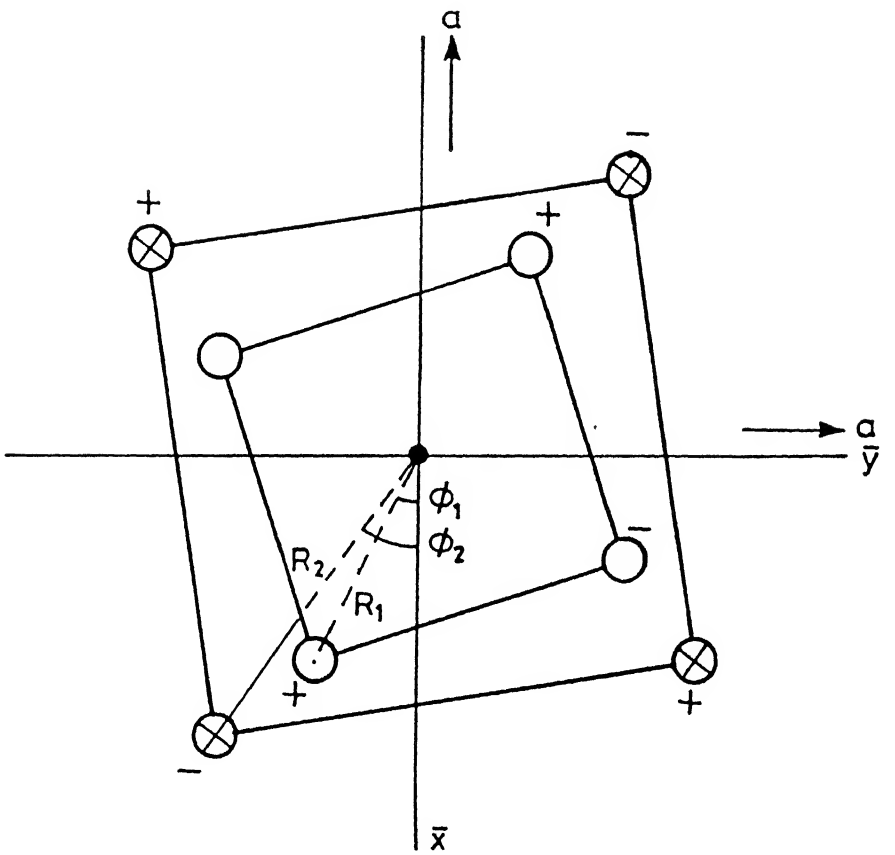

○ Fluorine ions (nearest neighbour)

⊗ Fluorine ions (next nearest neighbour)

● Y-ions

\+ Ions above the horizontal plane

− Ions below the horizontal plane

FIG.3.2 : PROJECTED POSITIONS OF FLUORINE NEAR NEIGHBOURS OF A Y ION IN $LiYF_4$ SINGLE CRYSTAL.

TABLE 3.3

IONIC RADII

S.No.	Element	Ionic radius(A°)
1.	Li^{+}	0.68
2.	Y^{3+}	0.893
3.	F^{-}	1.33
4.	Eu^{3+}	0.950

In the absence of the fluorine ions the symmetry of the unit cell would be D_{2d}. The two vertical reflection planes intersecting along the c-axis and the 2 two-fold rotation axes perpendicular to the c-axis can be easily visualized from Fig 3.1. The fluorine ions, however, do not possess these symmetry elements and the site symmetry of Y ions is lowered to S_4 with a 90^{o} rotation about the c-axis followed by a reflection in a plane perpendicular to the c-axis.

2.1 RARE EARTH DOPING IN $LiYF_4$ CRYSTALS

Like other scheelites, $LiYF_4$ can be readily doped with rare earth ions. Since these crystals have compact structure, interstitial substitution is very much unlikely. Therefore rare earth ions can replace either Y^{3+} or Li^{+} ions. If the rare earth ions were to replace Li^{+}, the resulting optical spectra would be very nearly unpolarized due to approximately cubic environment of the Li ions. The fact that the observed spectra are highly polarized suggests that the rare earths do not substitute for Li^{+} ions. Moreover, large differences in the ionic radii and ionic charges of rare earth and Li ions would make this substitution less likely. Conditions are much more favourable for a rare earth ion occupying a Y^{3+} site on both these counts. These considerations show that $LiYF_4$ is a superior host for rare earth doping.

3. EXPERIMENTAL SET-UP

3.1 EXPERIMENTAL SET-UP FOR ABSORPTION MEASUREMENTS

Figure 3.3 gives a schematic diagram of the set-up used for absorption measurements. Light from a white light source 'S' is focussed by the lenses L_1 and L_2 onto the sample mounted in a cryostat. The transmitted light is collected and focussed on the entrance slit of a double grating monochromator (GDM-1000). The spectrally dispersed light from the GDM-1000 is detected by the PMT (M12FC51) attached to the exit slit of the monochromator. The PMT signal is converted into a voltage signal by an $I_A - V_A$ converter and amplified by a lock-in-amplifier (HR-8, PARC). The source 'S' is a 1000 watts tungsten-halogen lamp with linear filament (Osram). The colour temperature of these lamps is 2800K. The lamp is water cooled (Fig 3.4). For measurements at liquid nitrogen temperature a glass dewar was fabricated using cold finger for sample cooling. The cryostat and the sample holder are shown in Figure 3.5. The sample holder was made from a copper block and brazed to the cold finger. The dewar is fitted with 4 windows of Corning 7059 glass.

The spectral range of the monochromator from 7500 cm^{-1} to 35000 cm^{-1} is scanned in two orders. The instrument resolution is 0.5 cm^{-1}. A 25 Hz chopper and a photodiode are built in the monochromator for lock-in-detection. The

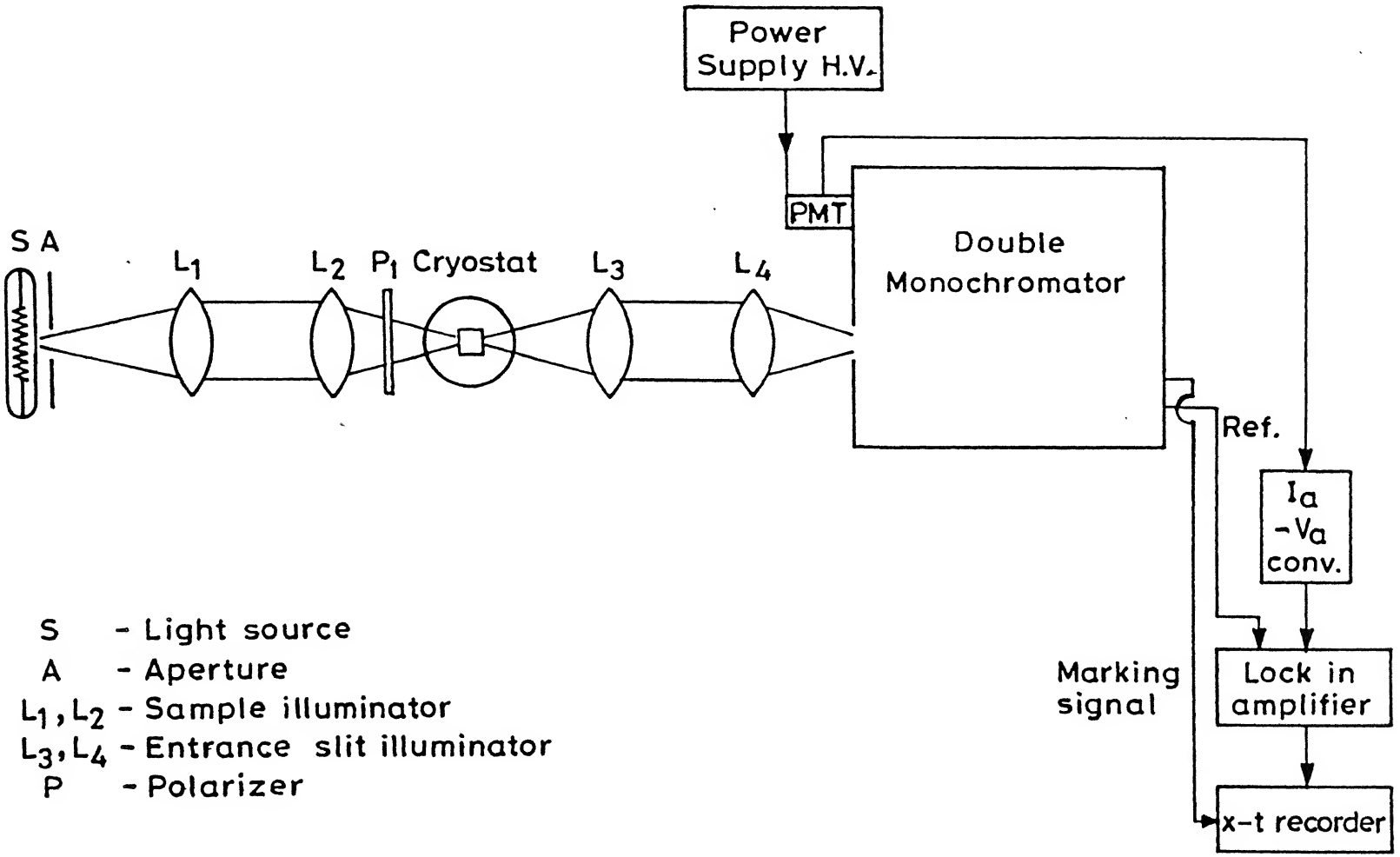

FIG.3.3 : SET-UP FOR ABSORPTION MEASUREMENT.

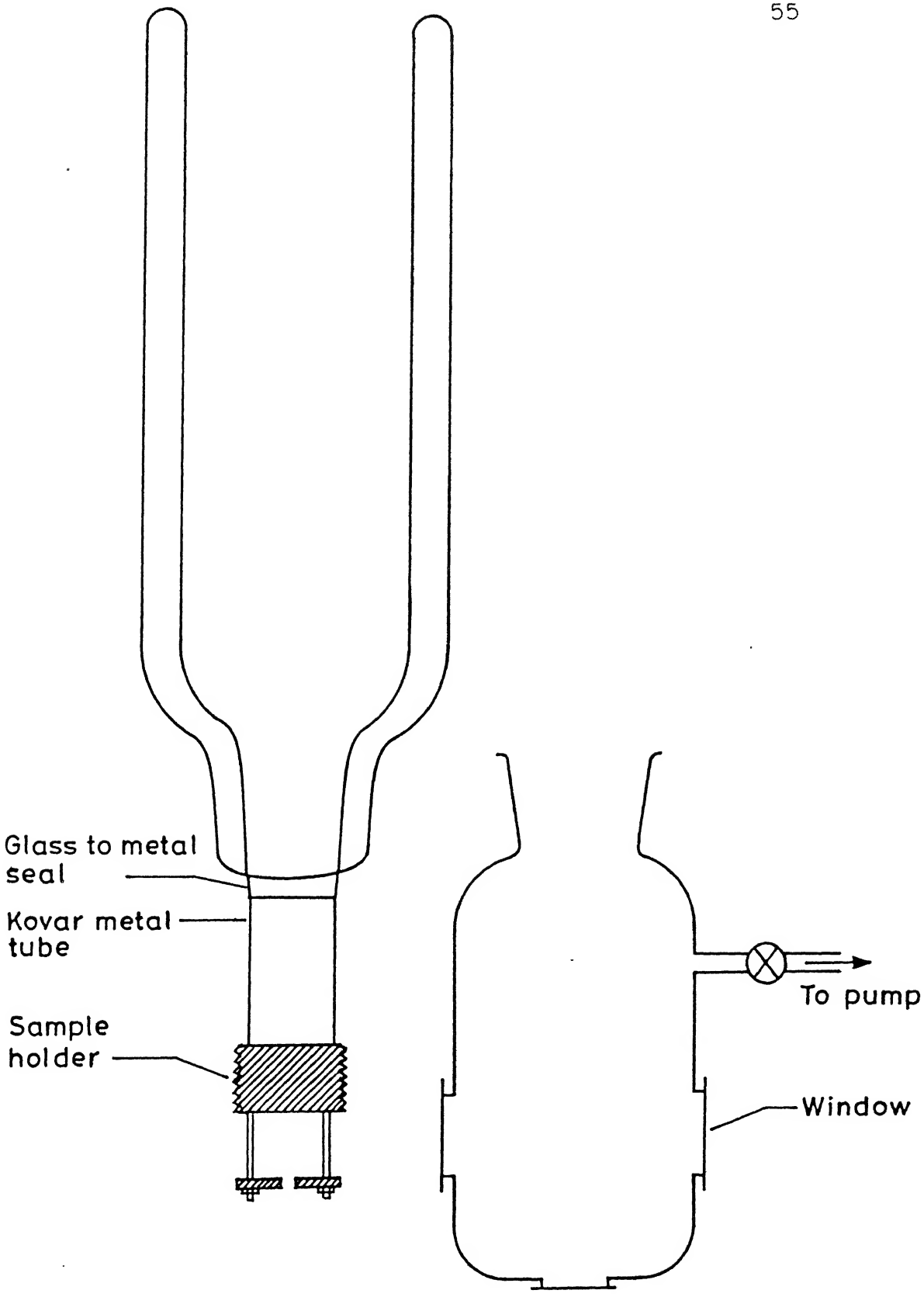

FIG.3.5 : THE CRYOSTAT AND THE SAMPLE HOLDER.

wave number read out of the monochromator was calibrated using low-pressure Hg and Ne discharges, and Ar^+ ion laser lines. Additional details of the GDM-1000 and its calibration are given in appendix II.

3.2 EXPERIMENTAL SET-UP FOR RECORDING FLUORESCENCE AND EXCITATION SPECTRA

Fig 3.6 shows schematically the arrangement used to record fluorescence and excitation spectra. In this setup, a laser beam from a Coherent ring dye laser using R6-G dye or a Coherent (Innova-100) 15-W Ar-ion laser, was incident on the sample and the emitted fluorescence was collected in the perpendicular geometry. The detection and the recording systems are identical to the absorption measurements.

To select σ and π polarizations a sheet polarizer was used. In order to compensate for the polarization characteristics of the monochromator, the spectral profile of the tungsten-halogen lamp was recorded by inserting the sheet polarizer between the lamp and the entrance slit of the monochromator. The lamp profiles were recorded with the sheet kept in σ and π positions and the necessary correction factors (I_π/I_σ) were obtained in the region of our interest. Fig 3.7 shows the σ-polarized, π-polarized and unpolarized lamp profiles, and Fig 3.8 shows the dependence of the correction factors (I_π/I_σ) on wave number. The experimental data for these plots are listed in appendix II.

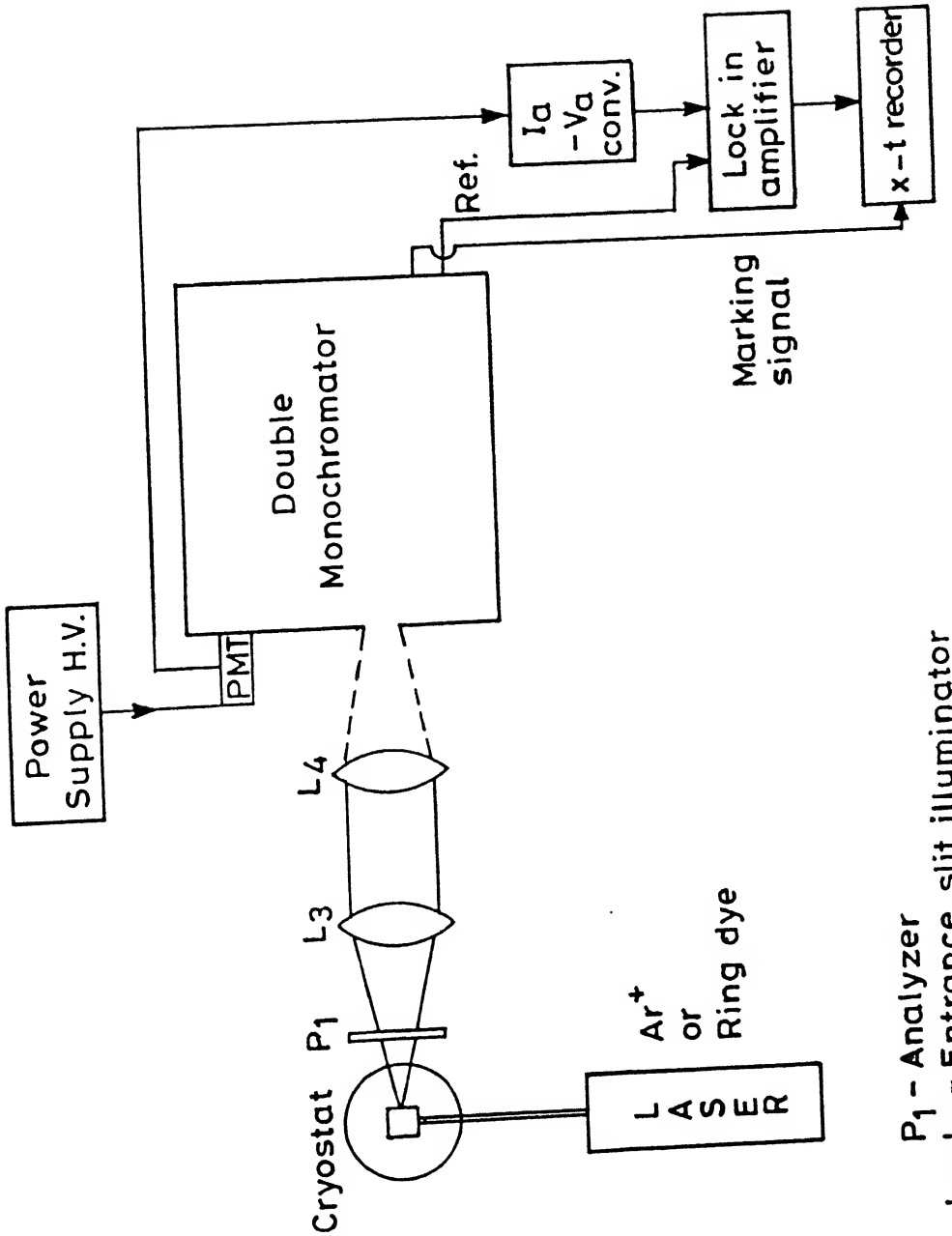

FIG.3.6 : SET-UP FOR FLUORESCENCE MEASUREMENTS.

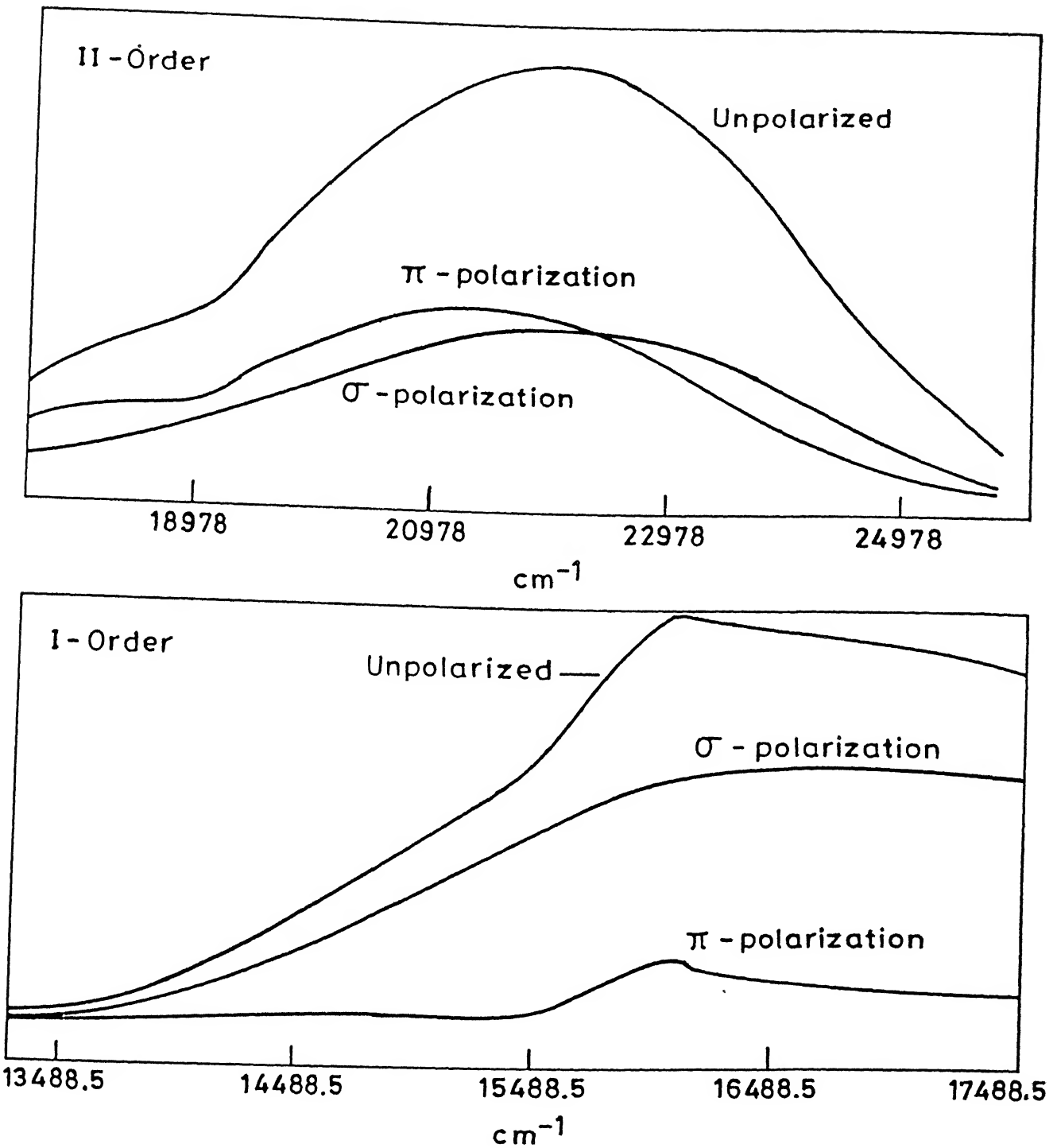

FIG.3.7 : RESPONSE OF 'GDM-1000' TO POLARIZED LIGHT.

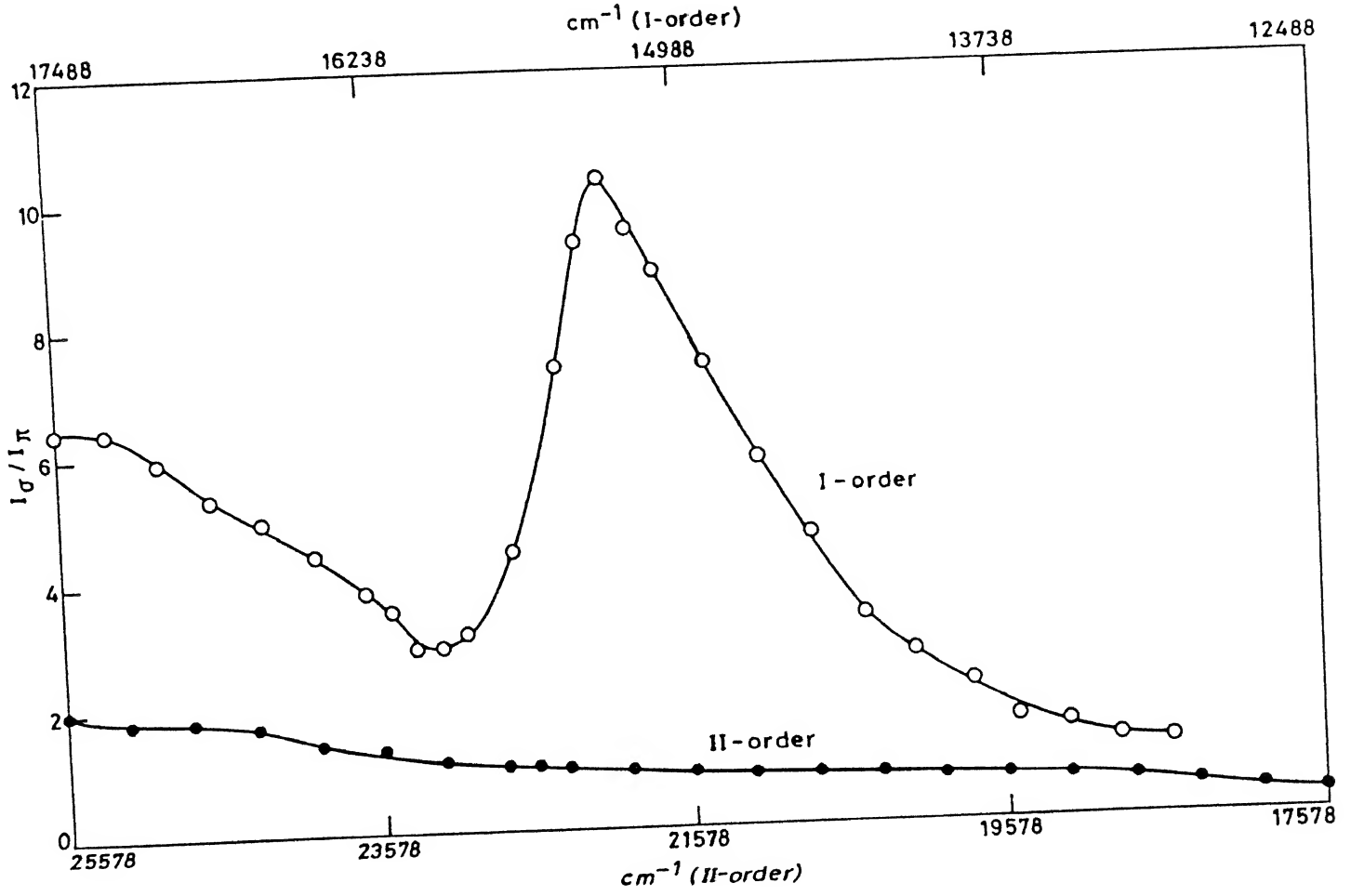

FIG.3.8 : PLOT OF THE POLARIZATION CORRECTION FACTOR (I_σ/I_π).

4. EXPERIMENTAL DATA

In this section, we present experimental data as obtained from absorption, fluorescence and excitation spectra. The wave numbers corresponding to the peak positions of spectral lines were measured from the chart recording with reference to the positions of marking signals and corrected for monochromator calibration. The accuracy of measurement of the peak positions is within ± 1 cm^{-1} for sharp lines and within ± 2 to ± 5 for broad and weak lines. The wave number assignments were found to be always reproducible and were within this precision. The experimental parameters and conditions such as slit-width, and the sample orientation with respect to the incident radiation and the direction of observation were identical for σ and π polarized spectra for any given group of transitions. Though we have tried our best to keep these conditions the same for recording the axial spectra as well, some departures are expected as the sample had to be physically rotated and because the axial spectra were usually recorded on different days. The sample temperature was slightly higher than the liquid nitrogen temperature because it was not in direct contact with the liquid nitrogen. This may affect the results because spectral line positions in the $LiYF_4:Eu^{3+}$ are temperature dependent. In fact, absorption spectral lines at room

temperature are shifted upto 7 cm^{-1} from those at liquid nitrogen temperature.

4.1 THE ABSORPTION DATA

The transverse and axial absorption spectra of $LiYF_4:Eu^{3+}$ were recorded at liquid nitrogen temperature in the spectral region 18500 cm^{-1} to 25500 cm^{-1}. The absorption spectra are reproduced in Fig 3.9 to Fig 3.12. We could not see any absorption corresponding to ^7F_o-^5D_o and ^7F_o-$^5D_3$ transitions in the regions 17200-17300 cm^{-1} and 24000 cm^{-1}-24500 cm^{-1} respectively. A slit width of 70μ and a scanning speed of 20 cm^{-1}/min were used for these measurements. Measured wave-number position of lines after correcting for the monochromator error are tabulated in Table 3.4.

4.2 FLUORESCENCE DATA

Information on the low lying energy levels can not be obtained from the absorption spectra. Fluorescence spectra maps the energy levels below the excited levels. Fluorescence spectra of the sample were recorded at liquid nitrogen temperature in the transverse and axial sample orientations. For recording the transverse spectra, the sample was excited along the c-axis and the observations were made along one of the a-axes, while for the axial spectra, excitation was done along an a-axis and observations were made along the c-axis. The slit width ranging

from 50 to 200μ was used depending upon the strength of the fluorescence of various groups of transitions. Commonly used scan speed was 4 cm^{-1}/min in 2^{nd} order and 2 cm^{-1}/min in the 1^{st} order. The sample fluoresces when irradiated with any of the Ar^+ laser lines, but the fluorescence is strongest for the excitation at 457.9 nm. We have recorded the fluorescence with the 457.9 nm and with the 514.5 nm lines of the Ar^+ ion laser. The 457.9 nm excitation gives fluorescence from $^5D_2$, $^5D_1$ and ^5D_o excited levels while the 514.5 nm produces fluorescence from the $^5D_1$ and ^5D_o levels only. To excite the ^5D_o level exclusively we used the R6-G dye laser lasing at 16938 cm^{-1} and 17630 cm^{-1}. The resonance excitation of ^5D_o at 17271 cm^{-1} is extremely weak as the ^7F_o-^5D_o direct transition is highly forbidden. To excitation of ^5D_o level by the 17640 cm^{-1} line of the dye laser is phonon assisted while excitation by the 16938 cm^{-1} line corresponds to the $^7F_1$-^5D_o transition indicating enough population of the $^7F_1$ level even at liquid nitrogen temperature. The fluorescence spectra are reproduced in Fig 3.13 through Fig 3.28. Tables 3.5, 3.6 and 3.7 list the observed line positions for 457.9 nm, 514.5 nm and R6-G excitations respectively. The lines marked 'r' and v are Raman and vibronic transitions respectively. The lines with marks 'a', 'b' and 'c' are unidentified, Hg-lines and Ar^+ - lines respectively.

4.3 EXCITATION DATA

We have not made a detailed study of the excitation spectra. Whatever measurements were made in this respect helped us to identify the interfering vibronic lines. They also helped us in ascertaining the position of the ^5D_o level of Eu^{3+} indirectly. To obtain the excitation spectra we monitored the ^5D_o-$^7F_1$ fluorescence at 16840 cm^{-1} and scanned the R6-G dye laser. The peak intensity of the fluorescence signal was plotted with respect to the birefringent micrometer reading which was then calibrated in wave numbers. This calibration is rather inaccurate with a maximum error of ± 6 cm^{-1}. The excitation spectra are reproduced in Fig 3.29 to Fig 3.32. Table 3.8 gives the position of the excitation peaks with the reported phonon-modes of $LiYF_4$ pure crystal [6]. Fig 3.33 reproduces the micrometer calibration curve.

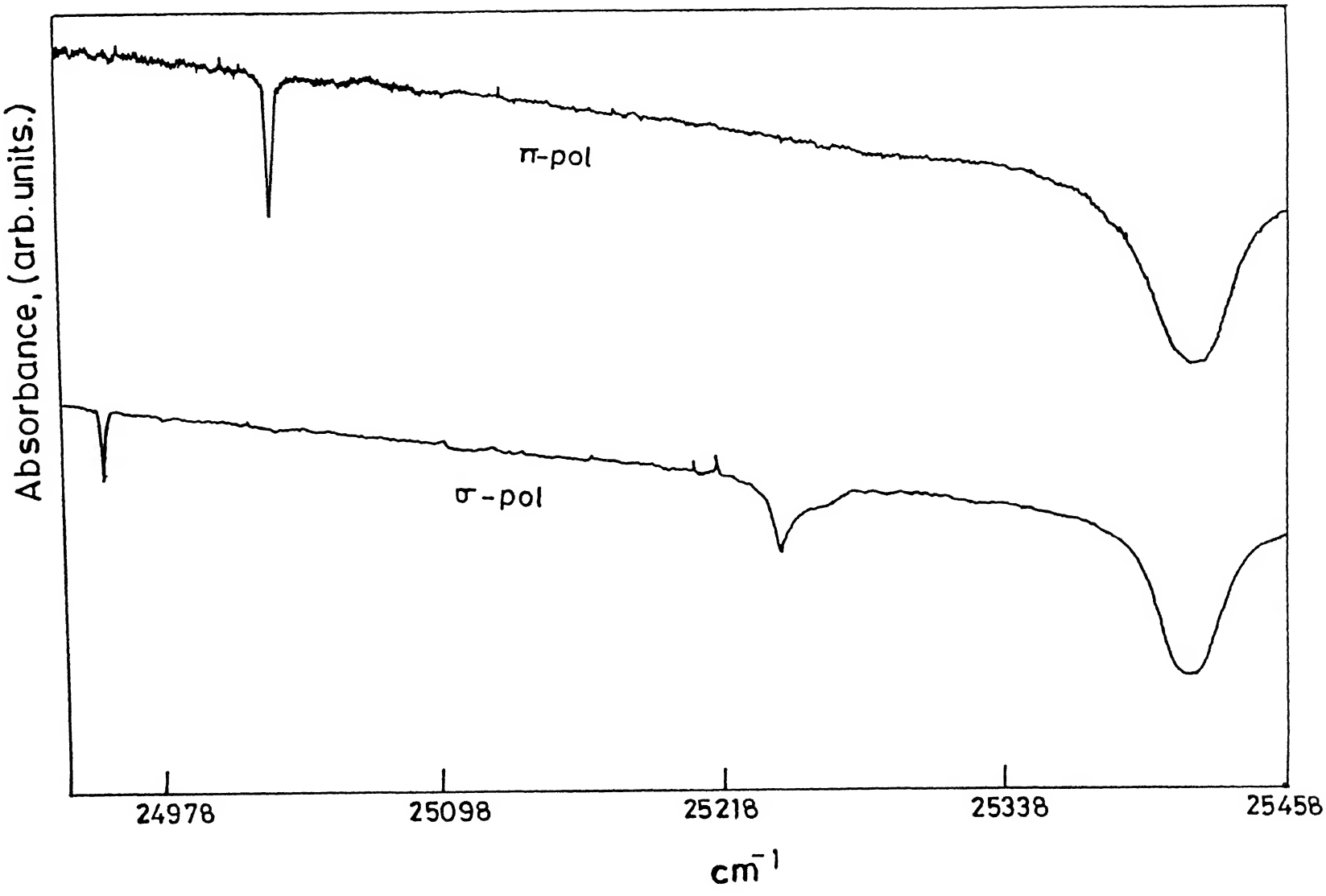

FIG.3.9 : ^7F_o-$^5L_6$ TRANSVERSE ABSORPTION SPECTRUM OF $LiYF_4:Eu^{3+}$ AT LIQUID N_2 TEMPERATURE.
(The cm^{-1} scale is without calibration correction)

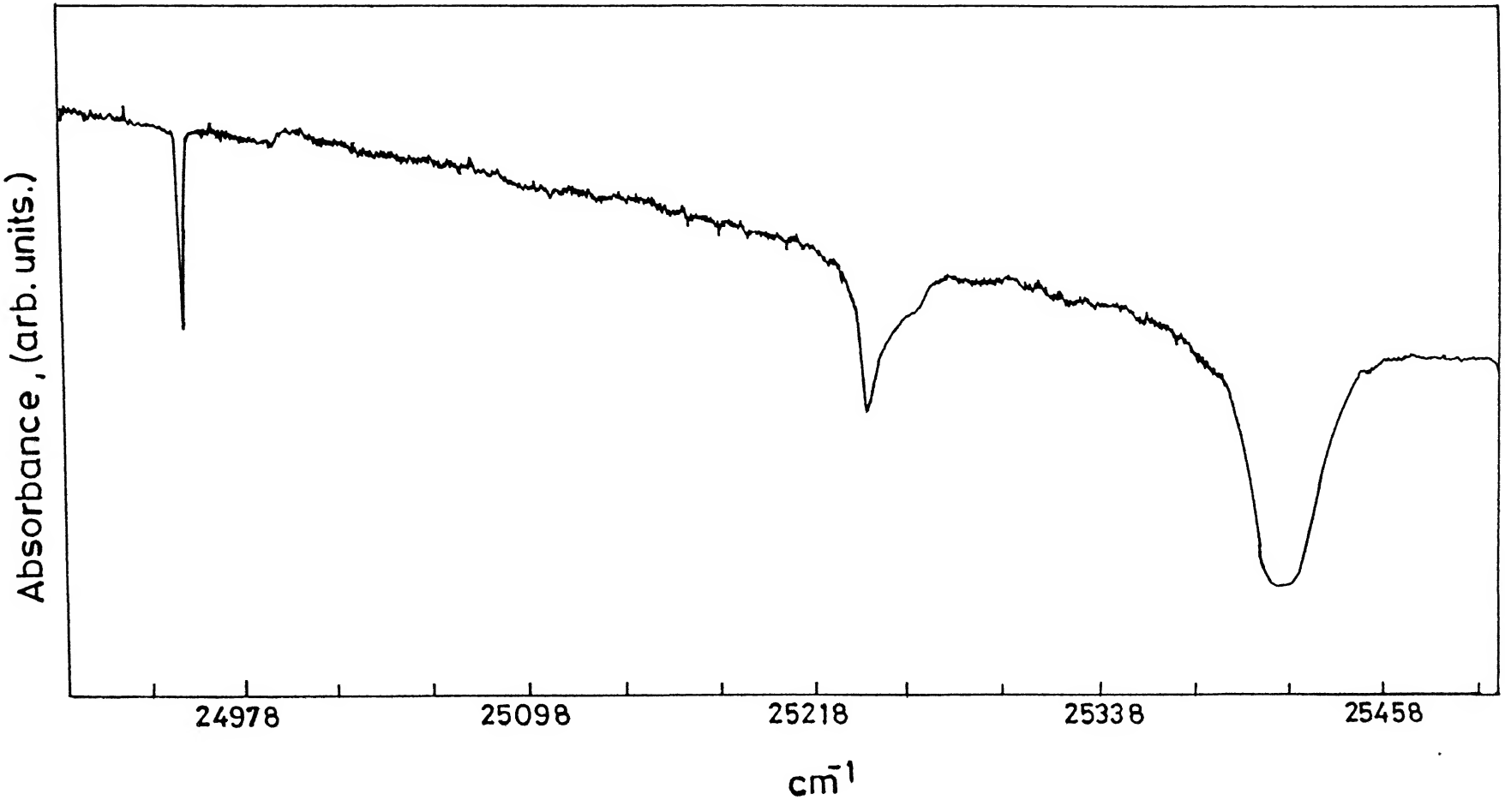

FIG.3.10: $^7F_o - ^5L_6$ AXIAL ABSORPTION SPECTRUM OF $LiYF_4:Eu^{3+}$ AT LIQUID N_2 TEMPERATURE.
(The cm^{-1} scale is without calibration correction)

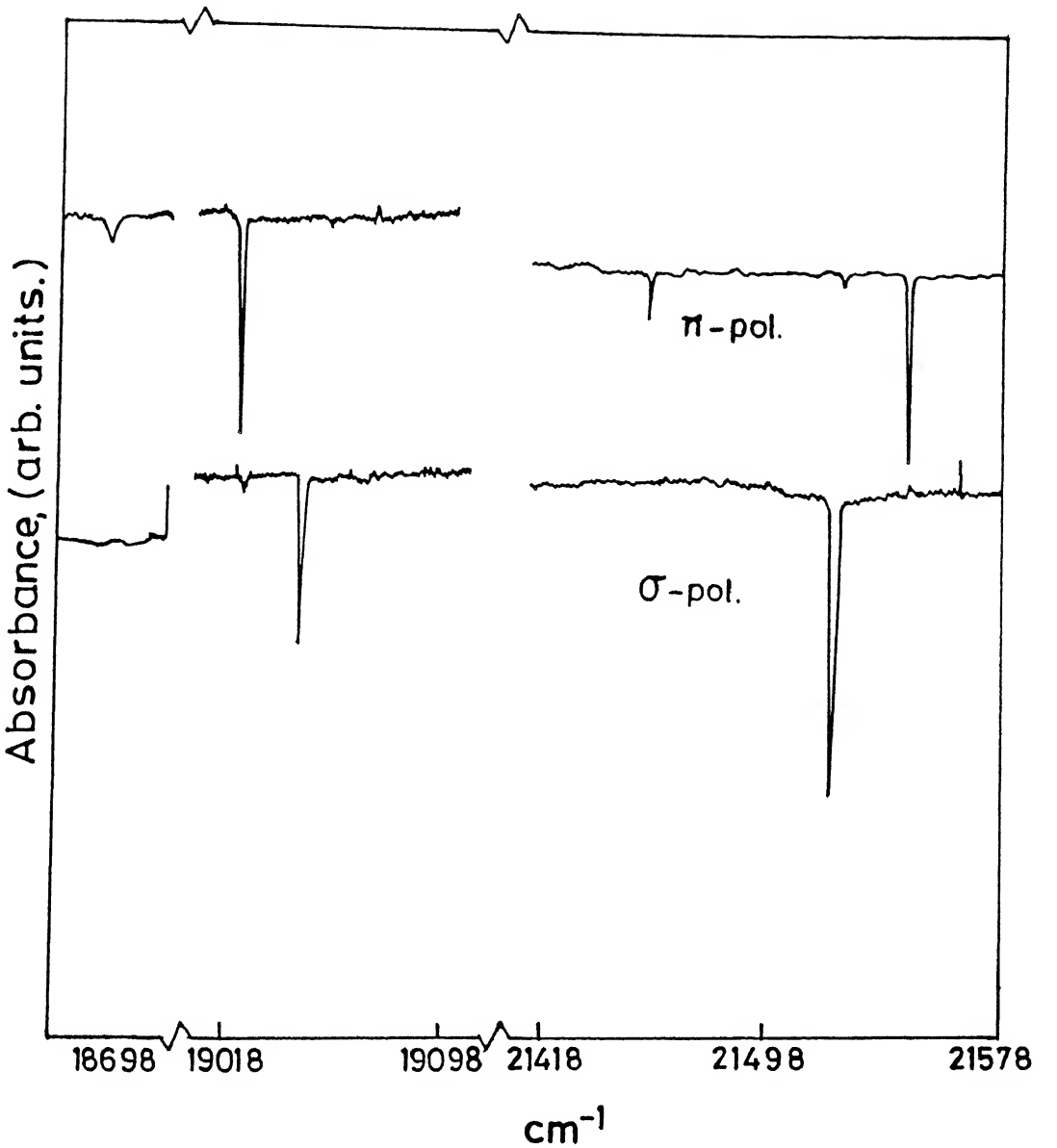

Fig.3.11 : $^7F_1$-^5D_o, ^7F_o-$^5D_1$ AND ^7F_o-$^5D_2$ TRANSVERSE ABSORPTION SPECTRA OF $LiYF_4$:Eu^{3+} AT LIQUID N_2 TEMPERATURE (The cm^{-1} scale is without calibration correction)

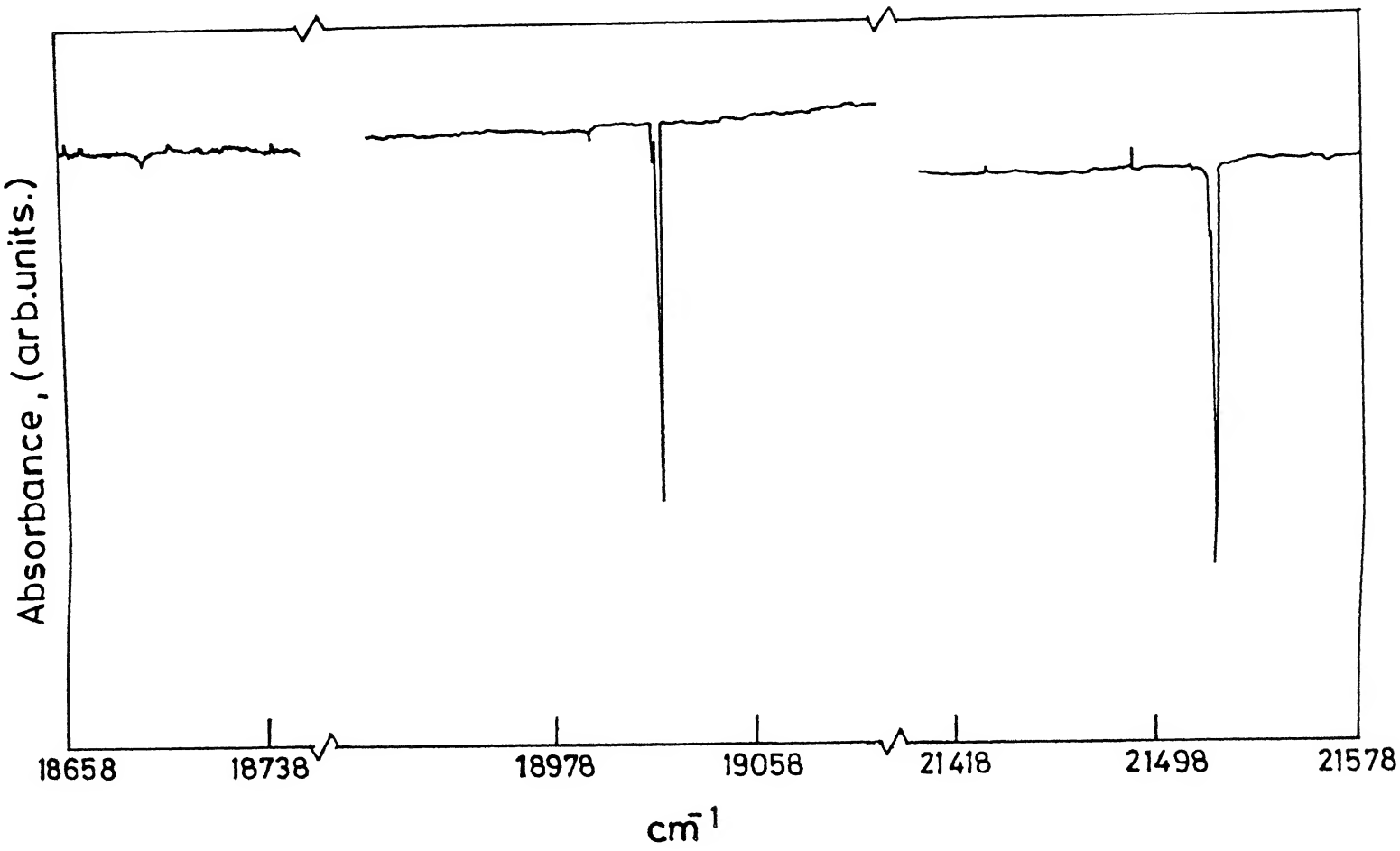

FIG.3.12 : $^7F_1$-^5D_o, ^7F_o-$^5D_1$ AND ^7F_o-$^5D_2$ AXIAL ABSORPTION SPECTRA OF $LiYF_4:Eu^{3+}$ AT LIQUID N_2 TEMPERATURE (The cm^{-1} scale is without calibration correction)

TABLE 3.4

ABSORPTION DATA FOR Eu^{3+} IN $LiYF_4$ AT LIQUID NITROGEN TEMPERATURE

SNo.	Line Position (cm^{-1})	FWHM (cm^{-1})	Relative Intensity (arbitrary units)			Transition Mech.	S_4-Symmetry assignment	Transition
			I_σ	I_π	I_{ax}			
1.	25416	34	189	141	284	πE σE	$\Gamma_1-\Gamma_2(2)$ $\Gamma_1-\Gamma_3(3)$	$^7F_o - {}^5L_6$
2.	25258[a]	12	17	0	16	-	-	-
3.	25241	14	29	0	50	σE	$\Gamma_1-\Gamma_3(2)$	$^7F_o - {}^5L_6$
4.	25027	4	0	17	0	πE	$\Gamma_1-\Gamma_2(1)$	$^7F_o - {}^5L_6$
5	24953	3	5.0	0	8.0	σE	$\Gamma_1-\Gamma_3(1)$	$^7F_o - {}^5L_6$
6.	21543	3	0	13	0	πE	$\Gamma_1-\Gamma_2(2)$	$^7F_o - {}^5D_2$
7.	21520	3	14	0	16	σE	$\Gamma_1-\Gamma_3$	$^7F_o - {}^5D_2$
8.	21518[s,a]	-	-	-	-	-	-	-
9.	21450	3	0	4	0	πE	$\Gamma_1-\Gamma_2(1)$	$^7F_o - {}^5D_1$
10.	19043	2	6.0	0	0	σM	$\Gamma_1-\Gamma_1$	$^7F_o - {}^5D_1$
11.	19042[s,a]	-	-	-	-	-	-	-
12.	19021	2	0	7.0	7.0	πM	$\Gamma_1-\Gamma_3$	$^7F_o - {}^5D_1$
13.	19019[s,a]	-	-	-	-	-	-	-
14.	18694[a]	B	0	3	-	-	-	-
15.	18684	4	0	4	3	πE	$\Gamma_3-\Gamma_3$	$^7F_1 - {}^5D_1$

a - refers to unidentified line

s - refers to weak shoulder

B - refers to broad and weak line

π and σ indicate whether the electric vector of the radiation is $\parallel$ or $\perp$ to the $\bar{c}$ crystal axis respectively.

E and M indicate electric dipole and magnetic dipole transitions.

-x-

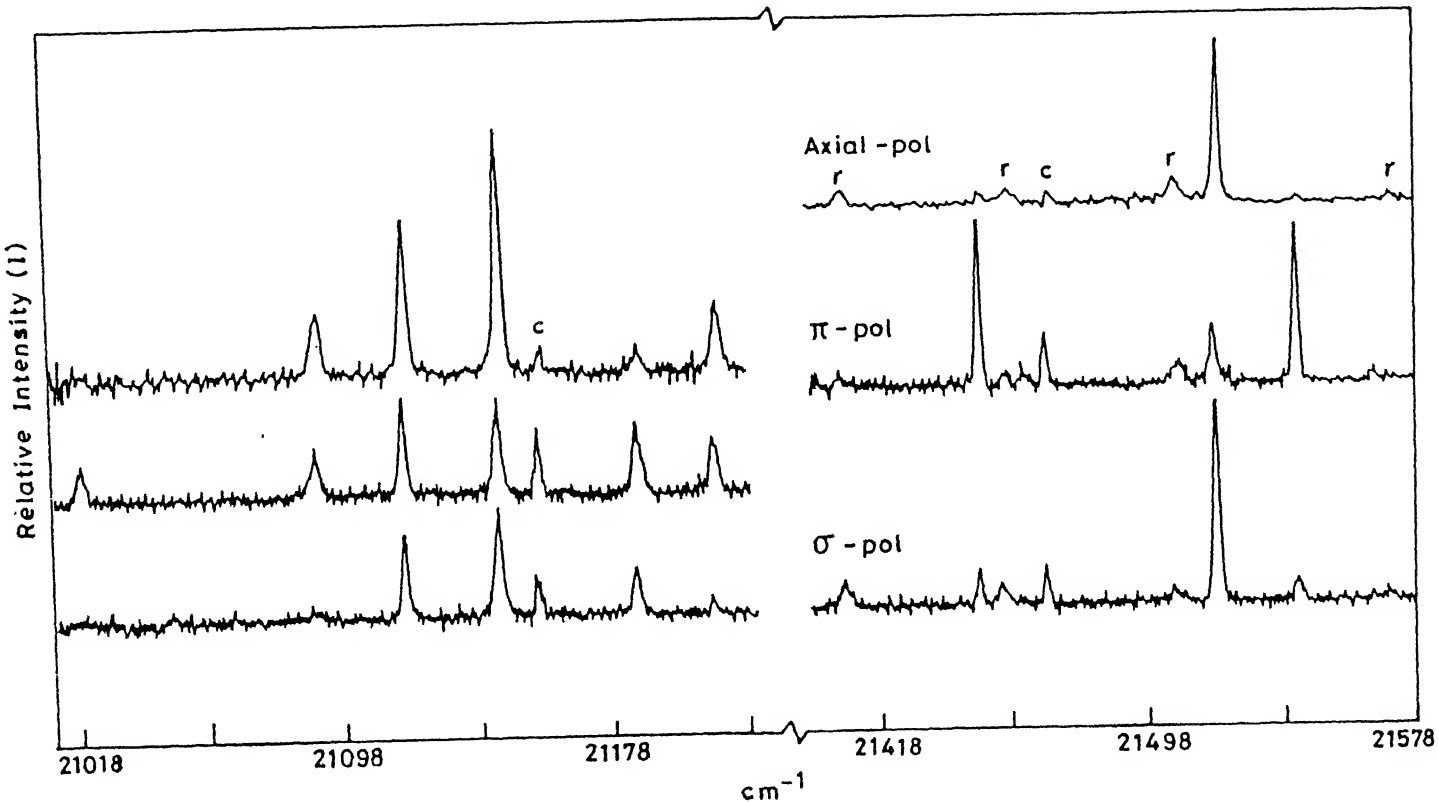

FIG.3.13 : $^5D_2$-^7F_o AND $^5D_2$-$^7F_1$ FLUORESCENCE OF $LiYF_4:Eu^{3+}$ AT LIQUID N_2 TEMPERATURE
(r and c indicate Raman lines and Ar^+ lines respectively; The cm^{-1} scale is without calibration correction)

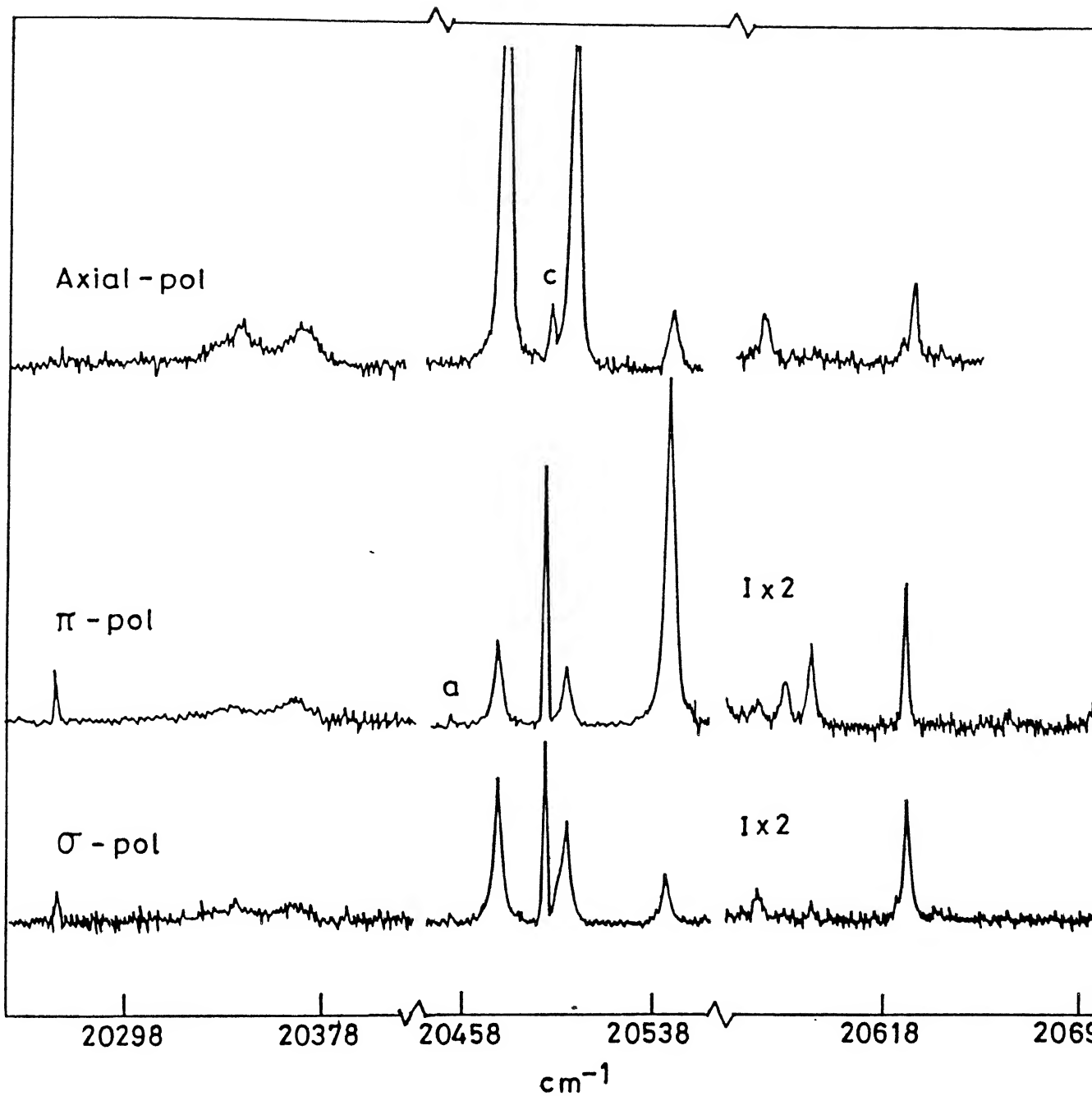

FIG.3.14 : $^5D_2$-$^7F_2$ FLUORESCENCE OF $LiYF_4$:Eu^{3+} AT LIQUID N_2 TEMPERATURE
(a and c indicate unidentified and Ar^+ lines respectively; The cm^{-1} scale is without calibration correction)

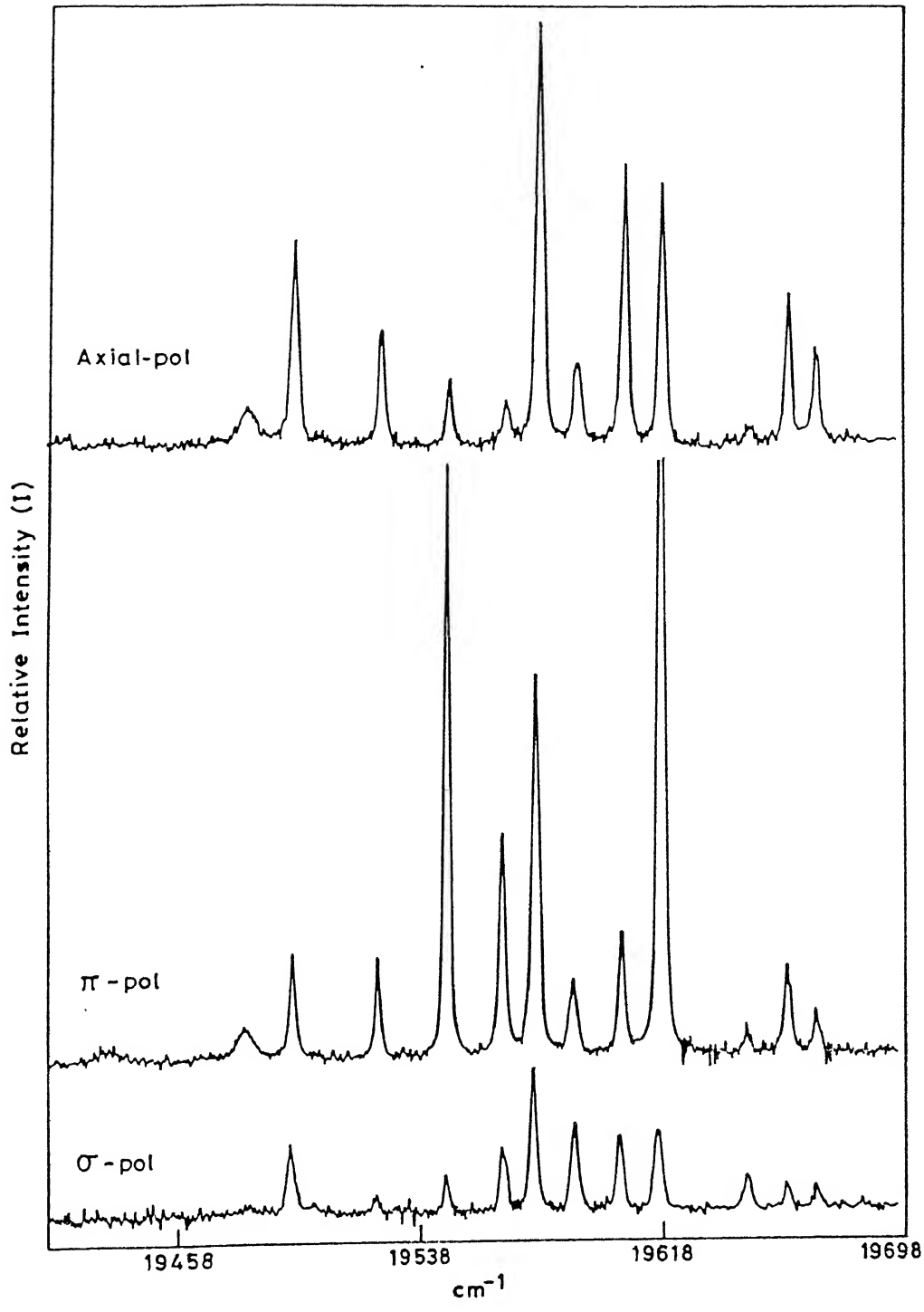

FIG.3.15 : $^5D_2$-$^7F_3$ FLUORESCENCE OF $LiYF_4:Eu^{3+}$ AT LIQUID N_2 TEMPERATURE
(The cm^{-1} scale is without calibration correction)

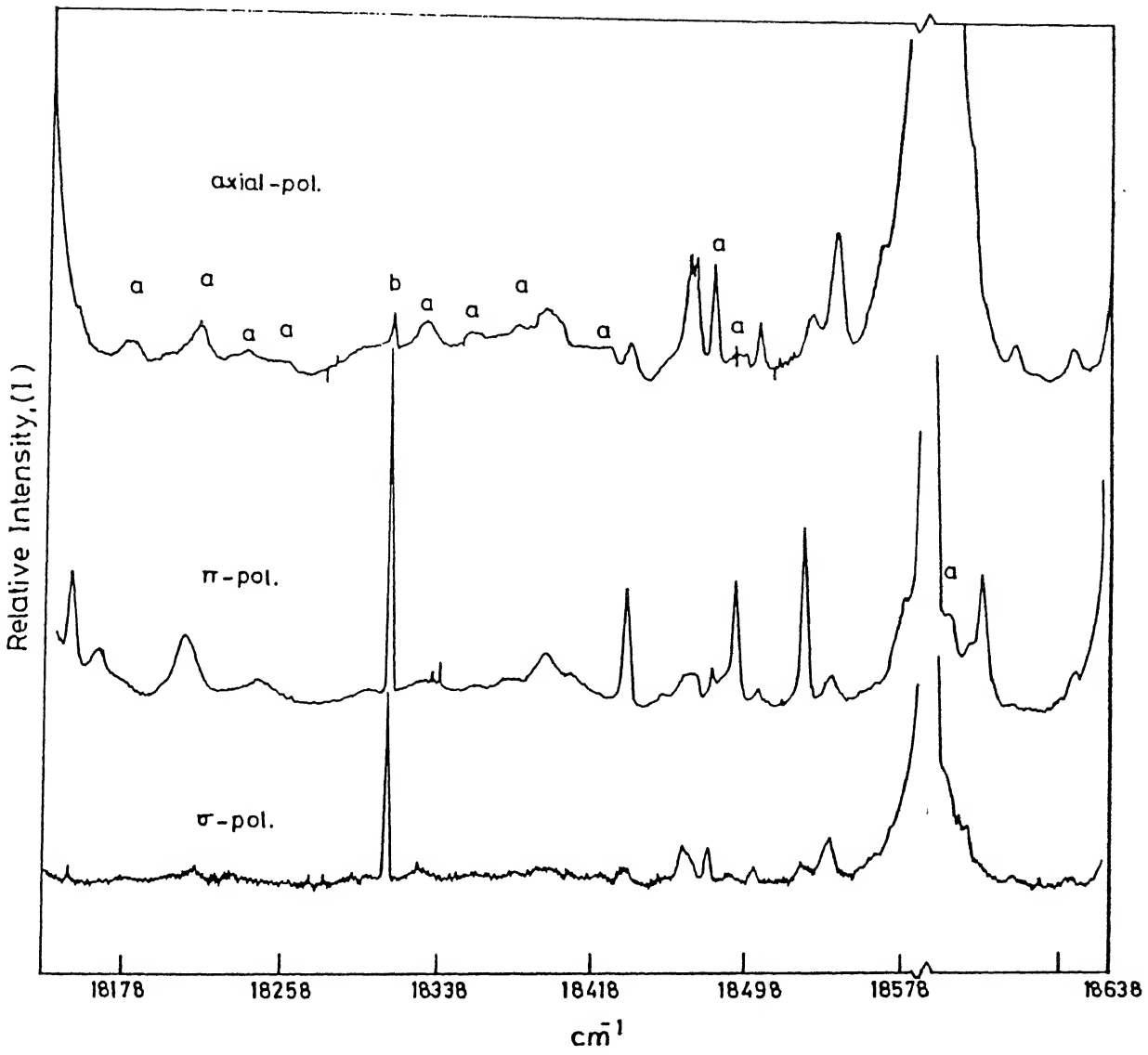

FIG.3.16 : $^5D_2$-$^7F_4$ FLUORESCENCE OF $LiYF_4:Eu^{3+}$ AT LIQUID N_2 TEMPERATURE
(a and b indicate unidentified and Hg-lines respectively; The cm^{-1} scale is without calibration correction)

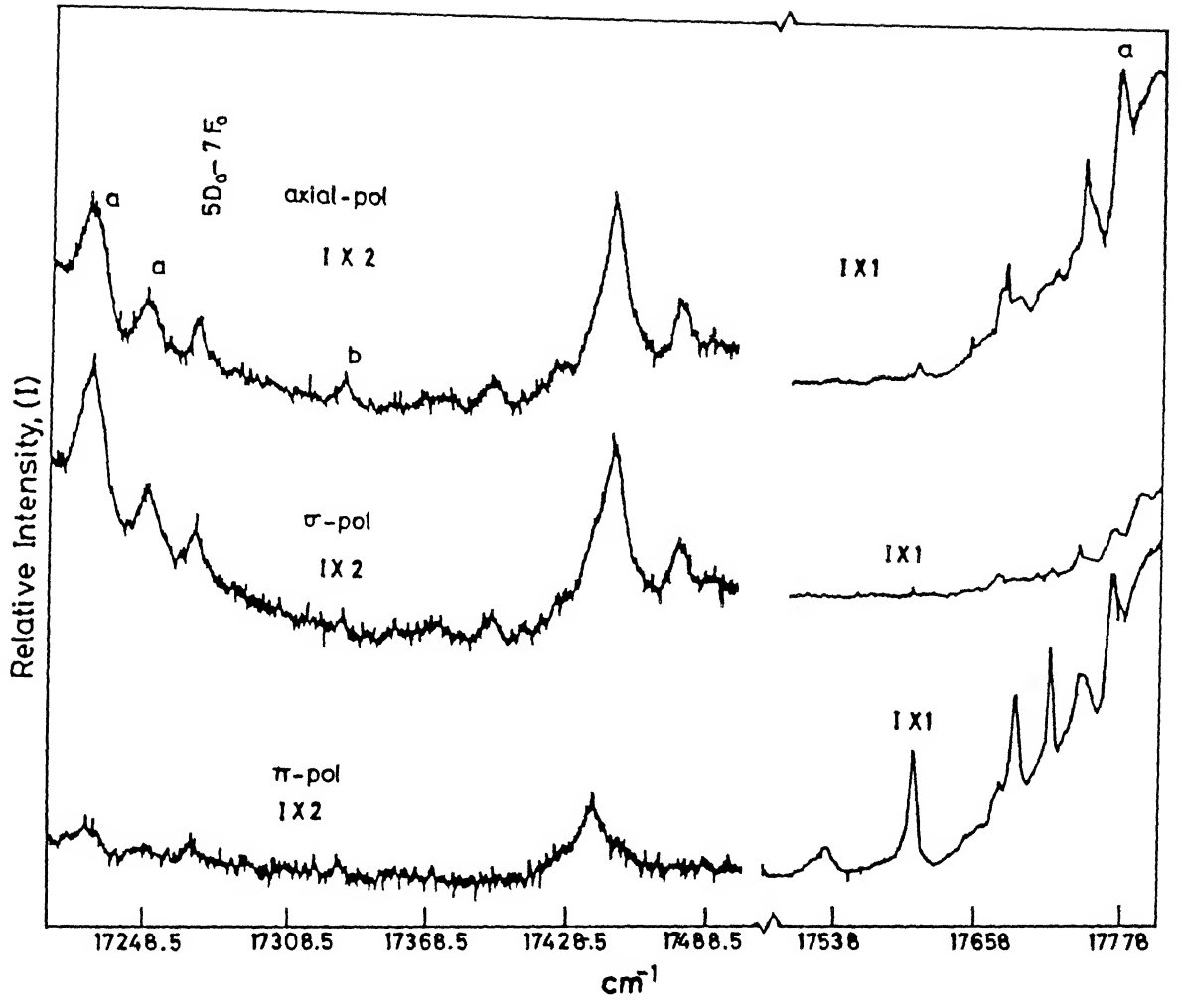

FIG.3.17 : $^5D_2-^7F_5$ FLUORESCENCE OF $LiYF_4:Eu^{3+}$ AT LIQUID N_2 TEMPERATURE
(a and b indicate unidentified and Hg-lines respectively; The cm^{-1} scale is without calibration correction)

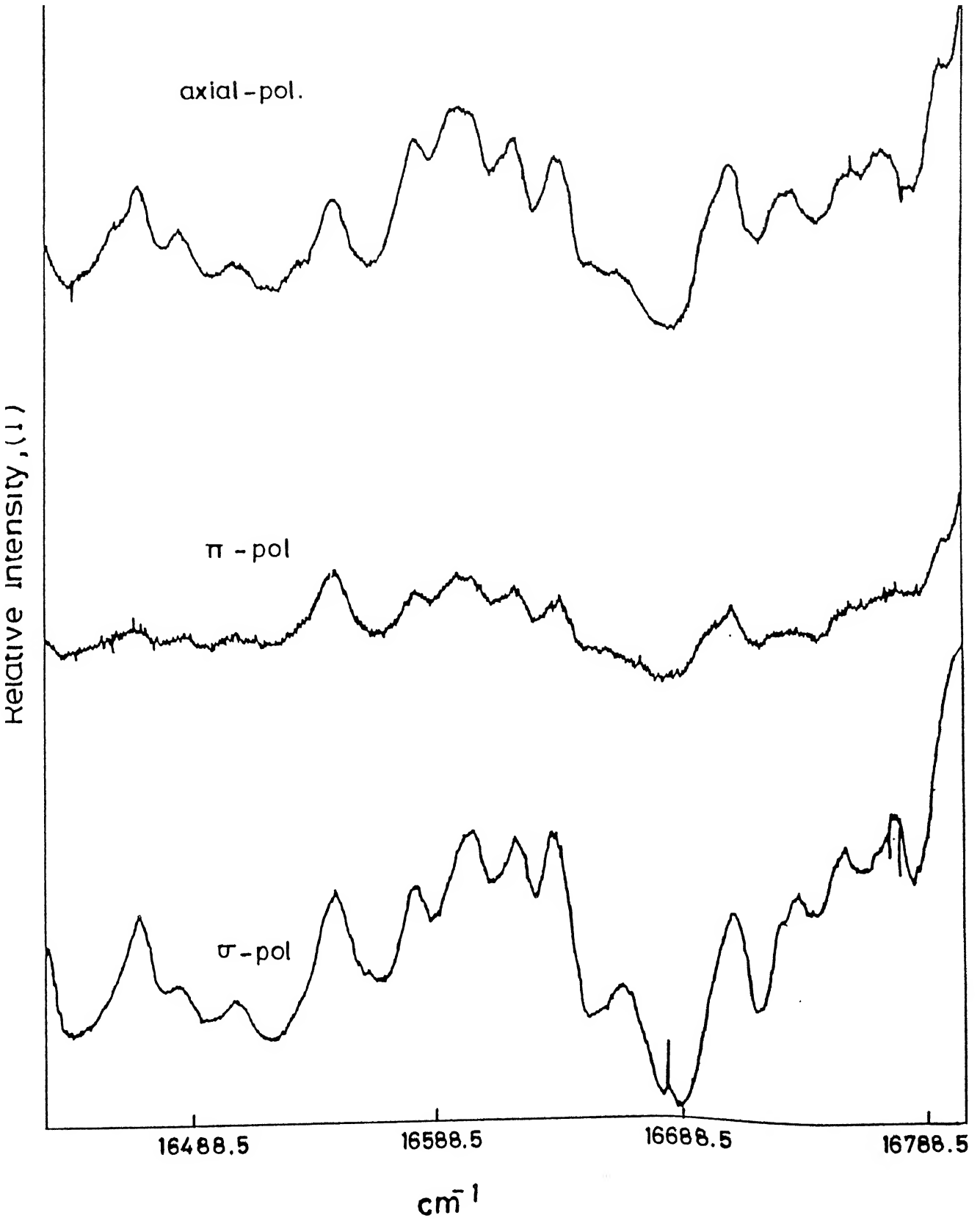

FIG.3.18 : $^5D_2$-$^7F_6$ FLUORESCENCE OF $LiYF_4:Eu^{3+}$ AT LIQUID N_2 TEMPERATURE
(This group has not been analyzed; The cm^{-1} scale is without calibration correction)

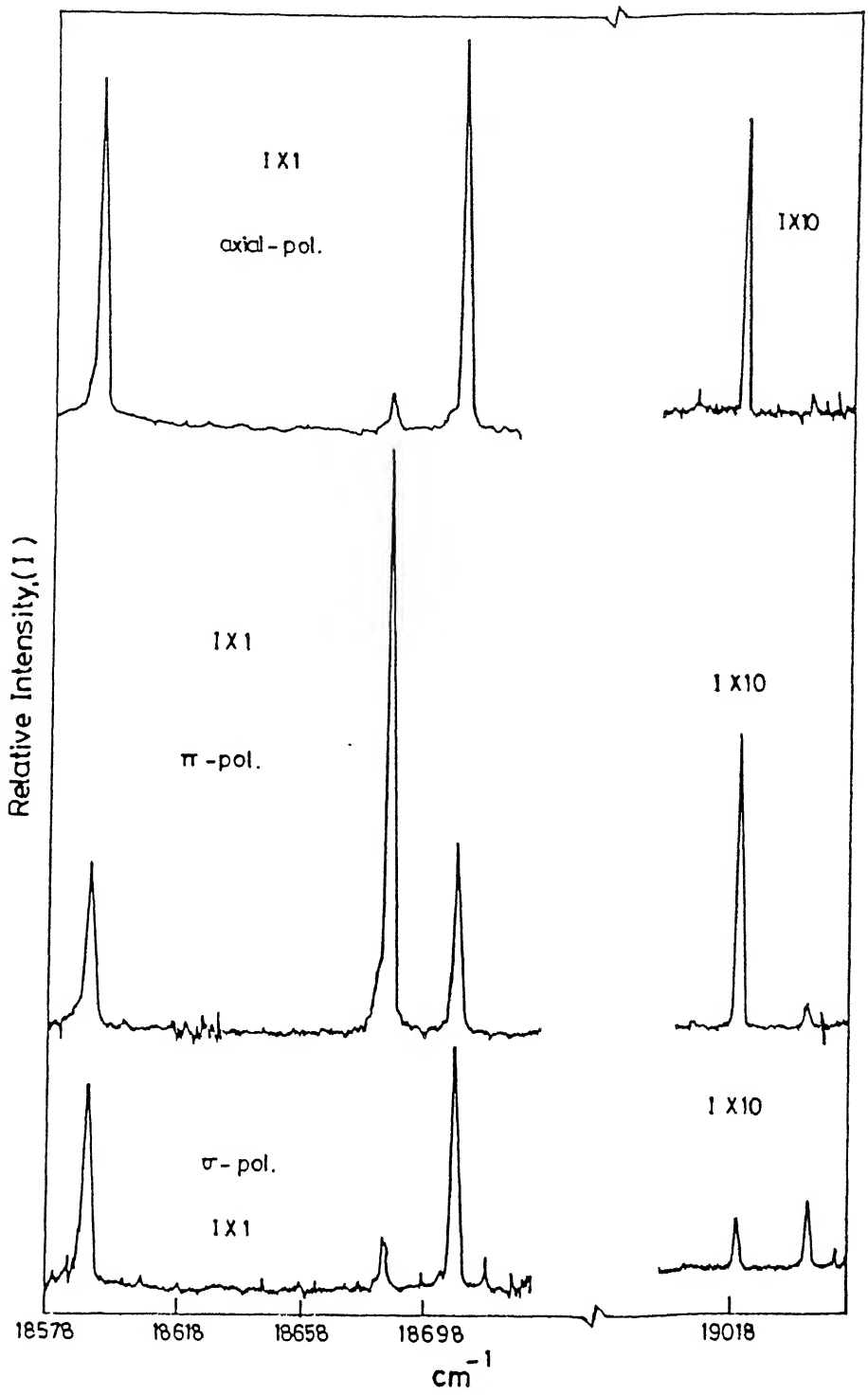

FIG.3.19 : $^5D_1-^7F_0$ AND $^5D_1-^7F_1$ FLUORESCENCE OF $LiYF_4:Eu^{3+}$ AT LIQUID N_2 TEMPERATURE
(The cm^{-1} scale is without calibration correction)

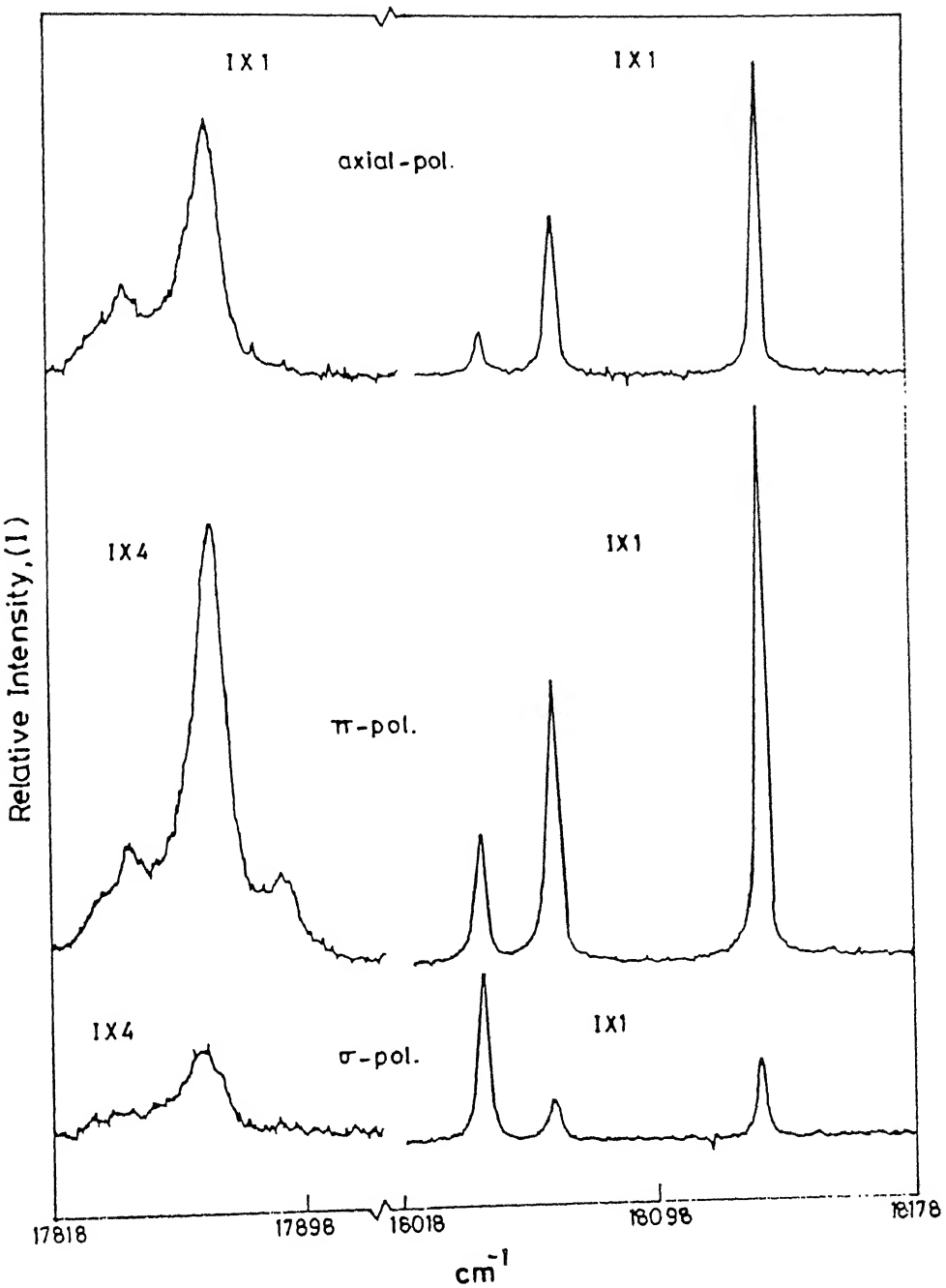

FIG.3.20 : $^5D_1$-$^7F_2$ FLUORESCENCE OF $LiYF_4:Eu^{3+}$ AT LIQUID N_2 TEMPERATURE
(The cm^{-1} scale is without calibration correction)

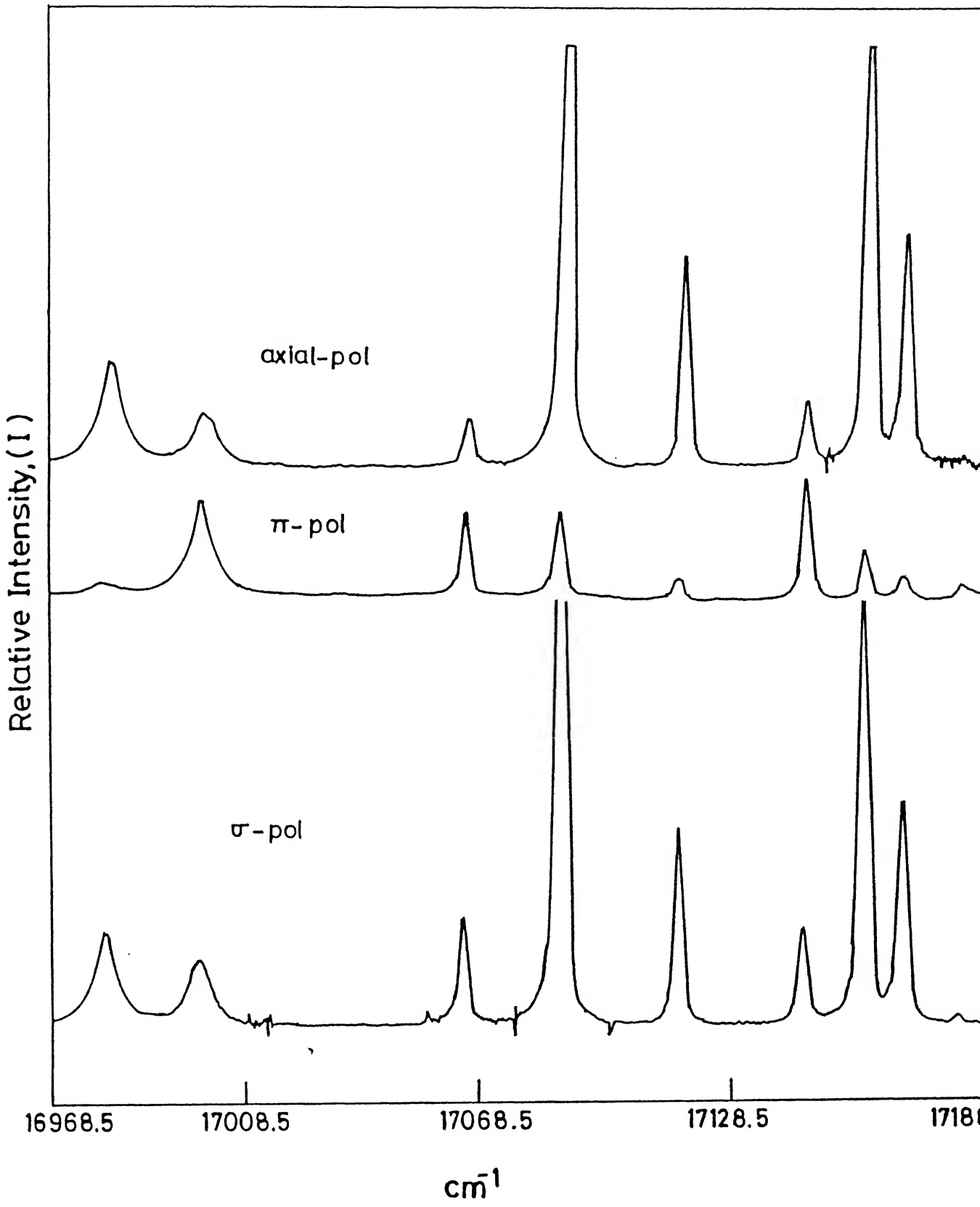

FIG.3.21 : $^5D_1$-$^7F_3$ FLUORESCENCE OF $LiYF_4:Eu^{3+}$ AT LIQUID N_2 TEMPERATURE
(The cm^{-1} scale is without calibration correction)

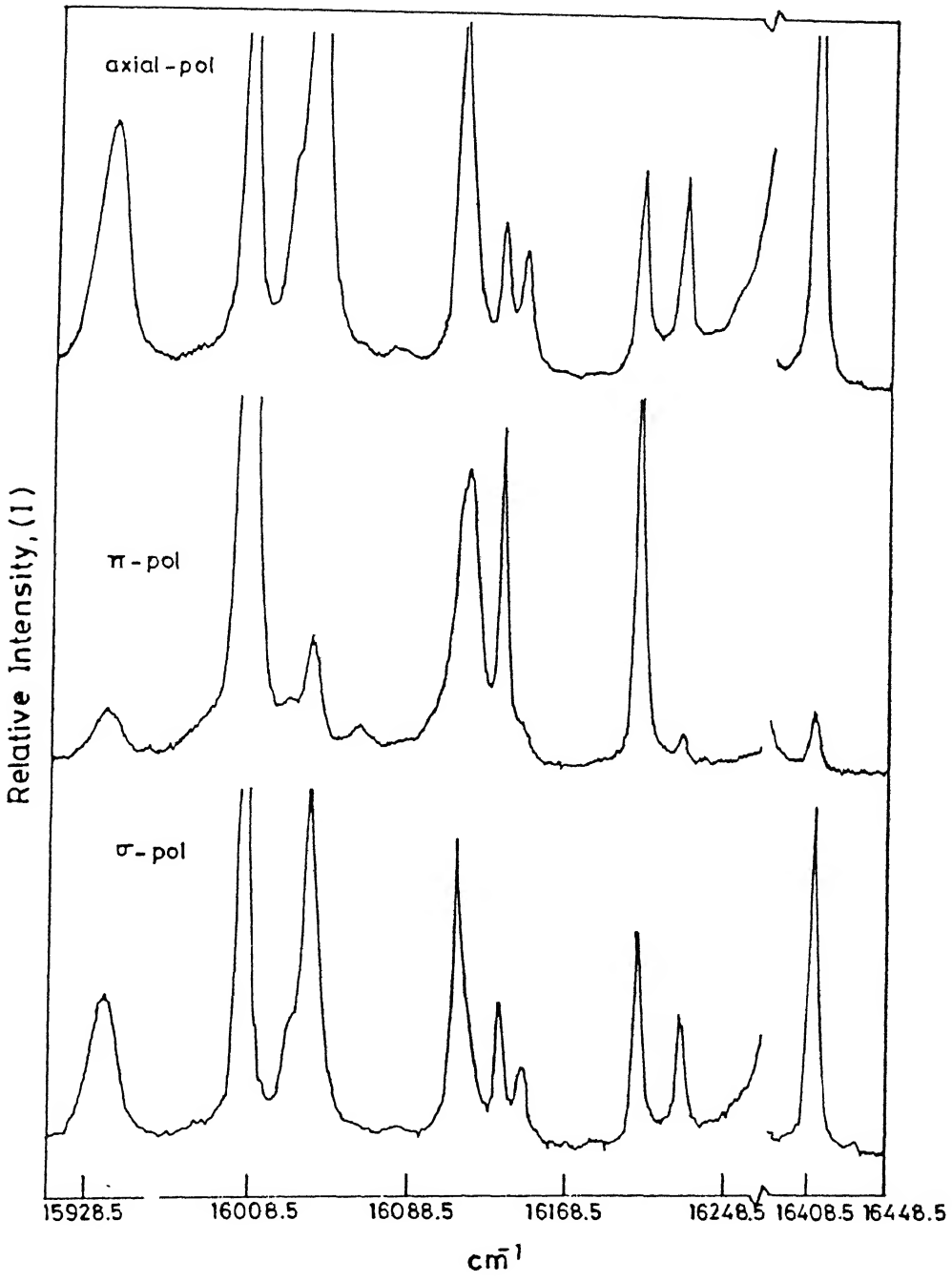

FIG.3.22 : $^5D_1$-$^7F_4$ FLUORESCENCE OF $LiYF_4:Eu^{3+}$ AT LIQUID N_2 TEMPERATURE
(The cm^{-1} scale is without calibration correction)

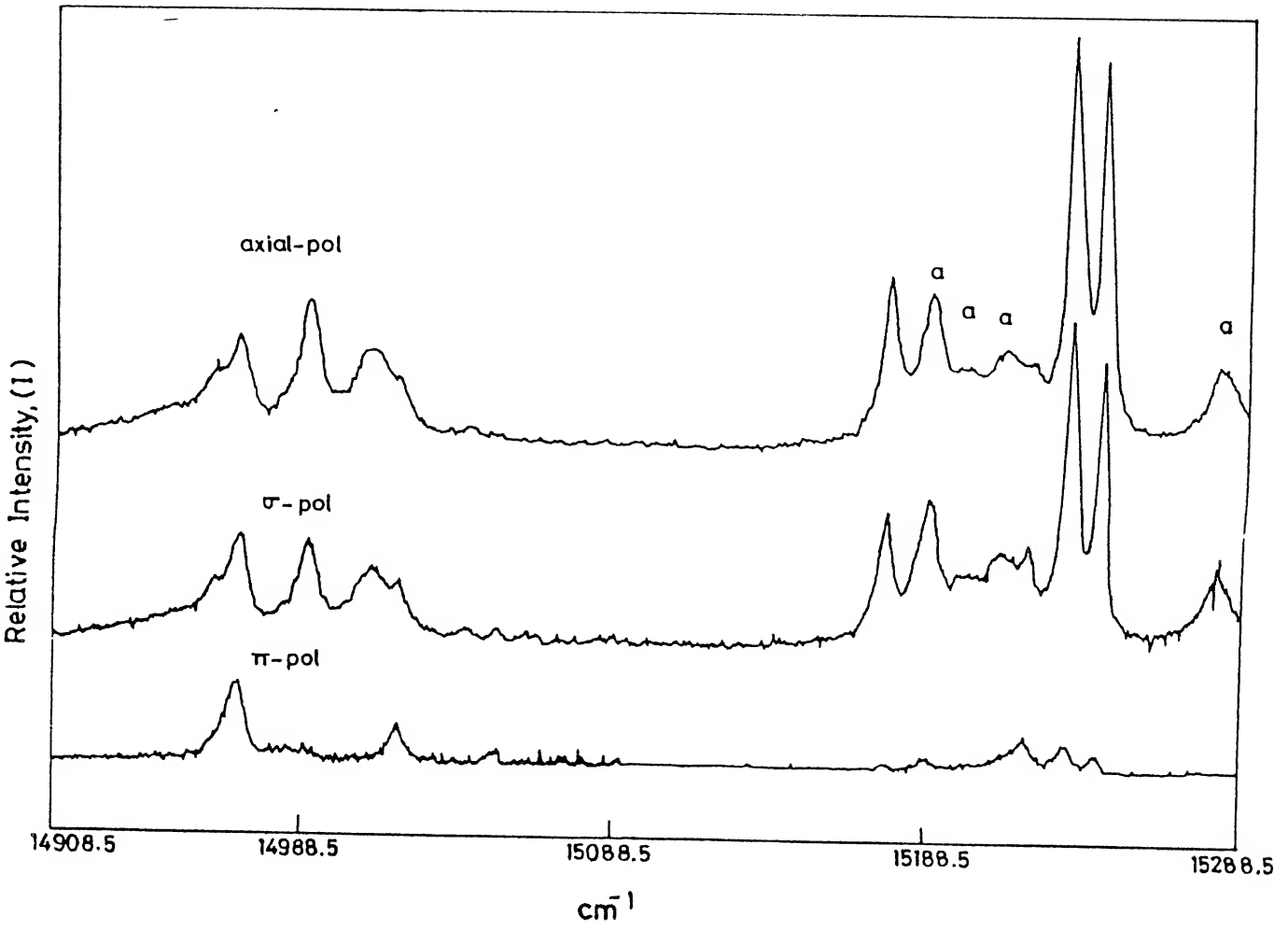

FIG.3.23 : $^5D_1$-$^7F_5$ FLUORESCENCE OF $LiYF_4:Eu^{3+}$ AT LIQUID N_2 TEMPERATURE

(a indicates unidentified lines; The cm^{-1} scale is without calibration correction)

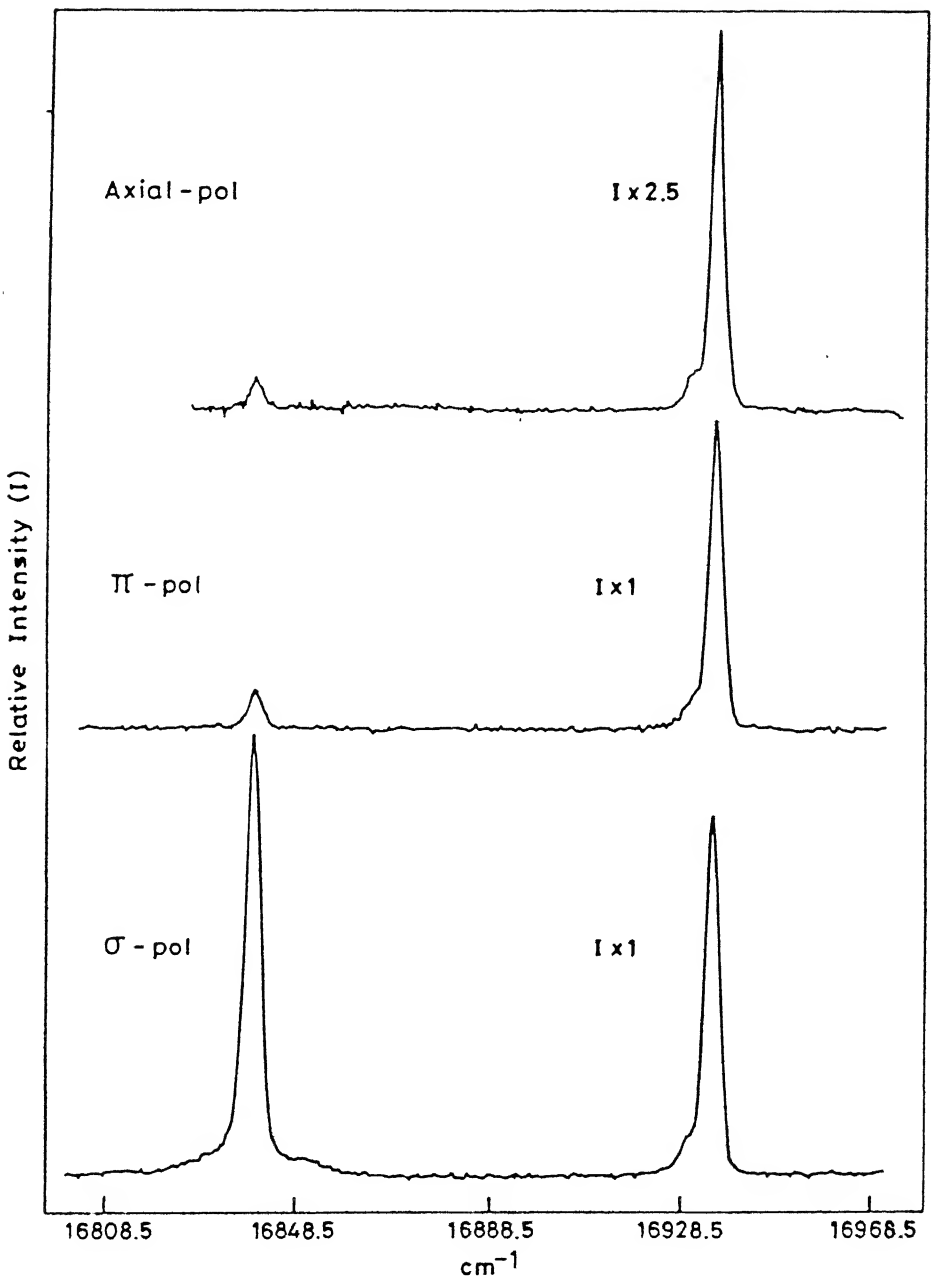

FIG.3.24 : $^5D_o - ^7F_1$ FLUORESCENCE OF $LiYF_4:Eu^{3+}$ AT LIQUID N_2 TEMPERATURE
(The cm^{-1} scale is without calibration correction)

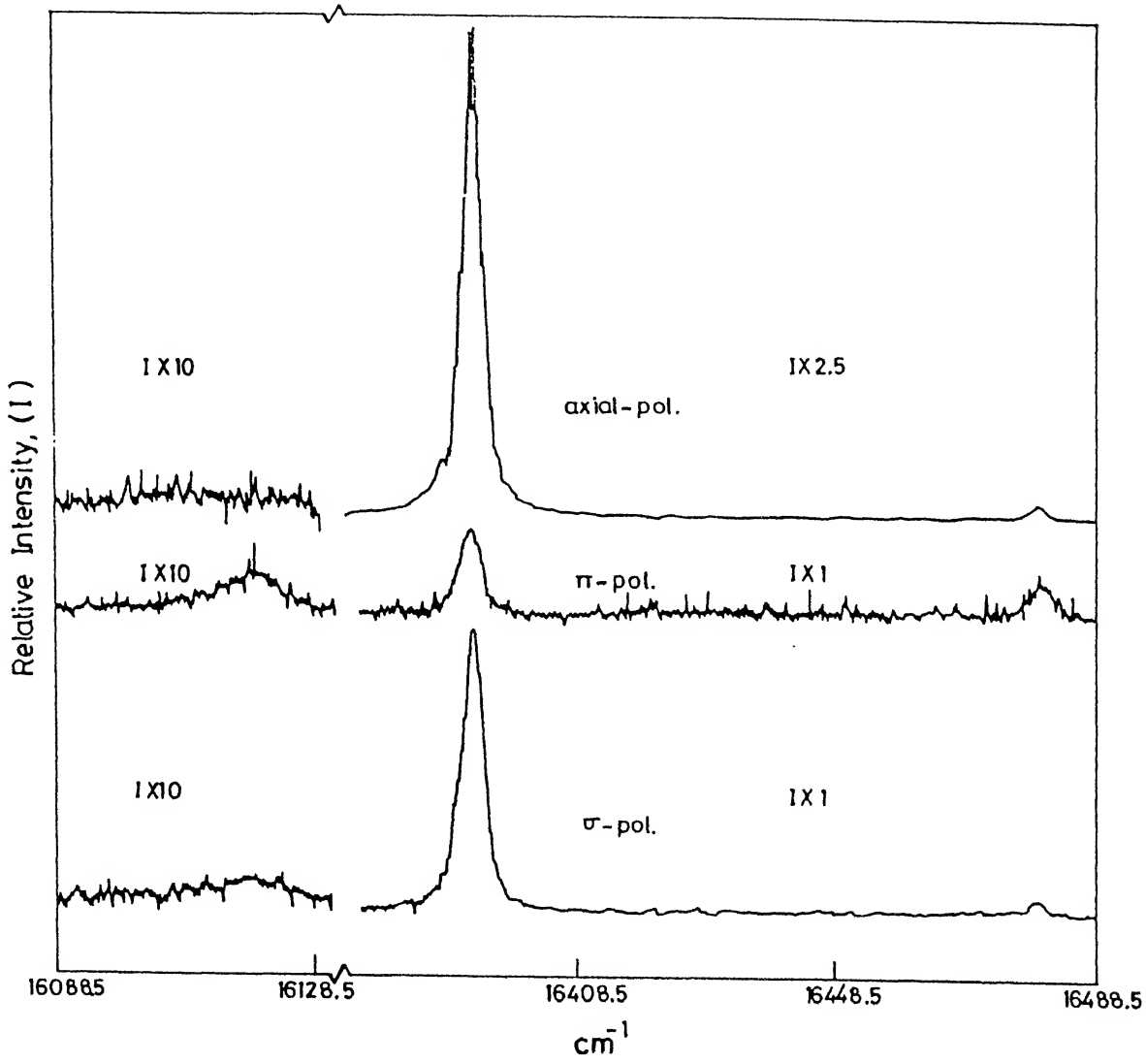

FIG.3.25 : $^5D_o - ^7F_2$ FLUORESCENCE OF $LiYF_4:Eu^{3+}$ AT LIQUID N_2 TEMPERATURE
(The cm^{-1} scale is without calibration correction)

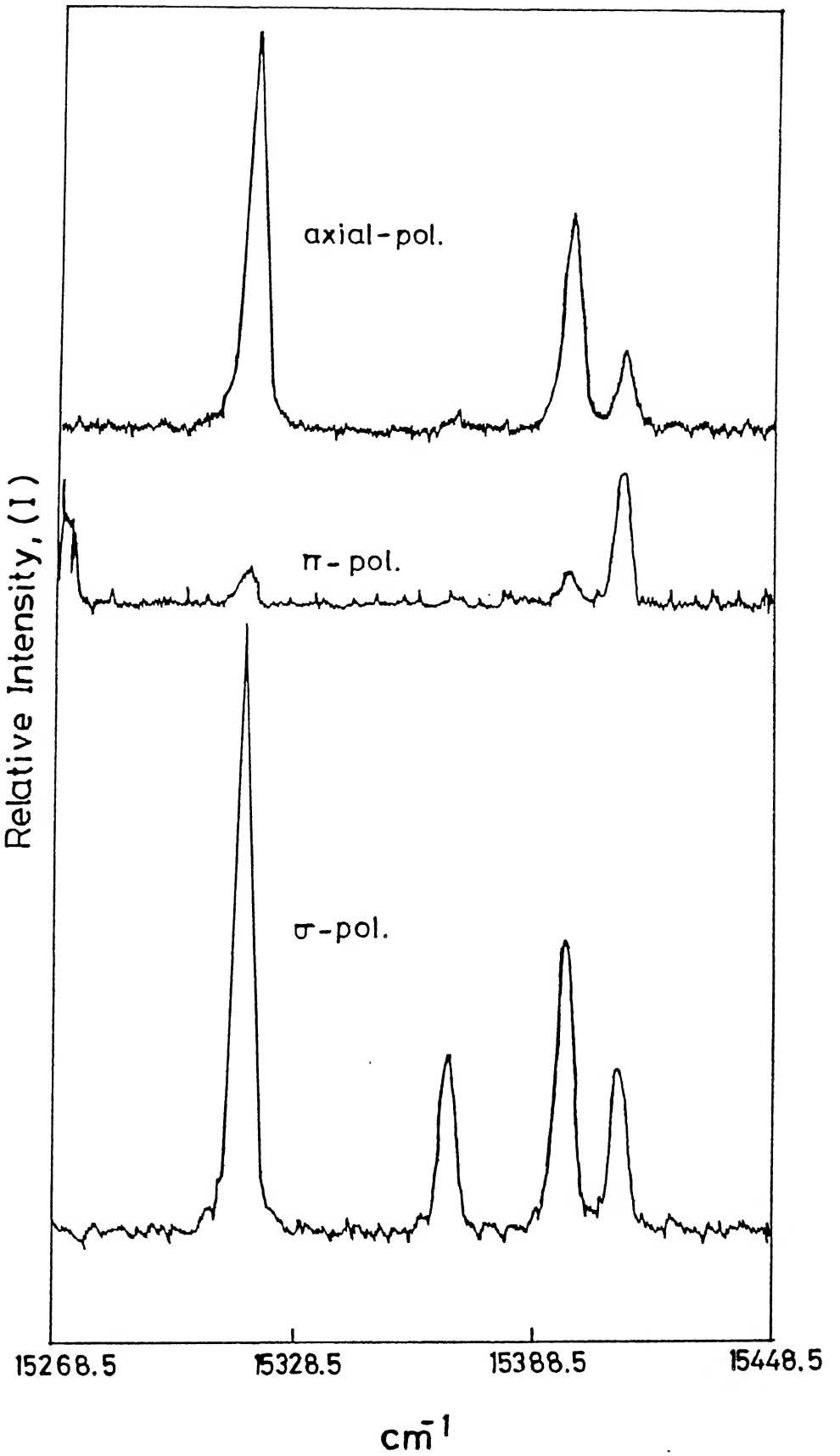

FIG.3.26 : $^5D_o - ^7F_3$ FLUORESCENCE OF $LiYF_4:Eu^{3+}$ AT LIQUID N_2 TEMPERATURE
(The cm^{-1} scale is without calibration correction)

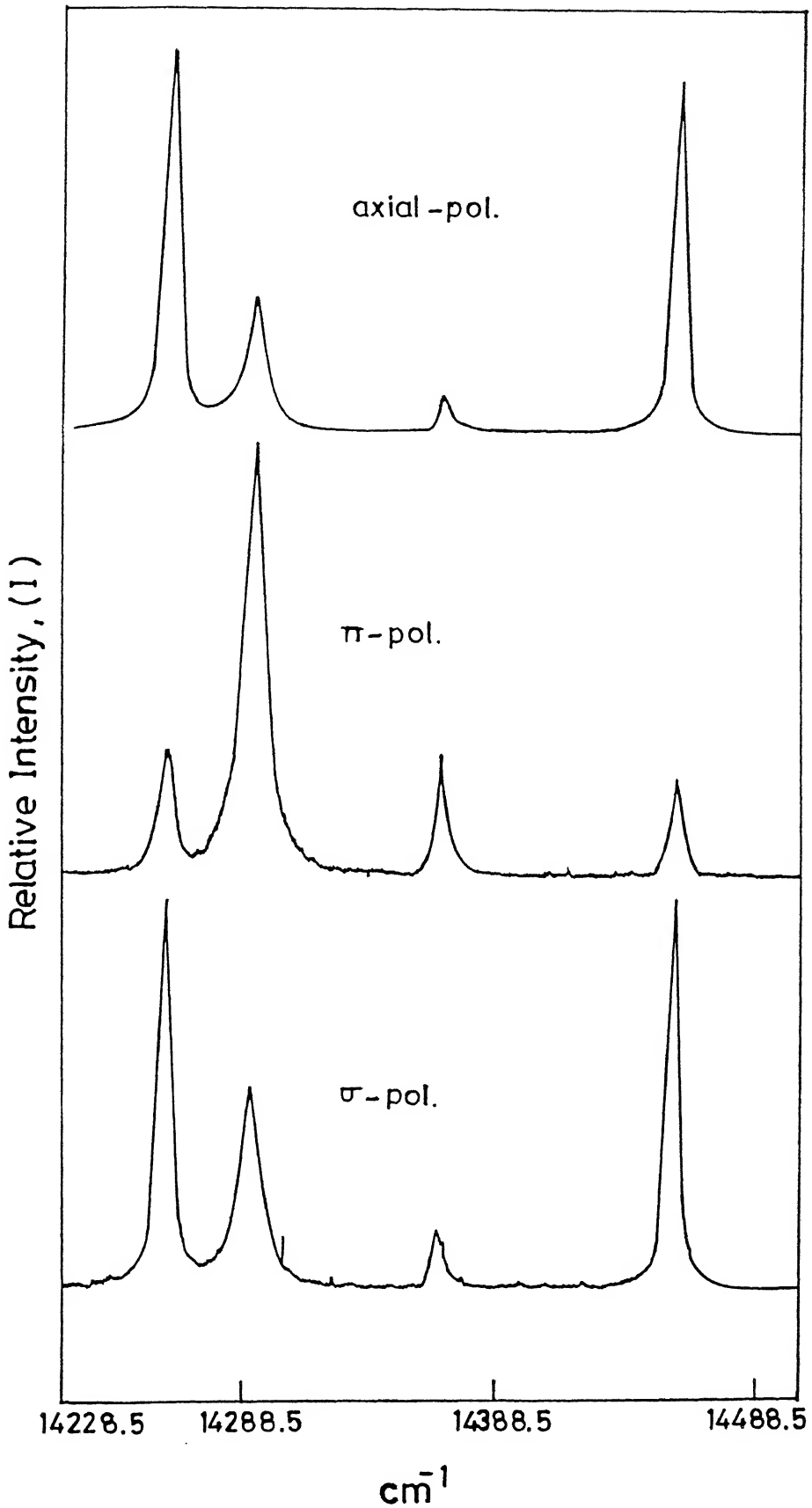

FIG.3.27 : ^5D_o-$^7F_4$ FLUORESCENCE OF $LiYF_4:Eu^{3+}$ AT LIQUID N_2 TEMPERATURE
(The cm^{-1} scale is without calibration correction)

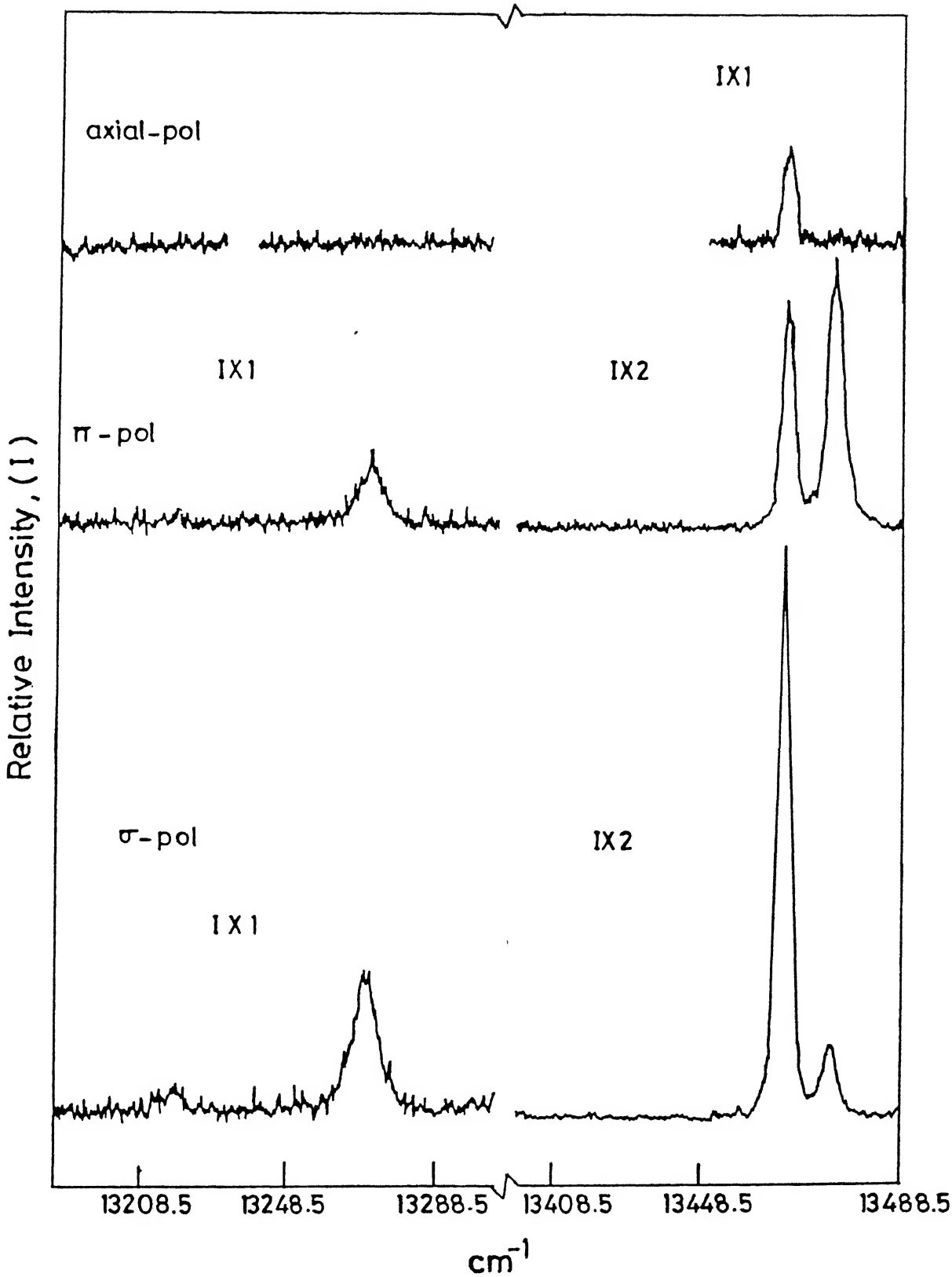

FIG.3.28 : $^5D_o - ^7F_5$ FLUORESCENCE OF $LiYF_4:Eu^{3+}$ AT LIQUID N_2 TEMPERATURE
(The cm^{-1} scale is without calibration correction)

TABLE 3.5

FLUORESCENCE DATA FOR THE 457.9 nm EXCITATION OF $Eu^{3+}:LiYF_4$ AT LIQUID NITROGEN TEMPERATURE

SNo.	Obs. Line Position (cm^{-1})	FWHM (cm^{-1})	Relative Intensity (arbitrary units)			Transition Mechanism	S_4-Symmetry assignment	Transition
			I_π	I_σ	I_{ax}			
1.	21570$^{\omega,r}$	-	-	-	-	-	-	-
2.	21543.	2.0	9.2	1.9	0.4	πE	$\Gamma_2(2)-\Gamma_1$	$^5D_2-^7F_0$
3.	21520.	2.0	3.6	18.0	10.5	σE	$\Gamma_3-\Gamma_1$	$^5D_2-^7F_0$
4.	21509^{r}	4.0	2.4	1.9	2.0	-	-	-
5.	21470^{r,c}	2.0	3.2	2.9	0.8	-	-	-
6.	21463^{r}	2.0	1.2	0.0	0.0	-	-	-
7.	21458^{r}	2.0	0.8	1.4	1.4	-	-	-
8.	21450.	2.0	10.0	2.4	0.8	πE	$\Gamma_2(1)-\Gamma_1$	$^5D_2-^7F_0$
9.	21408^{r}	3.5	0.4	3.4	1.2	-	-	-
10.	21209.	3.0	4.8	1.2	5.2	πM	$\Gamma_2(2)-\Gamma_3$	$^5D_2-^7F_1$
11.	21187.	3.0	6.0	4.2	2.4	$\pi E, \sigma M$	$\Gamma_3-\Gamma_3$	$^5D_2-^7F_1$
12.	21158^{c}	2.0	3.6	3.0	1.8	-	-	-
13.	21145.	2.5	7.0	11.5	19.4	$\sigma E, \pi M$	$\Gamma_1-\Gamma_3$	$^5D_2-^7F_1$
14.	21117.	2.5	7.0	7.2	12.6	$\pi M, \sigma E$	$\Gamma_2(1)-\Gamma_3$	$^5D_2-^7F_1$

15.	21090.	2.5	3.5	0.4	5.5	πM	$\Gamma_3-\Gamma_1$	$^5D_2-^7F_1$
16.	21048.[ω]	–	0.0	0.2	0.0	σM	$\Gamma_1-\Gamma_1$	$^5D_2-^7F_1$
17.	21021.	3.0	3.0	0.0	0.0	πE	$\Gamma_2(1)-\Gamma_1$	$^5D_2-^7F_1$
18.	20866.[d]	3.0	48.6	10.9	15.2	πE, σM	–	–
19.	20788.[d]	4.0	4.0	8.3	16.6	πM, σE	–	–
20.	20706.[a]	7.0	4.9	0.0	0.0	–	–	–
21.	20671.[ω, a]	4.0	2.0	0.0	0.0	–	–	–
22.	20629.	2.5	14.0	16.3	19.0	πM, σE	$\Gamma_3-\Gamma_2(1)$	$^5D_2-^7F_2$
23.	20589.	3.0	9.6	1.6	0.0	πE	$\Gamma_1-\Gamma_2(1)$	$^5D_2-^7F_2$
24.	20578.[ω, a]	4.5	8.1	0.0	0.0	–	–	–
25.	20567.	4.0	4.0	5.2	14.4	πM, σE	$\Gamma_2(2)-\Gamma_3$	$^5D_2-^7F_2$
26.	20545.	4.0	56.8	11.7	10.9	πE, (σM)	$\Gamma_3-\Gamma_3$	$^5D_2-^7F_2$
27.	20502	4.0	8.8	21.8	52.1	πM, σE	$\Gamma_1-\Gamma_3$	$^5D_2-^7F_2$
28.	20493.[c]	2.0	20.4	19.2	5.9	–	–	–
29.	20474.	4.0	12.8	30.2	72.3	πM, σE	$\Gamma_2(1)-\Gamma_3$	$^5D_2-^7F_2$
30.	20455.[ω, a]	–	0.4	0.4	0.0	–	–	–
31.	20390.[ω]	–	0.3	0.3	0.0	σM	$\Gamma_2(2)-\Gamma_2(2)$	$^5D_2-^7F$
32.	20369.[ω]	B	1.0	0.8	0.9	σE, πM	$\Gamma_2(2)-\Gamma_1$ and $\Gamma_3-\Gamma_2(2)$	$^5D_2-^7F_2$
33.	20344.[ω]	–	0.5	0.8	1.5	σE, (πM)	$\Gamma_3-\Gamma_1$	$^5D_2-^7F_2$

34.	20271.	3.0	4.8	4.2	0.0	πE	$\Gamma_2(1)-\Gamma_1$	$^5D_2-^7F_2$
35.	19669.	3.0	4.2	3.2	9.2	πM, σE	$\Gamma_2(2)-\Gamma_3(1)$	$^5D_2-^7F$
36.	19659.	2.5	7.5	3.2	12.5	πM, σE	$\Gamma_3-\Gamma_2(1)$	$^5D_2-^7F_3$
37.	19646.	3.0	2.4	3.8	2.3	πE, σM	$\Gamma_3-\Gamma_3(1)$	$^5D_2-^7F_3$
38.	19617.	2.5	69.0	11.3	21.1	πE and σE, πM	$\Gamma_1-\Gamma_2(1)$ and $\Gamma_3-\Gamma_1$	$^5D_2-^7F_3$
39.	19605.	2.5	10.5	9.0	22.6	πM, σE	$\Gamma_1-\Gamma_3(1)$	$^5D_2-^7F_3$
40.	19590.	3.0	7.8	12.6	7.5	πM, σE and σM	$\Gamma_2(2)-\Gamma_3(2)$ and $\Gamma_2(1)-\Gamma_2(1)$	$^5D_2-^7F$
41.	19576.	3.0	37.8	20.7	34.1	πM, σE and σM	$\Gamma_2(1)-\Gamma_3(1)$ and $\Gamma_1-\Gamma_1$	$^5D_2-^7F$
42.	19566.	2.5	18.5	7.5	4.3	πE, σM	$\Gamma_3-\Gamma_3(2)$	$^5D_2-^7F_3$
43.	19548.	2.5	49.0	3.6	5.0	πE	$\Gamma_2(1)-\Gamma_1$	$^5D_2-^7F_3$
44.	19525.	2.5	8.0	1.8	10.9	πM, (σE)	$\Gamma_1-\Gamma_3(2)$	$^5D_2-^7F_3$
45.	19504ω	-	0.0	0.5	0.3	σM	$\Gamma_2(2)-\Gamma_2(2)$	$^5D_2-^7F_3$
46.	19496.	3.0	10.2	8.3	19.6	πM, σE	$\Gamma_2(2)-\Gamma_3(2)$	$^5D_2-^7F_3$
47.	19480.	7.0	7.0	1.4	8.1	πM	$\Gamma_3-\Gamma_2(2)$	$^5D_2-^7F_3$
48.	19439ω	6.0	2.4	0.0	0.0	πE	$\Gamma_1-\Gamma_2(2)$	$^5D_2-^7F_3$
49.	19042.	2.0	6.0	45.6	10.0	σM	$\Gamma_1-\Gamma_1$	$^5D_1-^7F_o$
50.	19020.	2.5	96.0	15.0	35.0	πM, σE	$\Gamma_3-\Gamma_1$	$^5D_1-^7F_o$
51.	18912ω	-	-	-	-	-	$\Gamma_3-\Gamma_1(1)$	$^5D_2-^7F_4$

52.	18842$^{\omega}_{\cdot}$	-	-	-	-	-	$\Gamma_2(1)-\Gamma_1(1)$	$^5D_2-^7F_4$
53.	18793$^{\omega,a}_{\cdot}$	-	-	-	-	-	-	-
54.	18709.	2.0	11.6	25.2	24.6	πM, σE	$\Gamma_1-\Gamma_3$	$^5D_1-^7F_1$
55.	18687.	2.0	36.4	5.4	2.5	πE, σM	$\Gamma_3-\Gamma_3$	$^5D_1-^7F_1$
56.	18666.	6.0	12.0	2.7	12.7	πM, σE	$\Gamma_1-\Gamma_3(1)$	$^5D_2-^7F_4$
57.	18636.	5.0	0.0	4.5	14.4	σE	$\Gamma_2(1)-\Gamma_3(1)$	$^5D_2-^7F_4$
58.	18619$^{s}_{\cdot}$	-	-	-	-	-	$\Gamma_3-\Gamma_2(1)$	$^5D_2-^7F_4$
59.	18612$^{s,\omega}_{\cdot}$	-	-	-	-	-	$\Gamma_1-\Gamma_1$	$^5D_1-^7F_1$
60.	18602$^{s,a}_{\cdot}$	-	-	-	-	-	-	-
61.	18592.	3.0	15.0	33.5	22.2	πM, σE	$\Gamma_3-\Gamma_1$	$^5D_1-^7F_1$
62.	18580$^{s,a}_{\cdot}$	-	-	-	-	-	-	-
63.	18574$^{s,\omega}_{\cdot}$	-	-	-	-	-	$\Gamma_1-\Gamma_2(1)$	$^5D_2-^7F_4$
64.	18565$^{\omega}_{\cdot}$	-	-	-	-	-	$\Gamma_2(2)-\Gamma_2(2)$	$^5D_2-^7F_4$
65.	18542.	7.0	11.2	31.9	62.1	σE, πM σM	$\Gamma_3-\Gamma_2(2)$ $\Gamma_2(1)-\Gamma_2(1)$	$^5D_2-^7F_4$
66.	18528.	3.5	32.2	7.6	35.6	πM, σE	$\Gamma_2(2)-\Gamma_3(2)$	$^5D_2-^7F_4$
67.	18505	3.5	3.5	5.6	12.8	σE, πM	$\Gamma_3-\Gamma_3(2)$	$^5D_2-^7F_4$
68.	18492$^{a}_{\cdot}$	3.5	22.4	1.2	0.0	-	-	-
69.	18481$^{a}_{\cdot}$	4.0	8.0	12.6	18.6	-	-	-
70.	18471$^{s,\omega}_{\cdot}$	-	-	-	-	-	$\Gamma_2(1)-\Gamma_2(2)$	$^5D_2-^7F_4$
71.	18467.	B	1.8	3.6	6.0	σM, πE	$\Gamma_1-\Gamma_3(2)$	$^5D_2-^7F_4$

72.	$18455^{\omega,a}$	–	0.6	0.4	0.0	–	–	–	
73.	18436.	3.5	21.0	4.8	11.5	σE, πM	$\Gamma_3 - \Gamma_1(3)$	$^5D_2 - ^7F_$	
74.	$18425^{\omega,a}$	–	0.0	0.8	1.7	σE, πM	$\Gamma_2(1) - \Gamma_3(3)$		
75.	$18407^{\omega,a}$	–	1.6	1.3	0.0	–	–	–	
76.	18394^{ω}	–	2.6	1.7	3.8	–	–	–	
77.	$18379^{\omega,a}$	–	0.0	1.3	3.0	–	$\Gamma_1 - \Gamma_1(3)$	$^5D_2 - ^7F_4$	
78.	18373^{a}	B	1.4	0.0	3.0	–	–	–	
79.	18358^{a}	B	1.0	0.0	2.2	–	–	–	
80.	18332^{a}	B	1.4	18.5	3.1	–	–	–	
81.	18303^{a}	B	0.8	0.4	1.6	–	–	–	
82.	18247^{a}	B	1.4	0.0	0.0	–	–	–	
83.	18217^{a}	B	0.0	13.8	2.9	–	–	–	
84.	$18182^{\omega,a}$	–	–	–	–	–	–	–	
85.	$18179^{\omega,a}$	–	1.4	0.0	0.0	–	–	–	
86.	$18167^{\omega,a}$	–	2.8	0.0	0.0	–	–	–	
87.	18153^{ω}	–	0.2	0.0	0.0	πE	$\Gamma_1 - \Gamma_2(1)$	$^5D_1 - ^7F_2$	
88.	18144^{a}	5.5	38.5	0.0	0.0	–	–	–	
89.	18131.	3.0	50.4	17.3	54.3	πM, σE	$\Gamma_3 - \Gamma_2(1)$	$^5D_1 - ^7F_2$	
90.	18067.	3.5	30.1	14.0	48.0	πM, σE	$\Gamma_1 - \Gamma_3$	$^5D_1 - ^7F_2$	
91.	18043.	3.5	12.9	37.5	8.2	σM, πE	$\Gamma_3 - \Gamma_3$	$^5D_1 - ^7F_2$	

92.	17891.$^{\omega}$	-	4.0	0.0	0.0	πE	$\Gamma_1-\Gamma_2(2)$	$^5D_1-^7F_2$
93.	17870.	7.5	142.5	78.0	156.0	πM, σE	$\Gamma_3-\Gamma_2(2)$	$^5D_1-^7F_2$
94.	17845.^{s}	-	6.0	3.6	7.9	πM, σE	$\Gamma_3-\Gamma_1$	$^5D_1-^7F_2$
95.	17813.$^{\omega,a}$	-	1.6	1.1	1.6	-	-	-
96.	17771.^{a}	-	12.4	8.4	15.6	-	-	-
97.	17745.$^{\omega}$	-	8.2	6.2	10.8	πM, σE	$\Gamma_2(2)-\Gamma_3(1)$	$^5D_2-^7F_$
98.	17719.$^{\omega}$	-	9.4	3.4	5.7	πM, σE	$\Gamma_3-\Gamma_3(1)$	$^5D_2-^7F_5$
99.	17691.$^{\omega}$	-	7.4	0.0	4.5	πE	$\Gamma_1-\Gamma_2(1)$	$^5D_2-^7F_5$
100.	17678.$^{\omega}$	-	4.0	2.9	5.9	πM, σE	$\Gamma_1-\Gamma_3(1)$	$^5D_2-^7F_5$
101.	17605.	4.0	20.8	1.2	1.0	πE	$\Gamma_2(1)-\Gamma_1(1)$	$^5D_2-^7F_$
102.	17533.	9.0	9.0	0.0	0.0	πE	$\Gamma_2(2)-\Gamma_1(2)$	$^5D_2-^7F_$
103.	17480.$^{\omega}$	-	0.0	4.0	6.4	σE	$\Gamma_1-\Gamma_3(2)$	$^5D_2-^7F_5$
104.	17451.	B	0.0	8.2	11.9	σE	$\Gamma_2(1)-\Gamma_3(2)$	$^5D_2-^7F_$
105.	17443.	B	20.5	0.0	0.0	πE	$\Gamma_2(1)-\Gamma_1(2)$	$^5D_2-^7F_5$
106.	17428.	-	0.0	1.6	2.8	σE	$\Gamma_1-\Gamma_3(3)$	$^5D_2-^7F_5$
107.	17400.$^{\omega}$	-	0.0	0.8	1.4	σE	$\Gamma_2(1)-\Gamma_3(3)$	$^5D_2-^7F_5$
108.	17376.$^{\omega}$	-	0.0	0.6	0.6	σ	$\Gamma_2(1)-\Gamma_2(2)$	$^5D_2-^7F_5$
109.	17335.^{b}	B	3.9	0.8	1.4	-	-	-
110.	17272.**	B	9.0	4.8	5.0	-	$\Gamma_1-\Gamma_1$	$^5D_o-^7F_o$
111.	17253.^{v}	B	7.7	6.2	5.8	-	-	-

132. 16714.

133. 16686.

134. 16667.

135. 16656.

136. 16642.

137. 16640.

138. 16625.

139. 16607.

140. 16600.

141. 16583.

142. 16550.

143. 16511.

144. 16508.

145 16490.

146. 16486.

147. 16470.++

148.	16436$^{\omega}$	-	0.0	1.2	0.0	σM	$\Gamma_1-\Gamma_1(1)$	$^5D_1-^7F_4$
149.	16413.	5.0	57.4	87.0	154.4	πM, σE	$\Gamma_3-\Gamma_1(1)$	$^5D_1-^7F_4$
150.	16382.	3.0	122.4	17.5	21.5	πE	$\Gamma_1-\Gamma_2(1)$	$^5D_o-^7F_2$
151.	16295.	4.5	71.8	75.6	169.7	πM, σE	$\Gamma_1-\Gamma_3$	$^5D_o-^7F_2$
152.	16229.	6.0	38.9	34.0	82.6	πM, σE	$\Gamma_1-\Gamma_3(1)$	$^5D_1-^7F_4$
153.	16208.	4.5	160.6	28.0	42.6	πE, σM	$\Gamma_3-\Gamma_3(1)$	$^5D_1-^7F_4$
154.	16149.	6.0	42.0	25.2	71.2	σE, πM	$\Gamma_3-\Gamma_1(2)$	$^5D_1-^7F_4$
155.	16138.	5.0	283.8	38.0	73.9	πE, σM	$\Gamma_1-\Gamma_2(1)$	$^5D_1-^7F_4$
156.	16121.	14.0	-	-	-	πE	$\Gamma_1-\Gamma_2(2)$	$^5D_o-^7F_2$
157.	16116.	B	-	-	-	σE	$\Gamma_3-\Gamma_2(1)$	$^5D_1-^7F_4$
158.	16089$^{\omega}$	-	-	-	-	-	$\Gamma_1-\Gamma_1$	$^5D_o-^7F_2$
159.	16064$^{\omega}$	-	5.8	0.0	0.0	πE	$\Gamma_1-\Gamma_2(2)$	$^5D_1-^7F_4$
160.	16042.	10.0	191.4	184.0	331.9	πM, σE	$\Gamma_3-\Gamma_2(2)$	$^5D_1-^7F_4$
161.	16032^{s}	B	-	-	-	πM, σE	$\Gamma_1-\Gamma_3(2)$	$^5D_1-^7F_4$
162.	16009.	6.0	236.6	34.8	42.8	πE, σM	$\Gamma_3-\Gamma_3(2)$	$^5D_1-^7F_4$
163.	15940.	17.0	153.0	129.2	289.4	πM, σE	$\Gamma_3-\Gamma_1(3)$	$^5D_1-^7F_4$
164.	15411.	3.0	70.2	7.8	10.1	πE	$\Gamma_1-\Gamma_2(1)$	$^5D_o-^7F_3$
165.	15398.	3.0	16.6	21.0	45.0	σE, πM	$\Gamma_1-\Gamma_3(1)$	$^5D_o-^7F_3$
166.	15368.	3.0	0.0	12.6	0.9	σM	$\Gamma_1-\Gamma_1$	$^5D_o-^7F_3$
167.	15317.	3.3	29.7	40.3	81.2	σE, πM	$\Gamma_1-\Gamma_3(2)$	$^5D_o-^7F_3$

168.	15283[a]	10.0	0.0	26.0	37.9	–	–	–
169.	15245.	4.0	15.8	36.8	72.1	σE, πM	$\Gamma_1-\Gamma_3(1)$	$^5D_1-^5F_5$
170.	15236.	5.5	43.1	58.3	115.0	σE, πM	$\Gamma_1-\Gamma_2(2)$	$^5D_o-^7F_3$
							$\Gamma_3-\Gamma_2(1)$	$^5D_1-^7F_5$
171.	15223.	7.0	68.6	22.4	3.8	πE, (σM)	$\Gamma_3-\Gamma_3(1)$	$^5D_1-^7F_5$
172.	15214[ω]	–	0.0	3.0	4.4	–	–	–
173.	15203[ω]	–	0.0	0.0	3.5	–	–	–
174.	15191[a]	10.0	38.0	46.0	65.1	–	–	–
175.	15177.	6.0	11.3	25.2	54.7	σE, πM	$\Gamma_3-\Gamma_1(1)$	$^5D_1-^7F_5$
176.	15044[ω]		0.0	0.4	0.6	σE	$\Gamma_1-\Gamma_3(2)$	$^5D_1-^7F_5$
177.	15022.	5.0	49.2	10.0	0.0	πE, σM	$\Gamma_3-\Gamma_3(2)$	$^5D_1-^7F_5$
178.	15014.	11.0	0.0	26.4	47.9	σE	$\Gamma_3-\Gamma_1(2)$	$^5D_1-^7F_5$
179.	14994.	9.0	14.4	28.8	56.4	σE, πM	$\Gamma_1-\Gamma_3(3)$	$^5D_1-^7F_5$
180.	14971.	7.0	145.6	30.6	41.0	πE, σM	$\Gamma_3-\Gamma_3(3)$	$^5D_1-^7F_5$
181.	14963[ω, a]	–	0.0	2.0	3.1	–	–	–
182.	14457	4.5	71.3	74.0	87.3	πM, σE	$\Gamma_1-\Gamma_3(1)$	$^5D_o-^7F_4$
183.	14400.	9.0	4.9	43.2	1.3	σM	$\Gamma_1-\Gamma_1(2)$	$^5D_o-^7F_4$
184.	14367.	5.0	85.1	10.0	8.3	πE, σM	$\Gamma_1-\Gamma_2(1)$	$^5D_o-^7F_4$
185.	14293.	9.5	526.7	70.2	61.4	πE	$\Gamma_1-\Gamma_2(2)$	$^5D_o-^7F_4$
186.	14259.	7.0	107.5	87.6	122.9	πM, σE	$\Gamma_1-\Gamma_3(2)$	$^5D_o-^7F_4$

* - Relative intensities have meaning within a group.

a,b, c: - Refers to unidentified, Hg-line (tube light) and Ar^{+} lines respectively

d - Pr^{3+} lines

r - Refers to Raman lines

V - Refers to vibronic lines

s - Refers to soulder

ω - Refers to very weak lines

B - Refers to broad lines

** - Assignment of 17272 cm^{-1} is not certain

\+ - ++ This group of lines from 16816 cm^{-1} to 16470 cm^{-1} may correspond to $^{5}D_{2}-^{7}F_{6}$: We could not analysed these.

TABLE 3.6

FLUORESCENCE DATA FOR THE 514.5 nm EXCITATION OF Eu^{3+}:$LiYF_4$ AT LIQUID NITROGEN TEMPERATURE

SNo.	Obs. Line Position (cm^{-1})	FWHM (cm^{-1})	Relative* Intensity (arbitrary units) I_π	I_σ	I_{ax}	Transition Mechanism	S_4-Symmetry assignment	Transition
1.	19043.	2.0	1.2	5.7	0.8	σM	Γ_1-Γ_1	$^5D_1$-^7F_o
2.	19021.	2.0	18.0	4.3	13.0	πM,σE	Γ_3-Γ_1	$^5D_1$-^7F_o
3.	18710.	3.0	17.4	29.5	41.7	πM,σE	Γ_1-Γ_3	$^5D_1$-$^7F_1$
4.	18687.	2.5	33.3	5.1	4.5	πE,(σM)	Γ_3-Γ_3	$^5D_1$-$^7F_1$
5.	18593.	3.0	11.4	29.7	46.3	πM,σE	Γ_3-Γ_1	$^5D_1$-$^7F_1$
6.	18494[a].	2.5	5.0	2.0	3.8	-	-	-
7.	18467[a].	2.5	3.0	0.0	0.0	-	-	-
8.	18435[a].	2.5	1.0	2.0	2.9	-	-	-
9.	18419[a].	2.5	1.0	0.0	0.0	-	-	-
10.	18382[a].	2.5	3.5	0.0	0.0	-	-	-
11.	18153[ω].	-	0.8	0.0	0.0	πE	Γ_1-Γ_2(1)	$^5D_1$-$^7F_2$
12.	18132.	3.5	44.8	15.1	46.8	πM,σE	Γ_3-Γ_2(1)	$^5D_1$-$^7F_2$
13.	18067.	4.0	30.0	11.8	31.9	πM,σE	Γ_1-Γ_3	$^5D_1$-$^7F_2$

14.	18044.	4.0	8.0	37.7	4.1	πE, σM	$\Gamma_3-\Gamma_3$	$^5D_1-^7F_2$
15.	17892.	4.0	1.6	0.0	0.0	πE	$\Gamma_1-\Gamma_2(2)$	$^5D_1-^7F_2$
16.	17869.	4.5	9.9	2.6	25.4	πM, σE	$\Gamma_3-\Gamma_2(2)$	$^5D_1-^7F_2$
17.	17842.	9.0	3.6	0.0	2.9	πM	$\Gamma_3-\Gamma_1$	$^5D_1-^7F_2$
18.	17185.	3.5	8.7	0.1	0.6	πE	$\Gamma_1-\Gamma_2(1)$	$^5D_1-^7F_3$
19.	17171.	3.5	17.4	24.5	38.6	σE, πM	$\Gamma_1-\Gamma_3(1)$	$^5D_1-^7F_3$
20.	17162.	3.5	29.9	44.8	73.1	σE, πM	$\Gamma_3-\Gamma_2(1)$	$^5D_1-^7F_3$
21.	17149.	4.0	81.1	8.0	9.9	πE	$\Gamma_3-\Gamma_3(1)$	$^5D_1-^7F_3$
22.	17119.	3.5	16.8	20.3	24.7	σE, πM	$\Gamma_3-\Gamma_1$	$^5D_1-^7F_3$
23.	17091.	3.5	40.6	42.7	95.5	σE, πM	$\Gamma_1-\Gamma_3(2)$	$^5D_1-^7F_3$
24.	17069.	3.5	32.5	7.0	7.6	πE	$\Gamma_3-\Gamma_3(2)$	$^5D_1-^7F_3$
25.	17006.	6.0	80.6	6.6	13.0	πE	$\Gamma_1-\Gamma_2(2)$	$^5D_1-^7F_3$
26.	16983.	6.0	10.0	18.0	29.3	πE,(πM)	$\Gamma_3-\Gamma_2(2)$	$^5D_1-^7F_3$
27.	16938.	3.5	241.9	52.5	160.0	πM, σE	$\Gamma_1-\Gamma_3$	$^5D_o-^7F_1$
28.	16932[s,a]	-	-	-	-	-	-	-
29.	16842.	3.5	25.0	64.4	14.0	σM	$\Gamma_1-\Gamma_1$	$^5D_o-^7F_1$
30.	16411.	5.5	0.0	5.5	3.5	σE	$\Gamma_3-\Gamma_1(1)$	$^5D_1-^7F_4$
31.	16381.	4.5	25.2	1.8	4.0	πE	$\Gamma_1-\Gamma_2(1)$	$^5D_o-^7F_3$
32.	16294.	5.5	48.8	71.5	112.5	σE, πM	$\Gamma_1-\Gamma_3$	$^5D_o-^7F_3$
33.	16230[ω]	-	0.0	.2	.8	πM, σE	$\Gamma_1-\Gamma_3(1)$	$^5D_1-^7F_4$

34.	16208.	4.0	14.0	2.0	5.5	πE, σM	$\Gamma_3-\Gamma_3(1)$	$^5D_1-^7F_4$
35.	16138.	4.0	13.2	0.2	4.1	πE, σM	$\Gamma_1-\Gamma_2(1)$	$^5D_1-^7F_4$
36.	16149$^{\omega}$.	B	0.0	0.0	0.0	σE, πM	$\Gamma_3-\Gamma_1(2)$	$^5D_1-^7F_4$
37.	16121$^{\omega}$.	B	1.9	0.1	0.0	πE	$\Gamma_1-\Gamma_2(2)$	$^5D_o-^7F_3$
38.	16116$^{\omega}$.	B	1.9	0.5	1.8	πM, σE	$\Gamma_3-\Gamma_2(1)$	$^5D_1-^7F_4$
39.	16042$^{\omega}$.	8.0	10.0	6.4	27.8	πM, σE	$\Gamma_3-\Gamma_2(2)$	$^5D_1-^7F_4$
40.	16009.	6.0	73.1	6.0	17.0	πE, σM	$\Gamma_3-\Gamma_3(2)$	$^5D_1-^7F_4$
41.	15939$^{\omega}$.	B	0.0	0.2	4.8	σE	$\Gamma_3-\Gamma_1(3)$	$^5D_1-^7F_4$
42.	15411.	6.0	144.0	24.0	14.4	πE	$\Gamma_1-\Gamma_2(1)$	$^5D_o-^7F_3$
43.	15399.	5.0	36.8	37.0	39.0	πM, σE	$\Gamma_1-\Gamma_3(1)$	$^5D_o-^7F_3$
44.	15369.	4.5	0.0	20.7	1.2	σM	$\Gamma_1-\Gamma_1$	$^5D_o-^7F_3$
45.	15318.	5.0	40.0	76.0	72.7	πM, σE	$\Gamma_1-\Gamma_3(2)$	$^5D_o-^7F_3$
46.	15270^{a}.	5.0	0.0	2.0	0.0	-	-	-
47.	14458.	6.0	48.4	67.2	132.2	σE, πM	$\Gamma_1-\Gamma_3(1)$	$^5D_o-^7F_4$
48.	14366.	6.0	82.9	10.8	12.1	πE	$\Gamma_1-\Gamma_2(1)$	$^5D_o-^7F_4$
49.	14293^{s}.	10.0	528.0	70.0	81.8	πE	$\Gamma_1-\Gamma_2(2)$	$^5D_o-^7F_4$
50.	14260.	7.0	61.4	81.2	175.5	σE, πM	$\Gamma_1-\Gamma_3(2)$	$^5D_o-^7F_4$

a - refers to unidentified lines

ω - refers to very weak lines

s - refers to shoulder

B - refers to broad lines

* - Relative intensities have meaning within a group.

TABLE 3.7

FLUORESCENCE DATA FOR THE R6-G EXCITATION OF Eu^{3+}:$LiYF_4$ AT LIQUID NITROGEN TEMPERATURE

SNo.	Obs. Line Position (cm^{-1})	FWHM (cm^{-1})	Relative Intensity* (arbitrary units)			Transition Mech.	S_4-Symmetry assignment	Transition
			I_π	I_σ	I^{**}_{ax}			
1.	17292^{r}.	B	0.0	1.2	0.0	-	-	-
2.	17272.	B	1.0	2.4	0.0	σM	Γ_1-Γ_1	^5D_o-^7F_o
3.	17250^{r}.	B	0.0	2.2	0.0	-	-	-
4.	17232^{r}.	B	0.0	4.0	0.0	-	-	-
5.	16938.	2.3	121.5	45.0	58.1	πM,σM	Γ_1-Γ_3	^5D_o-$^7F_1$
6.	16933^{s,a}.	2.3	8.1	1.8	4.1	-	-	-
7.	16841.	2.3	18.4	28.8	5.4	σM	Γ_1-Γ_1	^5D_o-$^7F_1$
8.	16382.	3.5	22.0	2.1	1.5	πE	Γ_1-Γ_2(1)	^5D_o-$^7F_2$
9.	16295.	3.5	43.3	30.8	64.4	πM,σE	Γ_1-Γ_3	^5D_o-$^7F_2$
10.	16122.	9.0	36.7	5.4	0.0	πE	Γ_1-Γ_2(2)	^5D_o-$^7F_2$
11.	15411.	3.0	54.0	5.4	1.8	πE	Γ_1-Γ_2(1)	^5D_o-$^7F_3$
12.	15398.	3.0	16.6	11.4	5.1	σM,πE	Γ_1-Γ_3(1)	^5D_o-$^7F_3$
13.	15369.	3.0	0.0	7.5	0.0	σM	Γ_1-Γ_1	^5D_o-$^7F_3$
14.	15317.	3.0	18.2	23.4	8.7	σM,πE	Γ_1-Γ_2(2)	^5D_o-$^7F_3$

15.	14664.	6.0	0.0	6.0	0.0	σM	$\Gamma_1-\Gamma_1(1)$	$^5D_o-^7F_4$
16.	14584.[a]	18.0	0.7	9.7	0.9	-	-	-
17.	14558.[a]	B	0.0	0.3	0.0	-	-	-
18.	14538.[a]	7.0	0.8	5.0	0.3	-	-	-
19.	14458.	4.0	14.1	14.4	18.8	πM,σE	$\Gamma_1-\Gamma_3(1)$	$^5D_o-^7F_4$
20.	14400.	7.0	0.8	5.0	0.3	σM	$\Gamma_1-\Gamma_1(2)$	$^5D_o-^7F_4$
21.	14366.	4.0	16.3	0.2	1.5	πE	$\Gamma_1-\Gamma_2(1)$	$^5D_o-^7F_4$
22.	14294.	8.0	119.1	8.0	4.4	πE	$\Gamma_1-\Gamma_2(2)$	$^5D_o-^7F_4$
23.	14259.	6.0	11.5	15.6	23.2	πM,σE	$\Gamma_1-\Gamma_3(2)$	$^5D_o-^7F_4$
24.	13485.	5.0	55.5	10.0	0.0	πE	$\Gamma_1-\Gamma_2(1)$	$^5D_o-^5F_5$
25.	13472.	4.0	34.7	62.4	9.0	σE	$\Gamma_1-\Gamma_3(1)$	$^5D_o-^7F_5$
26.	13271.	8.0	20.8	30.4	0.0	σE	$\Gamma_1-\Gamma_3(2)$	$^5D_o-^7F_5$
27.	13219.	B	0.0	0.6	0.0	σE	$\Gamma_1-\Gamma_3(3)$	$^5D_o-^7F_5$

r - refers to Raman line

a - refers to unidentified line

s - refers to weak shoulder

B - refers to broad and weak line

* - Relative intensities have meaning within a group

**- The laser power used for axial spectrum was different from that for the other polarizations.

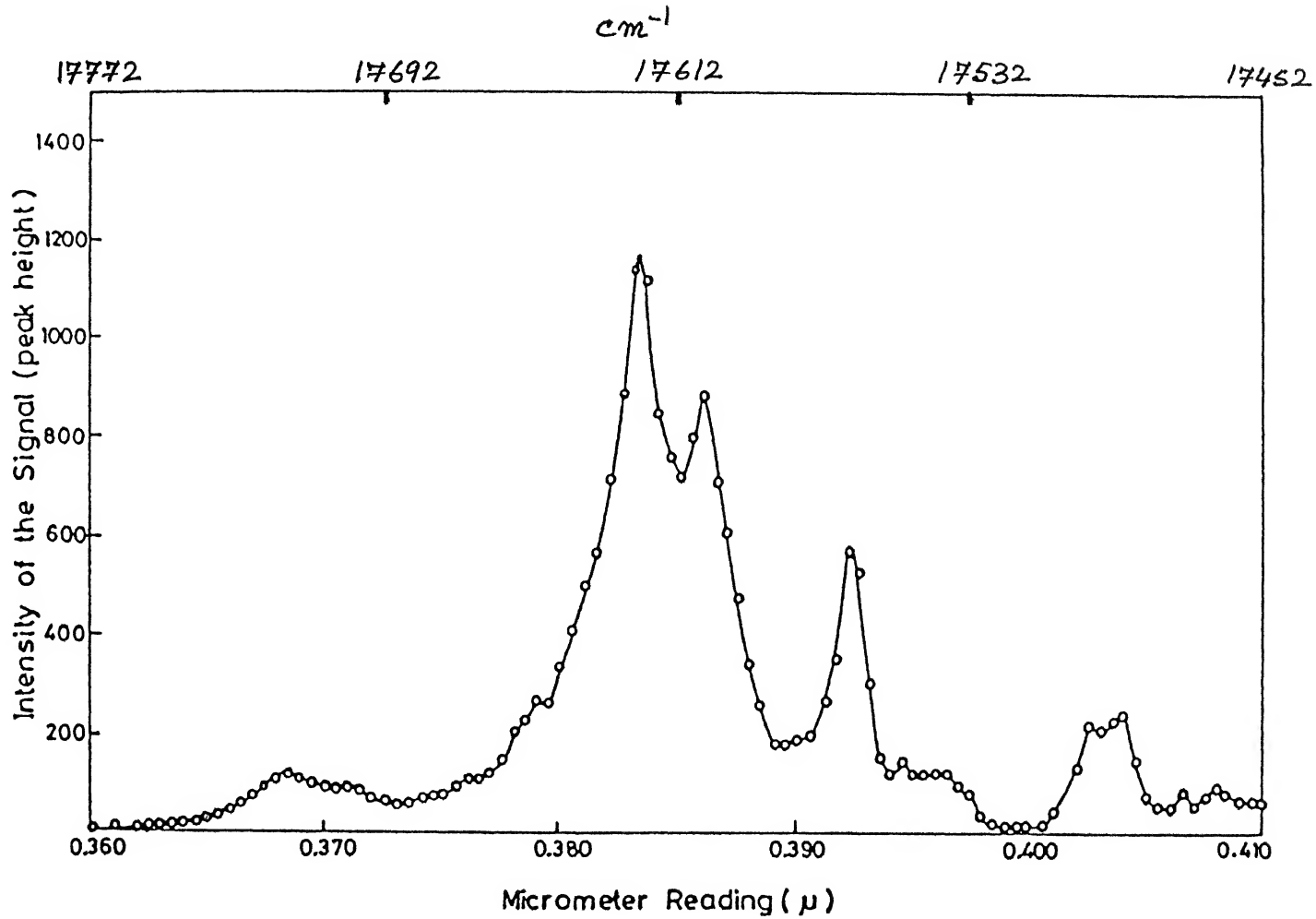

FIG.3.29 : EXCITATION SPECTRUM OF $LiYF_4:Eu^{3+}$ AT LIQUID N_2 TEMPERATURE.

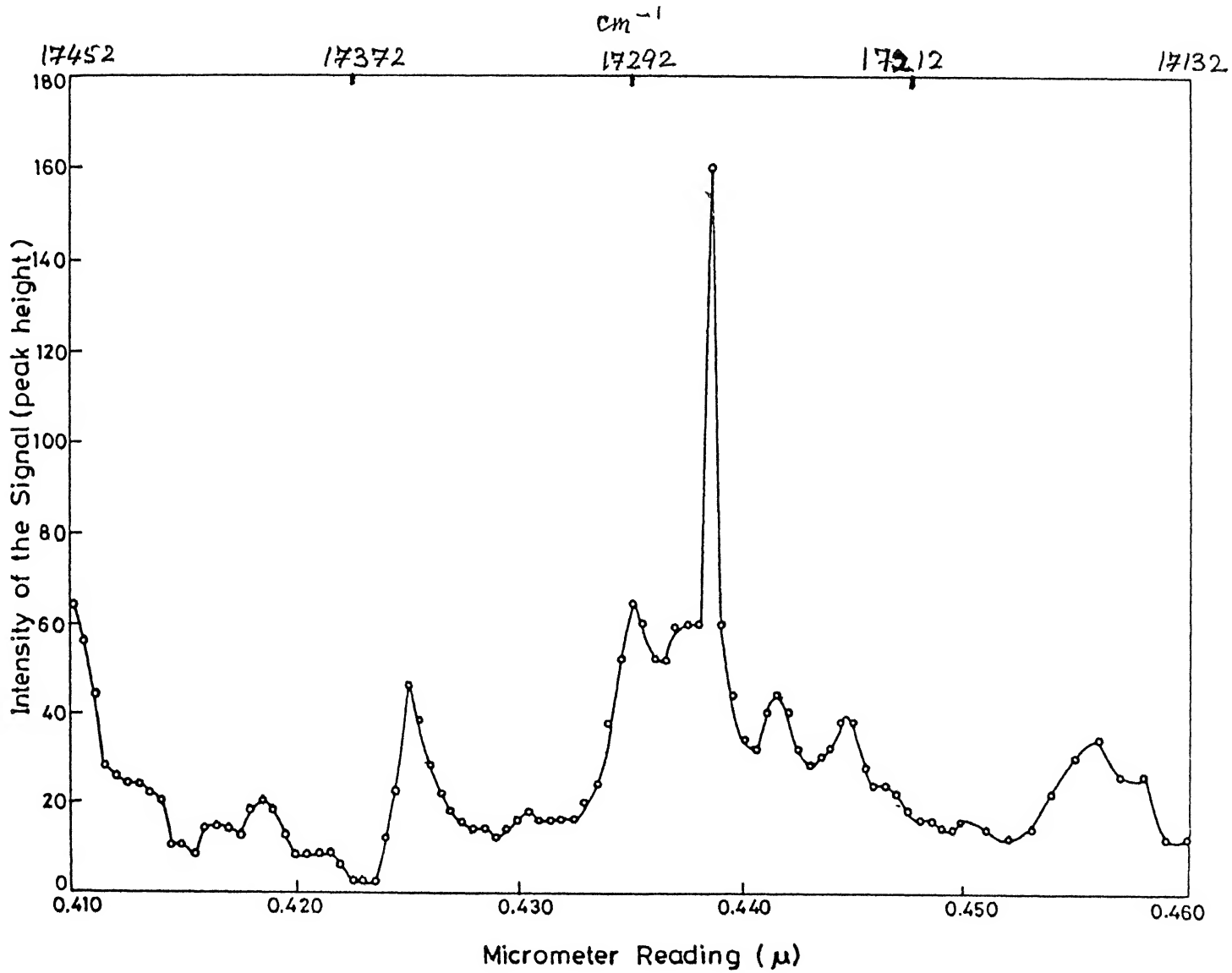

FIG.3.30 : EXCITATION SPECTRUM OF $LiYF_4:Eu^{3+}$ AT LIQUID N_2 TEMPERATURE.

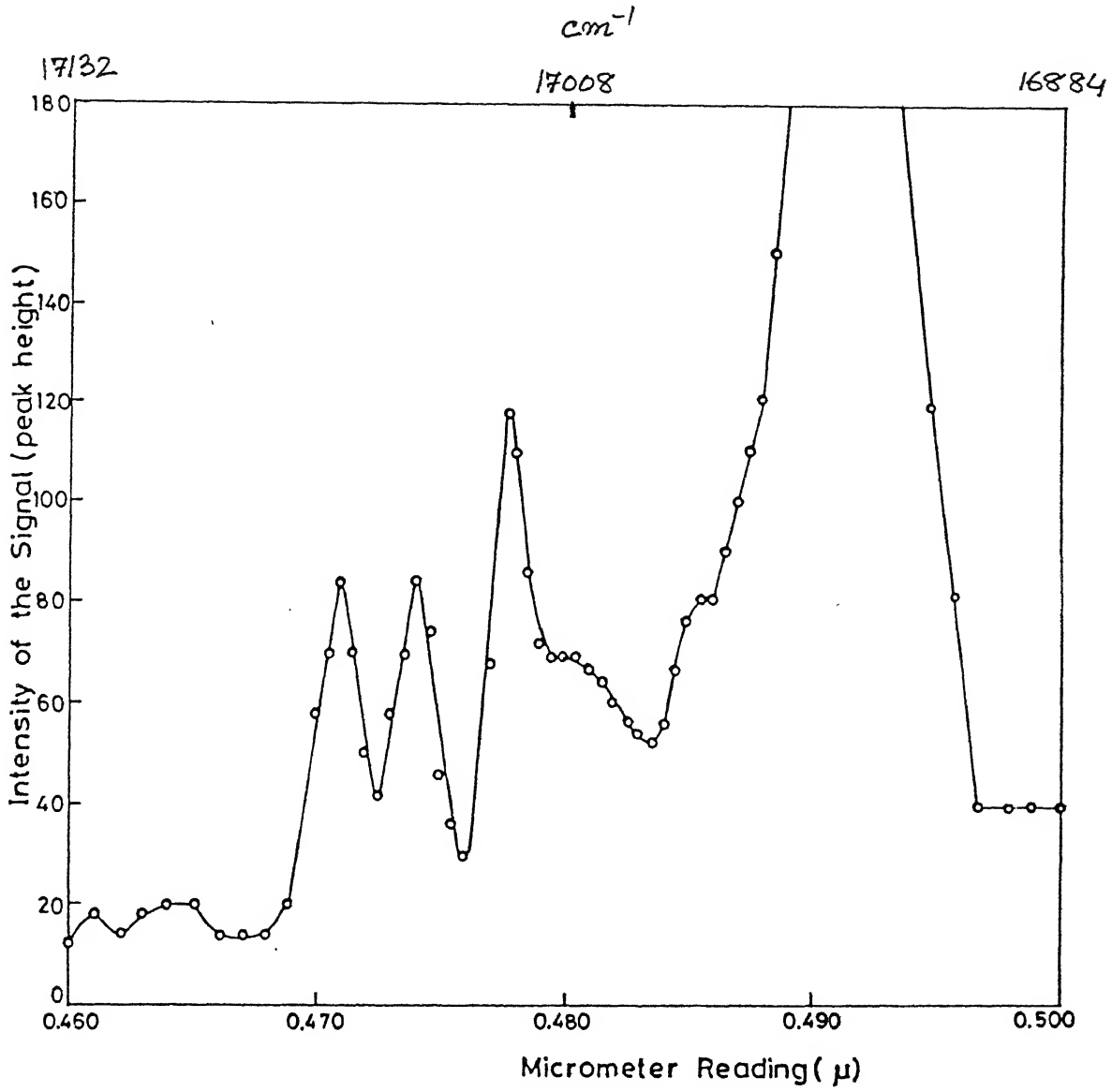

FIG.3.31 : EXCITATION SPECTRUM OF $LiYF_4:Eu^{3+}$ AT LIQUID N_2 TEMPERATURE

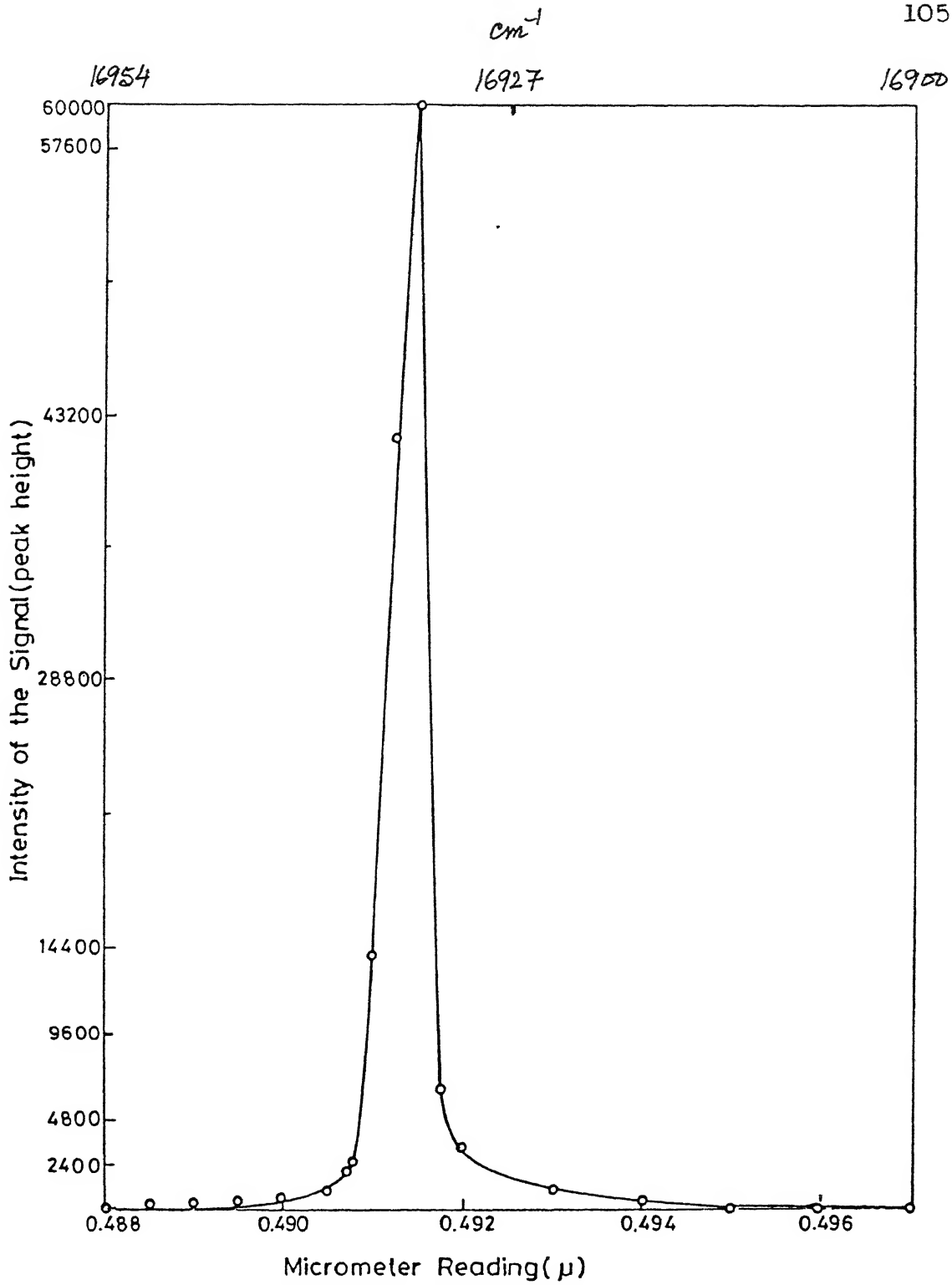

FIG.3.32 : EXCITATION SPECTRUM OF $LiYF_4:Eu^{3+}$ AT LIQUID N_2 TEMPERATURE

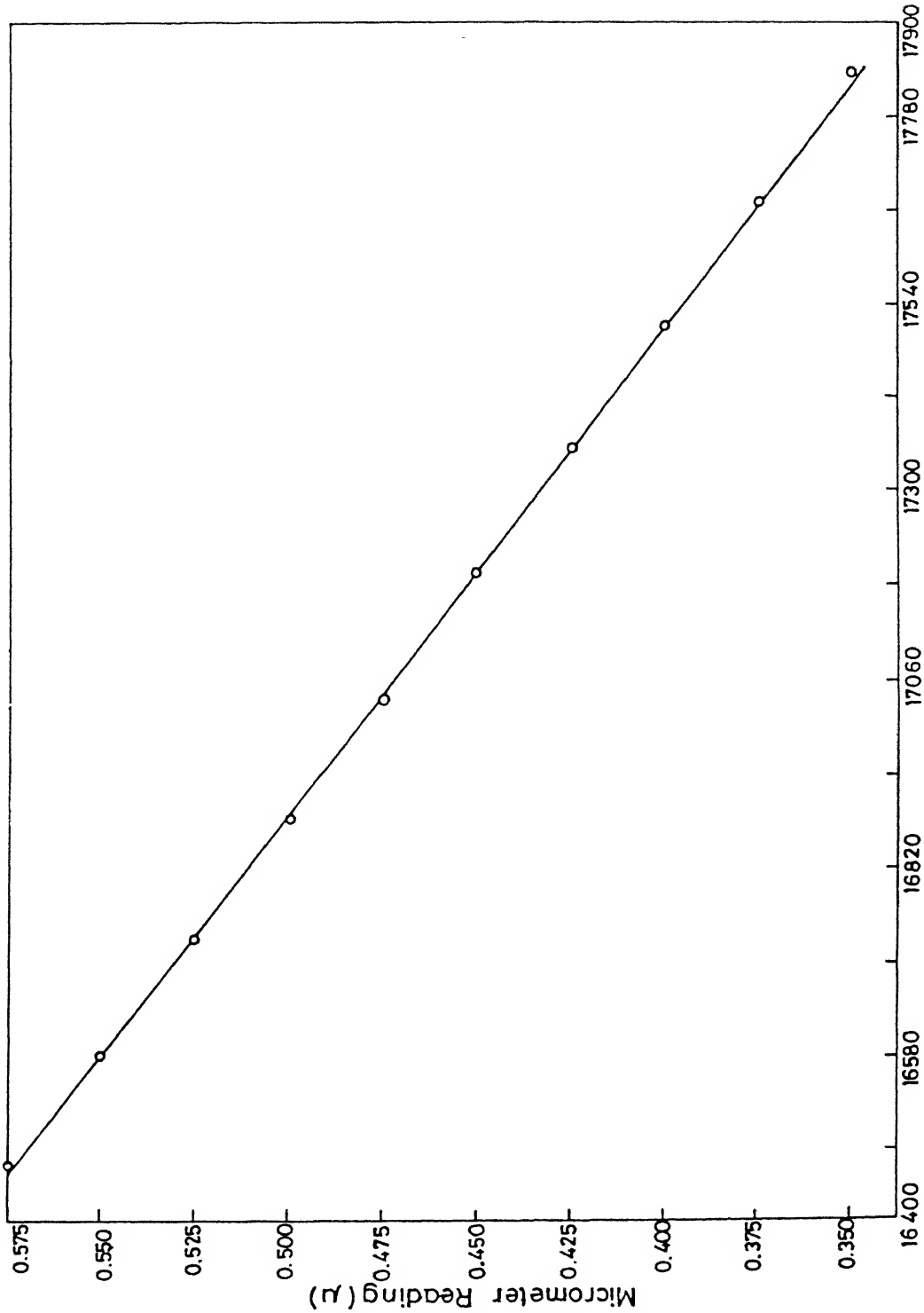

FIG.3.33 : DYE LASER CALIBRATION CURVE

TABLE 3.8

PEAK POSITIONS IN THE EXCITATION SPECTRA OF Eu^{3+}:$LiYF_4$ AT LIQUID NITROGEN TEMPERATURE AND ENERGY OF THE CORRESPONDING PHONONS

SNo.	Peak Positions (cm^{-1})	Difference from ^5D_o- ^7F_o transition at 17270 cm^{-1}	Difference from ^5D_o-$^7F_1(\Gamma_3)$ transition at 16936 cm^{-1}	Reported* Phonon energy (cm^{-1})
1.	17718	448	782	446Eg
2.	17702	432	766	425Ag/427Eg/ 424Eu
3.	17670	400	734	396Au
4.	17662	392	726	382Bg
5.	17624	354	688	368Eg/367Eu
6.	17608	338	672	329Bg/329Eg/ 326Eu
7.	17568	298	632	292/303Eu
8.	17552	282	616	283Au
9.	17500	230	564	-
10.	17492	222	556	224Au
11.	17474	204	538	199Eg
12.	17464	194	528	195Au
13.	17420	150	484	153Eg

14.	17410	140	474	143Eu
15.	17394	124	458	-
16.	17378	108	442	446Eg
17.	17354	86	420	425Ag/427Bg/424Eu
18.	17334	64	398	396Au
19.	17320	50	384	382Bg
20.	17292	22	356	368Eg/367Eu
21.	17276	6	340	-
22.	17270	0	334	-
23.	17250	20	314	-
24.	17230	40	294	292Eu
25.	17218	52	282	282Bg/283Au
26.	17204	66	268	264Ag
27.	17196	74	260	264Ag/252Au
28.	17158	112	222	224Au
29.	17144	126	208	$199E_3$
30.	17124	146	188	143Eu
31.	17104	166	168	173Eu/177Bg
32.	17060	210	124	-
33.	17040	230	104	224Eu

34.	17020	250	82	248/252Bg/Au
35.	17004	266	66	264Ag
36.	16972	298	34	292/303Eu
37.	16936	334	0	-

* - Reference [6].

REFERENCES

[1] Thoma et al; Inorg Chem 9 1096 (1970).

[2] R W G Wyckoff; The structure of crystals 2nd ed. The Chemical Catalog Company, Inc USA (1931).

[3] J P Sattler and J Nemarich; Phys Rev B (Solid State) 4 1 (1971).

[4] W A Shand; J Crystal Growth 5 143 (1969).

[5] Vishwamittar and S P Puri; J Phy C: Solid State Phys 7 1337 (1974).

[6] S A Miller et al; J Chem Phys 52 8 4172 (1970).

-x-

CHAPTER IV

RESULTS AND DISCUSSIONS

In this chapter we present the interpretation of the experimental data given in Chapter III. The spectra of the $LiYF_4:Eu^{3+}$ consist mainly of groups of sharp lines. These lines correspond to transitions among the Stark components belonging to various J-multiplets. The center of gravity of a certain group of lines gives the energy of the so called 'free ion level'. The symmetry assignments to Stark levels are made using E.D. and M.D. selection rules. The relative intensities of spectral lines in π, σ and axial spectra help decide the nature of the transition. Lines with comparable intensities appearing in $\sigma(\pi)$ and axial spectra are associated with ED(MD) transitions. Transitions are labelled as π-E.D., σ-E.D., π-M.D. and σ-M.D. where $\sigma(\pi)$ indicates that the electric vector of the emitted or absorbed radiation in the transition is perpendicular (parallel) to the $\bar{C}$-axis of the crystal and E.D.(MD) implies that the transition is electric dipole (magnetic dipole) in nature. The following general rule is helpful in deciding the nature of observed transitions.

A pure π-polarized E.D. transition must appear only in the π-polarized spectrum, a pure σ-polarized E.D. transition

must appear in σ and axial spectra but not in π-polarization. While a pure π-polarized M.D. transition must appear in π and axial-spectra but not in σ-polarization, and a pure σ-polarized M.D. transition must appear only in the σ polarization. Mixed transitions will appear in both (π and σ) the polarizations. Their relative intensities determine the dominant polarization and intensity in the axial-spectrum ditermines the nature of the transition. The criteria for mixed transitions are as follows.

$I_\pi < I_\sigma < I_{ax}$ = σ-E.D. (dominant), π.M.D.

$I_\sigma < I_\pi < I_{ax}$ = π-M.D. (dominant), σ-E.D.

$I_\sigma > I_\pi > I_{ax}$ = σ-M.D. (dominant), π-E.D.

$I_\pi > I_\sigma > I_{ax}$ = π-E.D. (dominant), σ-M.D.

A comparison of E.D. and M.D. selection rules shows that the combinations like (σ.E.D. + σ.M.D.) and (π.E.D. + π.M.D.) are not allowed.

1. ABSORPTION SPECTRA

The absorption spectrum directly gives the positions of the excited energy levels. The ground state of Eu^{3+} is a singlet ^7F_o with J=0. The ^7F_J multiplets with J=1- 6 lie next in energy. A survey of literature on the spectra of Eu^{3+} in various hosts and solutions reveals that the next higher level ^5D_o is expected to lie around 17270 cm^{-1} above ^7F_o, but we could not observe the ^7F_o- ^5D_o transition

in absorption. This transition is highly forbidden by several selection rules. The J=O $\longrightarrow$ J' =O transition is forbidden by E.D. and M.D. selection rules. F_o and D_o states both transform as Γ_1 representations of S_4 point group and the $\Gamma_1 \longrightarrow \Gamma_1$ transition is forbidden by the crystal field selection rules. We now describe the groups of levels observed in the absorption spectrum in the spectral range 18600 cm^{-1} to 25500 cm^{-1}.

$^7F_1$-$^5D_1$ ABSORPTION

The absorption spectra (Fig 3.11 and 3.12) show two lines at 18684 and 18694 cm^{-1}. The line at 18684 cm^{-1} is weak but sharp while the 18694 cm^{-1} line is very weak and broad. The literature survey and analysis of the rest of our experimental data indicate that these lines do not correspond to the $^7F_o \longrightarrow {}^5D_1$ transition. The line at 18684 cm^{-1} present in π-polarization, absent in σ-polarization, and extremely weak in the axial corresponds to an E.D. transition and satisfies the polarization and energy difference requirements for the $^7F_1(\Gamma_3) \longrightarrow {}^5D_1(\Gamma_3)$ transition. But we do not have any explanation for the very weak and broad line at 18694 cm^{-1}.

^7F_o- $^5D_1$ ABSORPTION

The J=1 multiplet splits into two Stark levels transforming as Γ_1 and Γ_3 (Table 2.3). For this group, we have observed two sharp and strong lines at 19043 and 19021 cm^{-1}

and two very weak shoulders at 19042 and 19019 cm^{-1} respectively (Figs 3.11 and 3.12). The line at 19043 cm^{-1} corresponds to a σ-polarized M.D. transition as it is strong in the σ-polarization but absent in π and axial spectra. We can assign this line to the $^7F_o(\Gamma_1) \longrightarrow {}^5D_1(\Gamma_1)$ transition. The line at 19021 cm^{-1} is strong in π and axial spectra but extremely weak in the σ-polarization. This indicates that it is a π-polarized magnetic dipole transition with a small admixture of σ-E.D. character. We can attribute this line to the $^7F_o(\Gamma_1) \longrightarrow {}^5D_1(\Gamma_3)$ transition. The weak shoulders remain unexplained.

^7F_o-$^5D_2$ ABSORPTION

Theoretically we expect 4 lines for this group according to the decomposition $D_2^+ \longrightarrow 1\Gamma_1+2\Gamma_2+1\Gamma_{3,4}$. There are three fairly strong and sharp lines at 21543 cm^{-1}, 21520 cm^{-1}, 21450 cm^{-1} and a weak shoulder at 21518 cm^{-1}, associated with the 21520 cm^{-1} line (Fig 3.11 and 3.12). The lines at 21543 cm^{-1} and 21450 cm^{-1} are π-polarized E.D. transitions as they are present in the π-spectrum but absent in σ and axial spectra. They can be assigned to the two expected $\Gamma_1 \longrightarrow \Gamma_2$ transitions. The line at 21520 cm^{-1} present in σ and axial but absent in the π-polarized spectrum, is σ-E.D. and can be attributed to the $\Gamma_1 \longrightarrow \Gamma_3$ transition. The shoulder 21518 cm^{-1} can not be assigned to the $\Gamma_1 \longrightarrow \Gamma_1$ transition as it does not

comply with the expected polarization behavior. Thus out of four, only three Stark components of the $^5D_2$-term are identified and the shoulder at 21518 also remains unexplained.

^7F_o-$^5L_6$ ABSORPTION

Four fairly strong and well separated lines at 25416 cm^{-1}, 25241 cm^{-1}, 25027 cm^{-1} and 24953 cm^{-1} and a broad shoulder at 25258 cm^{-1} associated with the 25241 cm^{-1} line are present in the spectral region 24900 cm^{-1} to 25500 cm^{-1}(Fig 3.9 and 3.10). A survey of the literature and our calculations indicate that the terms $^5D_3$, $^5L_6$ and $^5G_2$ must lie in the ranges 24300 cm^{-1}-24500 cm^{-1}, 24896-25400 cm^{-1} and 25900 cm^{-1}-26100 cm^{-1} respectively. Consequently, the observed spectral lines should correspond to the $^5L_6$ term. Theoretically a term with J=6 will split into 10 Stark components in the S_4 symmetry field according to the decomposition $(3\Gamma_1'+4\Gamma_2'+3\Gamma_3')$. It is reasonable to assume that Γ_1'—Γ_1' transitions will not appear for this group because M.D. transitions are forbidden for $\Delta J>\pm 1$. The line at 24953 cm^{-1} is very sharp and appears in σ and axial spectra only. It can, therefore, be assigned to the E.D., $^7F_o(\Gamma_1') \rightarrow\!\!\!- \; ^5L_6(\Gamma_3')$ transition. The line at 25027 cm^{-1} appearing only in π-polarization is π-E.D. type and can be assigned to the $^7F_o(\Gamma_1') \rightarrow\!\!\!- \; ^5L_6(\Gamma_2')$ transition. The line at 25241 cm^{-1} and its shoulder at 25258 cm^{-1} are

similarly σ-E.D. type. The relatively strong line at 25241 cm^{-1} can be attributed to the $^7F_0(\Gamma_1) \longrightarrow {}^5L_6(\Gamma_3)$ transition. The shoulder is somewhat difficult to account for, because theoretical calculations predict a $^5L_6(\Gamma_1)$ level just around this position, but the polarization characteristics of this 'shoulder' do not comply with the $\Gamma_1 \longrightarrow \Gamma_1$ transition. The line at 25416 cm^{-1} is very broad (FWHM 34 cm^{-1}) and strong, but its peak position in the π and σ spectra differs by 3 cm^{-1} and the peak position in the axial spectrum matches with that of the σ-polarization. In the π-polarization, the peak at 25418 cm^{-1} can be assigned to the π-E.D., $^7F_0(\Gamma_1) \longrightarrow {}^5L_6(\Gamma_2)$ transition and the σ-polarized 25415 cm^{-1} peak can be attributed to the σ-E.D., $^7F_0(\Gamma_1) \longrightarrow {}^5L_6(\Gamma_3)$ transition. Thus, out of the 10 expected Stark levels of $^5L_6$, five are identified. These assignments are in qualitative agreement with the theoretically calculated structure of $^5L_6$. However complete identification of the $^5L_6$ multiplet is not possible due to lack of sufficient experimental data and because precise calculations for the free ion energies were not possible. All observed absorption transitions are shown in Fig.4.1.

2. FLUORESCENCE SPECTRA

Resonance excitation of Eu^{3+} by any of the Ar^+ laser lines is not possible because of the mismatch of energies. However, $LiYF_4:Eu^{3+}$ fluoresces when excited with most of

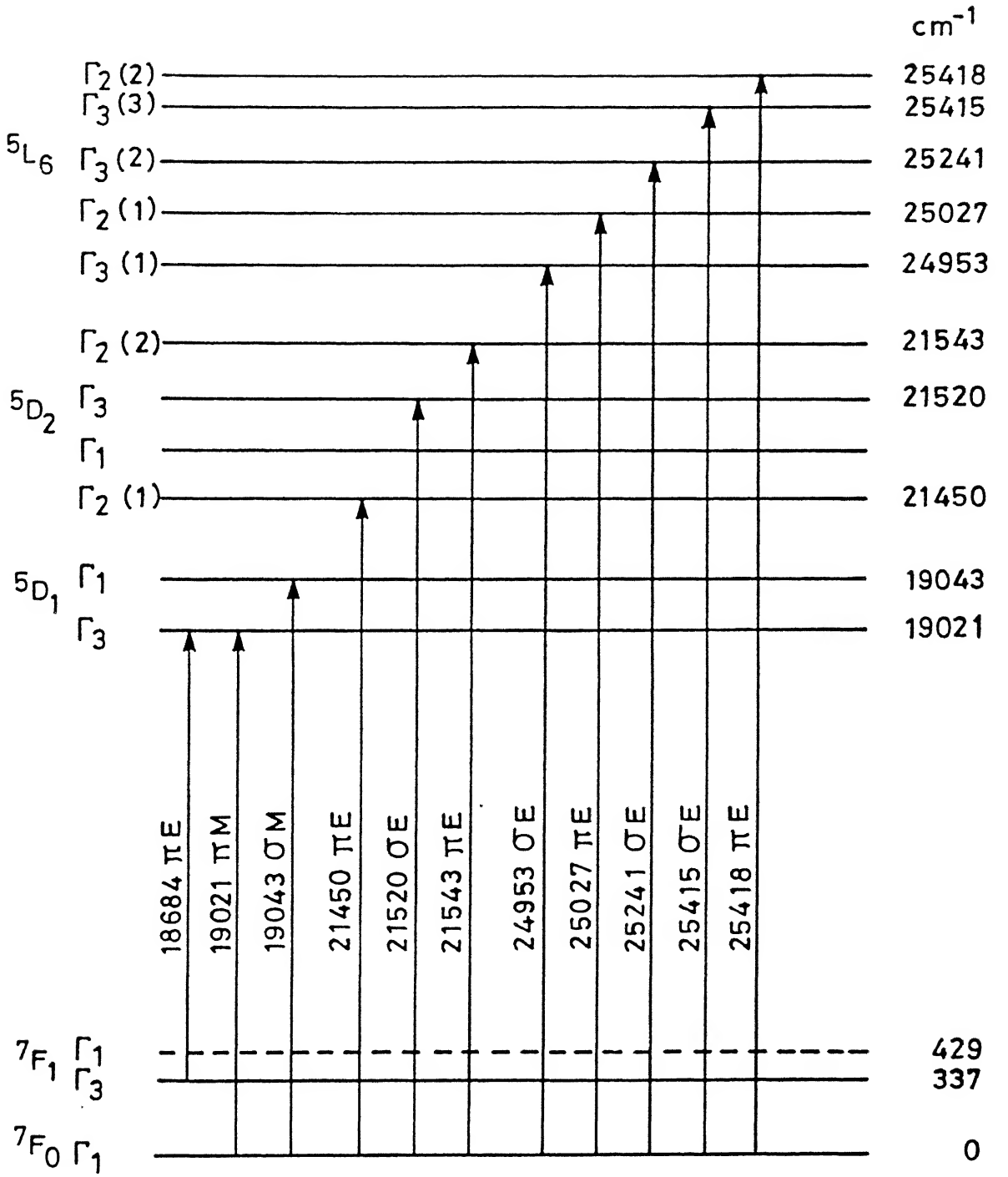

FIG.4.1 : OBSERVED ABSORPTION TRANSITIONS

the Ar^+-laser lines. The 457.9 nm (21838 cm^{-1}) laser line can excite $^5D_2$ levels of Eu^{3+} by phonon assisted processes. This excitation produces fluorescence from $^5D_1$ and ^5D_o as well. The exact mechanism of energy transfer (radiative or non-radiative) from $^5D_2$ to $^5D_1$ and ^5D_o multiplets could not be ascertained because of spectral range limitations of the monochromator, but radiative transitions are expected to be primarily responsible for this transfer. Similarly the 514.5 nm (19436 cm^{-1}) line can excite $^5D_1$ and ^5D_o levels. But the fluorescence with 514.5 nm excitation is relatively weaker than the fluorescence with 457.9 nm excitation. The ^5D_o level at 17271 cm^{-1} falls in the tuning range of the R 6G dye. Attempts to excite ^5D_o from the ground level ^7F_o using dye laser were not successful because of severe restriction on the ^7F_o —— ^5D_o transition. The excitation spectrum monitored with ^5D_o—— $^7F_1(\Gamma_1)$ transition at 16840 cm^{-1} shows that the ^5D_o level can be excited quite efficiently with the dye laser lasing at 16938 cm^{-1} and 17640 cm^{-1}. The excitation at 17640 cm^{-1} is a phonon assisted one while 16938 cm^{-1} corresponds to the $^7F_1(\Gamma_3)$—— $^5D_o(\Gamma_1)$ transition. We discuss below the symmetry assignments for various groups of fluorescence lines.

^5D_o-^7F_o FLUORESCENCE

This transition is forbidden by many selection rules (ie (J=0 to J'=0 is forbidden for E.D. and M.D. both and Γ_1—— Γ_1

is forbidden for E.D.). This was the reason why it was not observed in the absorption spectrum. A very weak and broad line at 17271 cm^{-1} corresponding to the highly forbidden $^5D_o(\Gamma_1') \longrightarrow {}^7F_o(\Gamma_1')$ transition was observed when the sample was excited by the 457.9 nm line of the Ar^+ laser and 16938 cm^{-1} lines of R 6G laser. The detection of this line was made difficult due to the presence of a Hg line at 17269 cm^{-1}. Another evidence of the position of the ^5D_o level comes from the excitation spectrum, which shows a sharp excitation at 17270 cm^{-1} (Section 4.3 of Chapter III). Polarization characteristics of this line are consistant with a pure σ-M.D. transition. Additional weak but persistent lines observed at 17292 cm^{-1}, 17250 cm^{-1} and 17231 cm^{-1} can be associated with the vibronic lines (c.f. Table 3.8).

$^5D_1$-^7F_o FLUORESCENCE

This group has two lines at 19043 cm^{-1} and 19021 cm^{-1} in agreement with the ^7F_o-$^5D_1$ absorption spectrum (Fig 3.19). The 19043 cm^{-1} line corresponds to the $^5D_1(\Gamma_1')$-$^7F_o(\Gamma_1')$, M.D. transition, while the line at 19021 cm^{-1} corresponds to the $^5D_1(\Gamma_3')$-$^7F_o(\Gamma_1')$, E.D. transition. The position of both the Stark components of $^5D_1$ are well established.

$^5D_2$-^7F_o FLUORESCENCE

The spectrum corresponding to this group of transitions could be obtained only with the 457.9 nm excitation. This

group has 4 sharp and medium strong lines at 21543 cm^{-1}, 21520 cm^{-1}, 21470 cm^{-1}, 21450 cm^{-1} and 5 very weak lines at positions 21570 cm^{-1}, 21509 cm^{-1}, 21463 cm^{-1}, 21458 cm^{-1} and 21408 cm^{-1} (Fig 3.13). The lines 21543 cm^{-1} and 21450 cm^{-1} are strong in π-spectrum and very weak in σ and axial spectra. These are π-E.D. transitions attributed to the $\Gamma_2(2) - \Gamma_1$ and $\Gamma_2(1) - \Gamma_1$ transitions. The line at 21520 cm^{-1}, strong in σ and axial spectra, but weak in the π-polarization, corresponds to the σ-E.D. $\Gamma_3 - \Gamma_1$ transition. It has a small contribution from π-M.D. transition as well. The 21470 cm^{-1} line can not be assigned to the remaining Stark component $^5D_2(\Gamma_1)$, because it is not consistent with the other group of transitions. All of the weak lines are Raman or vibronic lines with the phonon energies 268 cm^{-1}, 329 cm^{-1}, 375 cm^{-1}, 380 cm^{-1} and 430 cm^{-1}. The line at 21470 cm^{-1} is quite different from the Raman lines and corresponds to the Ar^+ line at 465.8 nm. Thus all the lines of this group are explained. The observed fluorescence transitons terminating on the ^7F_o are shown in Fig.4.2. The $^5D_2(\Gamma_1)$ component is not yet identified.

$^5D_o - ^7F_1$ FLUORESCENCE

The $^7F_1$ multiplet has two Stark component (Γ_1, $\Gamma_{3,4}$). The observed spectrum has two sharp and extremely strong lines at 16938 cm^{-1}, 16842 cm^{-1} and a weak shoulder at

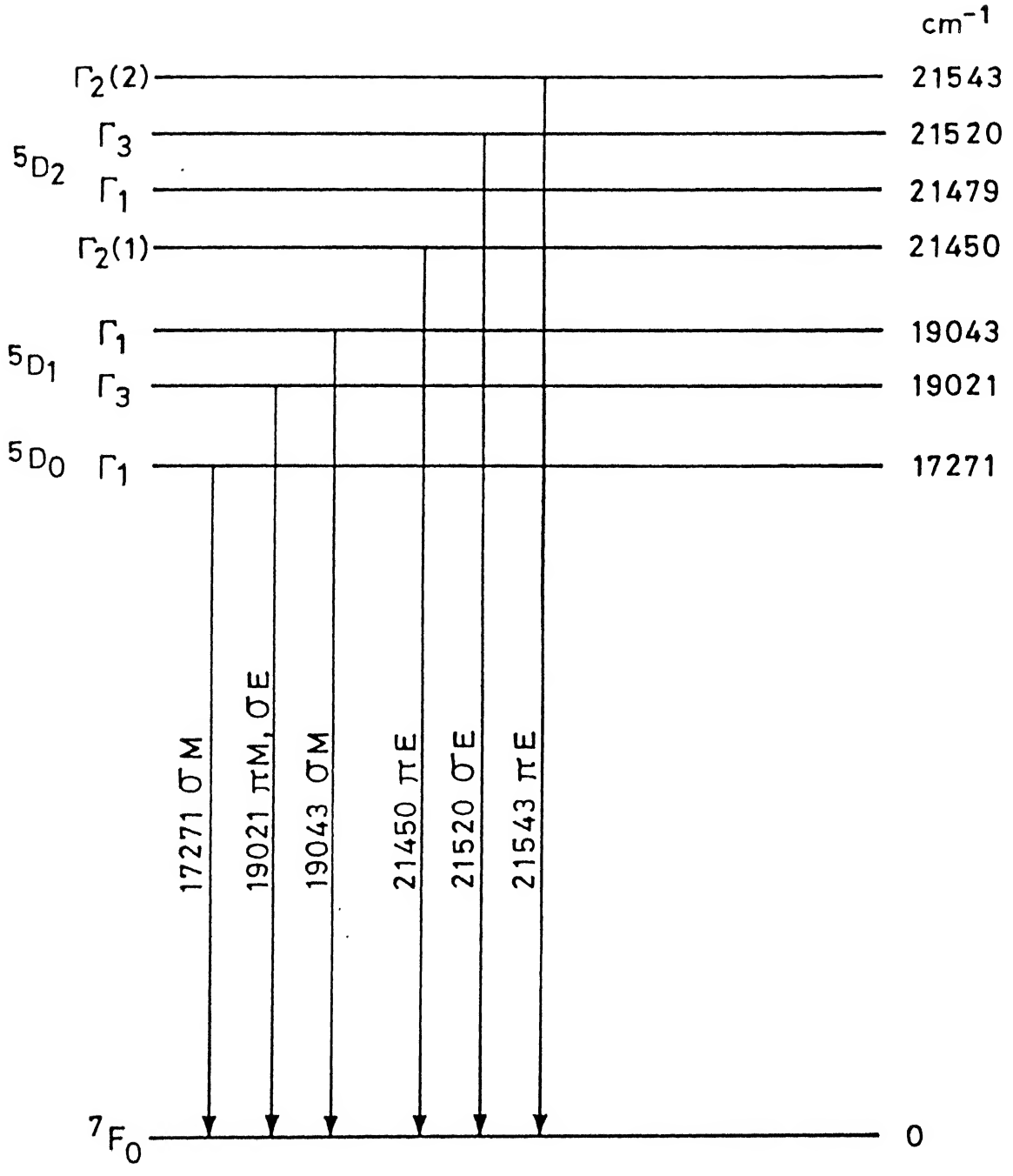

FIG.4.2 : FLUORESCENCE TRANSITIONS TERMINATING ON THE GROUND TERM ^7F_o.

16933 cm^{-1} (Fig 3.24) for excitations by 457.9 mm, 514.5 m and R 6G (Tables 3.5, 3.6, 3.7). The line at 16938 cm^{-1} is a π-M.D. dominant transition with a small contribution from σ-E.D. and corresponds to the $\Gamma_1 - \Gamma_3$ transition. This gives the position of the $^7F_1(\Gamma_3)$ level at 333 cm^{-1}. The line at 16842 cm^{-1} appearing strongly in σ-polarization, but weakly in the axial and π-spectra, is a σ-M.D. transition corresponding to the $\Gamma_1 - \Gamma_1$ transition. This would establish the second Stark component (Γ_1) of $^7F_1$ at 429 cm^{-1}. The appearance of the 16842 cm^{-1} line in π and axial spectra is difficult to explain. The observed intensities are however weak. The shoulder at 16933 cm^{-1} remains unexplained.

$^5D_1 - ^7F_1$ FLUORESCENCE

Theoretically we expect four lines for this group. We have observed three fairly strong lines at 18710 cm^{-1}, 18687 cm^{-1} and 18593 cm^{-1} (Fig 3.19 and Tables 3.5; 3.6). The lines at 18710 cm^{-1} and 18593 cm^{-1} are dominant σ-E.D. transitions with a fair contribution of π-M.D. character. They correspond to the $\Gamma_1 - \Gamma_3$ and $\Gamma_3 - \Gamma_1$ transitions respectively. The line at 18687 cm^{-1} is strong in π-polarization but very weak in σ and axial spectra, indicating a π-E.D. dominant character. The only possible assignment for this line is $\Gamma_3 - \Gamma_3$. The $\Gamma_1 - \Gamma_1$ transition has not been observed. These transitions re-confirm the two Stark components of $^7F_1$ at 333 $cm^{-1}(\Gamma_3)$ and 429 $cm^{-1}(\Gamma_1)$.

$^5D_2$-$^7F_1$ FLUORESCENCE

Eight lines are observed for this group in the spectral range 21021 cm^{-1}-21209 cm^{-1} (Fig 3.13 and Table 3.5). The line at 21209 cm^{-1} is dominantly π-M.D. and corresponds to the $\Gamma_2'(2)$-Γ_3' transition. The 21187 cm^{-1} line is dominant π-E.D. but with a fair contribution of σ-M.D. character. This line can be associated with the $\Gamma_3' - \Gamma_3'$ transition. The line at 21158 cm^{-1} corresponds to the Ar^+ line at 472.7 nm. The fairly strong line at 21145 cm^{-1} is a σ-E.D. (dominant) transition with a fair contribution of π-M.D. character. Consistent with this observation, this line could possibly be assigned to the $\Gamma_1' - \Gamma_3'$, $\Gamma_3' - \Gamma_1'$ and $\Gamma_2' - \Gamma_3'$ transitions. The last two assignments are ruled out by energy difference considerations. The assignment $\Gamma_1' - \Gamma_3'$ would put the $^5D_2(\Gamma_1')$ Stark level at 21478 (21145+333) cm^{-1}. This assignment is further confirmed by the σ-M.D. transition $\Gamma_1' - \Gamma_1'$ appearing at 21048 cm^{-1} (21048+429 = 21477 cm^{-1}). Out of the remaining three lines, the line at 21117 cm^{-1} has equal intensity in π and σ polarizations and is stronger in axial spectrum indicating comparable contributions from σ-E.D. and π-M.D. transitions. This line can be associated with $\Gamma_2'(1) - \Gamma_3'$ or with $\Gamma_2'(2) - \Gamma_1'$ transition. More exact assignment is not possible for this line. The lines at 21090 cm^{-1} and 21021 cm^{-1} are π-M.D. and π-E.D. transitions attributed to the $\Gamma_3' - \Gamma_1'$ and $\Gamma_2'(1) - \Gamma_1'$ transitions respectively. All the observed

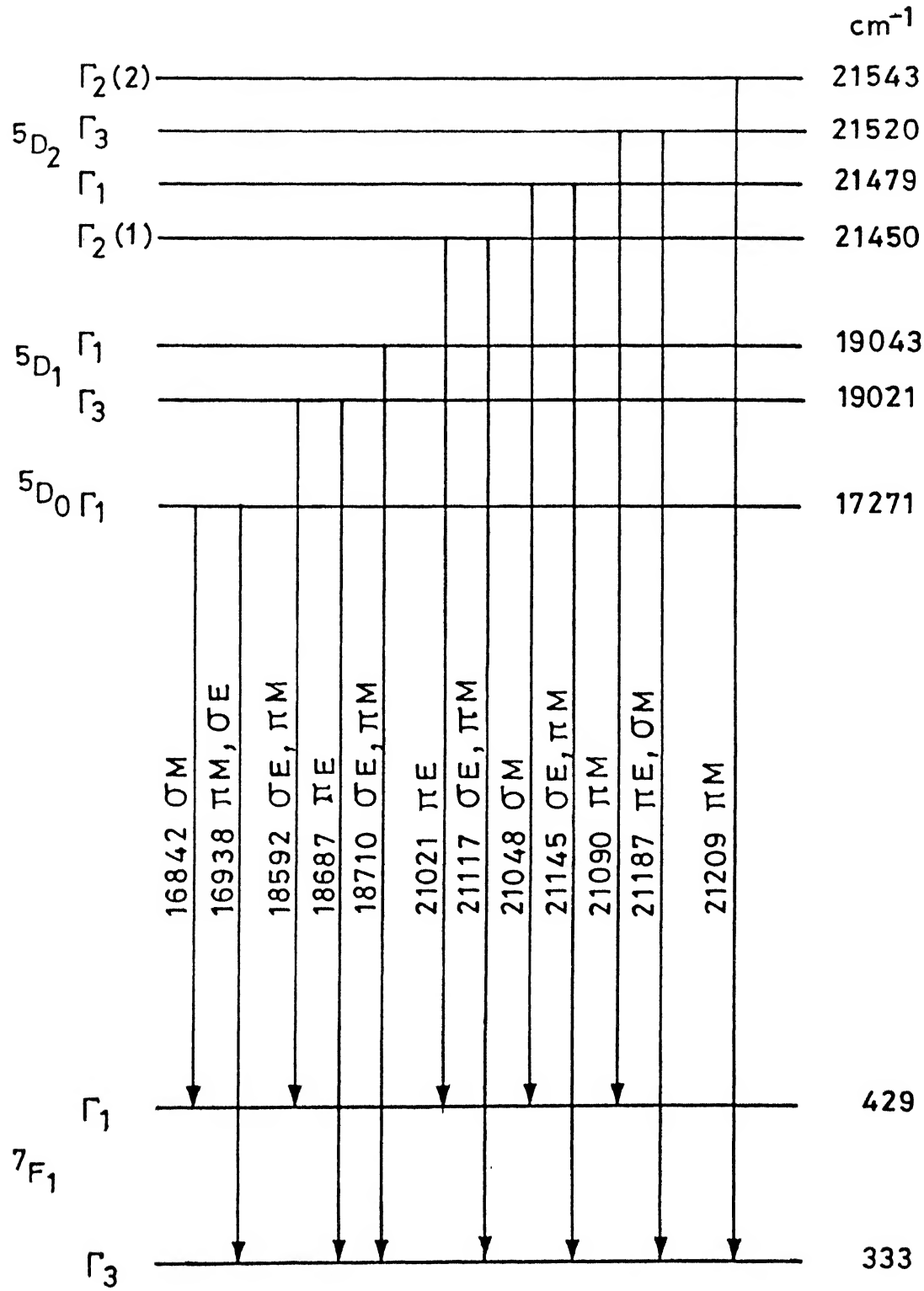

FIG.4.3 : FLUORESCENCE TRANSITIONS TERMINATING ON THE $^7F_1$ MULTIPLET.

fluorescence transitions terminating on the $^7F_1$ multiplet are shown in Fig 4.3.

^5D_o-$^7F_2$ FLUORESCENCE

Using dye laser excitation, we have observed three lines for this group at 16382 cm^{-1} 16295 cm^{-1} and 16122 cm^{-1} (Fig 3.25 Table 3.7). With other excitations these lines fall in the overlapping regions of the $^5D_1$-$^7F_4$ and $^5D_2$-$^7F_6$ transitions. The lines at 16382 cm^{-1} and 16122 cm^{-1} are dominantly π-polarized E.D. type and one assigned to the $^5D_o(\Gamma_1)$ - $^7F_2$ $\Gamma_2(1)$ and $^5D_o(\Gamma_1)$ — $^7F_2\Gamma_2(2)$ transitions respectively. This assignment would place the two Γ_2 Stark levels of $^7F_2$ at 889 cm^{-1} and 1151 cm^{-1}. The line at 16295 cm^{-1} is a dominant π-M.D. with comparable contribution of σ-E.D. character and would be consistent with the Γ_1 -Γ_3 assignment. We infer the position of the Γ_3 component of $^7F_2$ at 976 cm^{-1}. The Γ_1 -Γ_1 transition could not be seen.

$^5D_1$-$^7F_2$ FLUORESCENCE

The seven lines observed in the spectral range 17840 cm^{-1}-18155 cm^{-1} belong to this group (Fig 3.20 ; Tables 3.5 and 3.6). The weak line at 18142 cm^{-1} however does not belong to Eu^{3+}. The very weak but pure π-E.D. transitions at 18153 cm^{-1} and 17892 cm^{-1} are the Γ_1 -$\Gamma_2(1)$ and Γ_1 -$\Gamma_2(2)$ transitions terminating at 890 cm^{-1} and 1152 cm^{-1} respectively. The lines at 18132 cm^{-1}, 18067 cm^{-1} and 17869 cm^{-1} are dominant

π-M.D. with some contribution of σ-E.D. character and are assigned to the $\Gamma_3 - \Gamma_2(1)$, $\Gamma_1 - \Gamma_3$ and $\Gamma_3 - \Gamma_2(2)$ transitions. The line at 18044 cm^{-1} is dominantly σ-M.D. and is attributed to the $\Gamma_3 - \Gamma_3$ transition. The line at 17846 cm^{-1} is the π-M.D. ($\Gamma_3 - \Gamma_1$) transition and gives the position of the $^7F_1(\Gamma_1)$ level as 1175 cm^{-1}.

$^5D_2$-$^7F_2$ FLUORESCENCE

Theoretically, we expect 16 lines for this group. We have observed 13 lines in the spectral range 20270 cm^{-1} - 20650 cm^{-1} (Fig 3.14,Table 3.5). The line at 20629 cm^{-1} with mixed σ-E.D.(dominant) and π-M.D. character can be assigned to the $\Gamma_3 - \Gamma_2(1)$ transition and the 20589 cm^{-1} line with π-E.D. character is assigned to the $\Gamma_1 - \Gamma_2(1)$ transition. The lines at 20567 cm^{-1}, 20502 cm^{-1} and 20474 cm^{-1} are σ-E.D. (dominant) with some π-M.D. character, while the line at 20545 cm^{-1} is dominant π-E.D. with a small contribution from σ-M.D. They respectively correspond to the $\Gamma_2(2) - \Gamma_3$, $\Gamma_1 - \Gamma_3$, $\Gamma_2(1) - \Gamma_3$ and $\Gamma_3 - \Gamma_3$ transitions and give the position of the terminal level $^7F_2(\Gamma_3)$ at 976 cm^{-1}, 977 cm^{-1}, 976 cm^{-1} and 975 cm^{-1} respectively. The 20390 cm^{-1} line is extremely weak and can be assigned to the $\Gamma_2(2) - \Gamma_2(2)$ σ-M.D. transition suggesting the terminal level $^7F_2$ $\Gamma_2(2)$ to lie at 1153 cm^{-1}. The broad line at 20369 cm^{-1} appears unpolarized and may correspond to the two

transition $\Gamma_3 - \Gamma_2(2)$ and $\Gamma_2(2) - \Gamma_1$ terminating on the 1151 cm^{-1} and 1174 cm^{-1} levels of $^7F_2$ respectively. The weak lines at 20344 cm^{-1} and 20271 are assigned to the (σ E.D., π M.D.) $\Gamma_3 - \Gamma_1$ and π-E.D. $\Gamma_2(1) - \Gamma_1$ transitions respectively giving the positions of the terminal levels at 1176 and 1179 cm^{-1} although the polarization behavior of the 20271 cm^{-1} line is not quite consistent with this assignment. Out of the remaining three lines, the one at 20493 cm^{-1} being quite sharp and strong corresponds to the 488.0 nm of Ar^+ line and the extremely weak lines at 20578 cm^{-1} and 20455 cm^{-1} remain unexplained. Fig. 4.4 shows all the observed transitions terminating on the $^7F_2$ multiplet.

$^5D_o - ^7F_3$ FLUORESCENCE

The J=3 multiplet splits into five Stark components in S_4 symmetry ($\Gamma_1 + 2\Gamma_2 + 2\Gamma_{3,4}$). We have observed 4 well separated lines for this group (Fig 3.26, Tables 3.5, 3.6 and 3.7) in the spectral range 15300 cm^{-1} - 15420 cm^{-1}. The line at 15411 cm^{-1} is π-E.D. dominant and corresponds to the $\Gamma_1 - \Gamma_2(1)$ transition. It assigns the level at 1860 cm^{-1} to one of the Γ_2 components of $^7F_2$. The 15398 cm^{-1} and 15317 cm^{-1} lines with dominant σ-E.D. character with fair contribution from π-M.D. is assigned to the $\Gamma_1 - \Gamma_3$ transitions. From these assignments, we deduce the $\Gamma_3(1)$ and $\Gamma_3(2)$ components of $^7F_2$ at 1873 cm^{-1} and 1954 cm^{-1} respectively

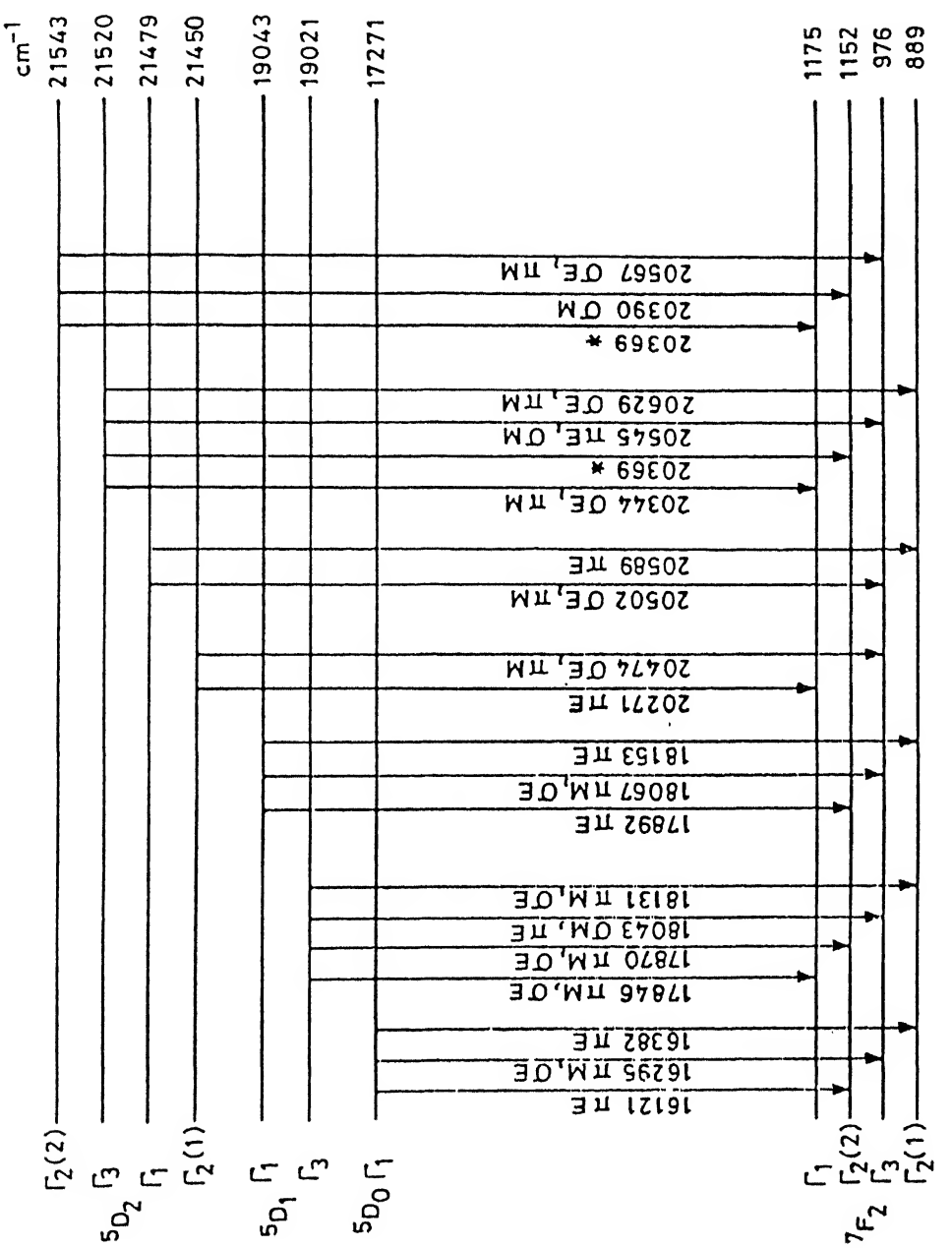

FIG.4.4 : FLUORESCENCE TRANSITIONS TERMINATING ON THE $^7F_2$ MULTIPLET.

(*Indicates wavenumbers corresponding to two transitions)

The line at 15369 cm^{-1} is a pure σ-M.D. ($\Gamma_1 - \Gamma_1$) transition and gives the position of the $^7F_2(\Gamma_1)$ level as 1902 cm^{-1}.

$^5D_1$-$^7F_3$ FLUORESCENCE

Out of the expected ten lines belonging to this group, we have observed nine in the spectral range 16950 cm^{-1} to 17200 cm^{-1}. There are 4 lines of mixed nature (σ-E.D. + π-M.D.) with σ-E.D. dominant at 17172 cm^{-1}, 17162 cm^{-1}, 17119 cm^{-1} and 17092 cm^{-1}. These lines are attributed to the $\Gamma_1 - \Gamma_3(1)$, $\Gamma_3 - \Gamma_2(1)$, $\Gamma_3 - \Gamma_1$ and $\Gamma_1 - \Gamma_3(2)$ transitions respectively giving the terminal levels of the $^7F_3$ multiplet at 1871 cm^{-1}, 1859 cm^{-1}, 1902 cm^{-1} and 1951 cm^{-1}. The line at 17185 cm^{-1}, overall weak but dominantly π-E.D. corresponds to the $\Gamma_1 - \Gamma_2(1)$ transition terminating at 1858 cm^{-1}. The three lines at 17149 cm^{-1}, 17069 cm^{-1} and 17006 cm^{-1} are predominantly π-E.D. with small intensity in σ-polarization correspond to the $\Gamma_3 - \Gamma_3(1)$, $\Gamma_3 - \Gamma_3(2)$ and $\Gamma_1 - \Gamma_2(2)$ transitions respectively. The terminal levels are 1872 cm^{-1}, 1952 cm^{-1} and 2038 cm^{-1}. The remaining one line has comparable contribution from π-M.D. and σ-E.D. transition and is attributed to the $\Gamma_3 - \Gamma_2(2)$ transition with the $^7F_3(\Gamma_2)$ at 2038 cm^{-1}. Thus this group gives all the Stark components of $^7F_3$ and confirms the assignments of the ^5D_o-$^7F_3$ group.

assigned to the $\Gamma_3 - \Gamma_3(2)$ transition, terminating at 1954 cm^{-1}. The 19548 cm^{-1} is dominantly π-E.D. $\Gamma_2(1) - \Gamma_1$ transition, terminating at the 1902 cm^{-1} level, but its weak appearance in the σ and axial spectra is not consistent with this assignment. The lines at 19525 cm^{-1} and 19480 cm^{-1} are dominantly π-M.D. assigned to the $\Gamma_1 - \Gamma_3(2)$ and $\Gamma_3 - \Gamma_2(2)$, transitions, terminating at 1954 cm^{-1} and 2040 cm^{-1} respectively. The transition corresponding to 19496 cm^{-1} is π-M.D. with comparable contribution from σ-E.D. and is attributed to the $\Gamma_2(1) - \Gamma_3(2)$, transition with Γ_3 at 1954 cm^{-1}. The last line at 19439 cm^{-1} is extremely weak but pure π-E.D. ($\Gamma_1 - \Gamma_2(2)$) transition, terminating at 2040 cm^{-1}. These assignments are in agreement with the assignments made in the previous two groups. Fig. 4.5 shows all transitions terminating on the $^7F_3$ multiplet.

$^5D_0 - ^7F_4$ FLUORESCENCE

The multiplet with J=4 splits into 7 Stark components in a crystal field of the S_4 symmetry ($3\Gamma_1+2\Gamma_2+2\Gamma_3$). We have observed 4 strong peaks and two very weak lines for this group in the spectral region 14200 cm^{-1}-14700 cm^{-1} (Fig 3.27 and Tables 3.5, 3.6 and 3.7). The spectra in the range 14500 cm^{-1} - 14700 cm^{-1} are not included in the Fig 3.27 . The two weak lines at 14664 cm^{-1} and 14400 cm^{-1} are σ-M.D. $\Gamma_1 - \Gamma_1$ transitions, terminating on the $\Gamma_1(1)$ and $\Gamma_1(2)$ levels at 2607 cm^{-1} and 2871 cm^{-1} respectively. The

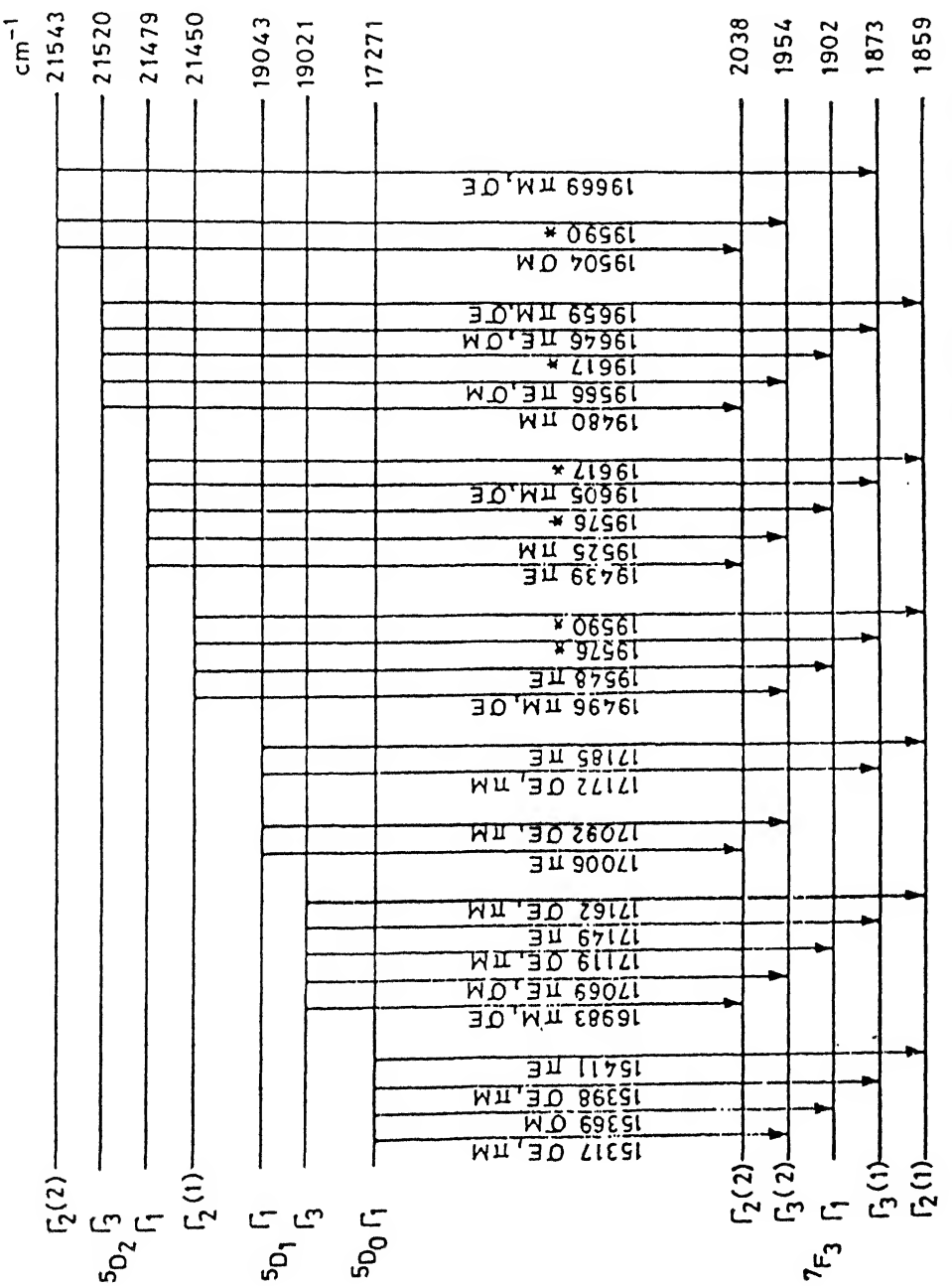

FIG.4.5 : FLUORESCENCE TRANSITIONS TERMINATING ON THE $^7F_3$ MULTIPLET.

(*Indicates wavenumber corresponding to two transitions)

lines at 14458 cm^{-1} and 14259 cm^{-1} are (π-M.D.+ σ-E.D.) $\Gamma_1 - \Gamma_3$ transitions. They predict the two Γ_3 components of $^7F_4$ at 2813 cm^{-1} and 3012 cm^{-1}. The remaining two lines at 14366 cm^{-1} and 14294 cm^{-1} are π-E.D., $\Gamma_1 - \Gamma_2$ transitions and assigned the positions of the two Γ_2 components at 2905 cm^{-1} and 2977 cm^{-1}.

$^5D_1 - ^7F_4$ FLUORESCENCE

We have observed 11 lines belonging to this group out of 14 expected lines (Fig 3.22 Table 3. 5 and 3. 6). The line 16436 cm^{-1} observed only with the 457.9 cm^{-1} excitation is extremely weak σ-M.D. type attributed to the $\Gamma_1 - \Gamma_1(1)$ transition yielding $^7F_4(\Gamma_1)$ level at 2607 cm^{-1}. The line at 16413 cm^{-1} is dominantly σ-E.D., $\Gamma_3 - \Gamma_1(1)$ transition with terminal level Γ_1 at 2608 cm^{-1}. The line at 16229 cm^{-1} having comparable contribution from π-M.D. and σ-E.D. corresponds to the $\Gamma_1 - \Gamma_3(1)$ transition, terminating at 2814 cm^{-1}. The line at 16208 cm^{-1}, π-E.D. (dominant) + σ-M.D. is the $\Gamma_3 - \Gamma_3(1)$ transition suggesting the $^7F_4(\Gamma_3)$ level at 2813 cm^{-1}. The lines at 16149 cm^{-1} and 16138 cm^{-1} are not well resolved, but their observed polarization behavior predicts them to be (σ-E.D.+π-M.D.) $\Gamma_3 - \Gamma_1(2)$, and π-E.D. ($\Gamma_1 - \Gamma_2(1)$) transition corresponding to the $^7F_4(\Gamma_1)$ at 2872 cm^{-1} and $^7F_4(\Gamma_2)$ at 2905 cm^{-1} respectively. The extremely weak line at 16064 cm^{-1} shows up only in the π-polarization and hence can be assigned to the $\Gamma_1 - \Gamma_2(2)$,

π-E.D. transition. The strong line at 16042 cm^{-1} has comparable contribution from σ-E.D. and π-M.D., $\Gamma_3 - \Gamma_2(2)$ transitions. Both the transitions assign to the $\Gamma_2(2)$ level a position of 2979 cm^{-1}. The line 16009 cm^{-1} is very strong and dominantly π-E.D. type assigned to the $\Gamma_3 - \Gamma_3(2)$ transition with 3012 cm^{-1} as the position of $^7F_4$ (Γ_3) line. A shoulder at 16032 cm^{-1} associated with the 16042 cm^{-1} line also corresponds to the $\Gamma_1 - \Gamma_3(2)$ transition and gives the $\Gamma_3(2)$ level a position of 3011 cm^{-1}. The line at 15940 cm^{-1} is (π-M.D.+σ-E.D.) type and can be assigned to the $\Gamma_3 - \Gamma_1(3)$, transition giving $\Gamma_1(3)$ a position of 3081 cm^{-1}. Thus all the seven Stark components of the $^7F_4$ are identified.

$^5D_2$-$^7F_4$ FLUORESCENCE

The spectrum in the spectral range corresponding to this group is somewhat complex. The strong transitions belonging to the $^5D_1$-$^7F_1$ may mask many of the lines of the $^5D_2$-$^7F_4$ group. Some of the lines are not well resolved, others are very weak. We have been able to identify some 16 lines belonging to this group out of the 28 lines expected theoretically. There are many extra lines which could not be explained in terms of Eu^{3+} transitions and remain unassigned (Fig 3.16 ,Table 3.5). There are two extremely weak lines at 18912 cm^{-1} and 18842 cm^{-1} (not shown in the Fig), which correspond to the $\Gamma_3 - \Gamma_1(1)$ and $\Gamma_2(1) - \Gamma_1(1)$ transitions if the energy differences are

matched. The terminal level $\Gamma_1(1)$ is at 2608 cm^{-1}. The two weak lines at 18666 cm^{-1}, 18636 cm^{-1} are (π-M.D. (dominant)+σ-E.D.) and σ-E.D. respectively and are assigned to the $\Gamma_1 - \Gamma_3(1)$ and $\Gamma_2(1) - \Gamma_3(1)$ transitions respectively. The line at 18619 cm^{-1} appearing fairly strong in σ-polarization is somewhat masked by the 18595 cm^{-1} line of the $^5D_1 - ^7F_1$ group, corresponds to the $\Gamma_3 - \Gamma_2(1)$ transition with $^7F_4(\Gamma_2)$ level at 2901 cm^{-1}. The line at 18574 cm^{-1} a clear shoulder in the π-and σ-polarization but masked in the axial spectra by the 18595 cm^{-1} strong line may correspond to the $\Gamma_1 - \Gamma_2(1)$ transition with $\Gamma_2(1)$ at 2905 cm^{-1}. Again at 18565 cm^{-1} is a weak shoulder appearing more clearly in σ-polarization, which corresponds to the $\Gamma_2(2) - \Gamma_2(2)$ transition with $^7F_4(\Gamma_2)$ level at 2978 cm^{-1}. The line at 18542 cm^{-1} is σ-E.D. (dominant)+π-M.D. $\Gamma_3 - \Gamma_2(2)$ transition with $\Gamma_2(2)$ level at 2978 cm^{-1}. The line at 18528 cm^{-1} is π-M.D. (dominant)+σ-E.D., $\Gamma_2(2) - \Gamma_3(2)$ transition and confirms the $^7F_4(\Gamma_3)$ position at 3015 cm^{-1}. By energy difference consideration alone, the line at 18505 cm^{-1} can be assigned to the $\Gamma_3 - \Gamma_3(2)$ transition though polarization behavior does not quite satisfy this assignment. There are two overlapping lines at 18471 cm^{-1} and 18467 cm^{-1} which correspond to the $\Gamma_2(1) - \Gamma_2(2)$ and $\Gamma_1 - \Gamma_3(2)$ transitions. The line at 18436 cm^{-1} π-M.D.(dominant)+σ-E.D. is a superposition of the $\Gamma_3 - \Gamma_1(3)$ and $\Gamma_2(1) - \Gamma_3(2)$ transitions. The line at 18394 cm^{-1} corresponds to the $\Gamma_1 - \Gamma_1(3)$ transition according to energy

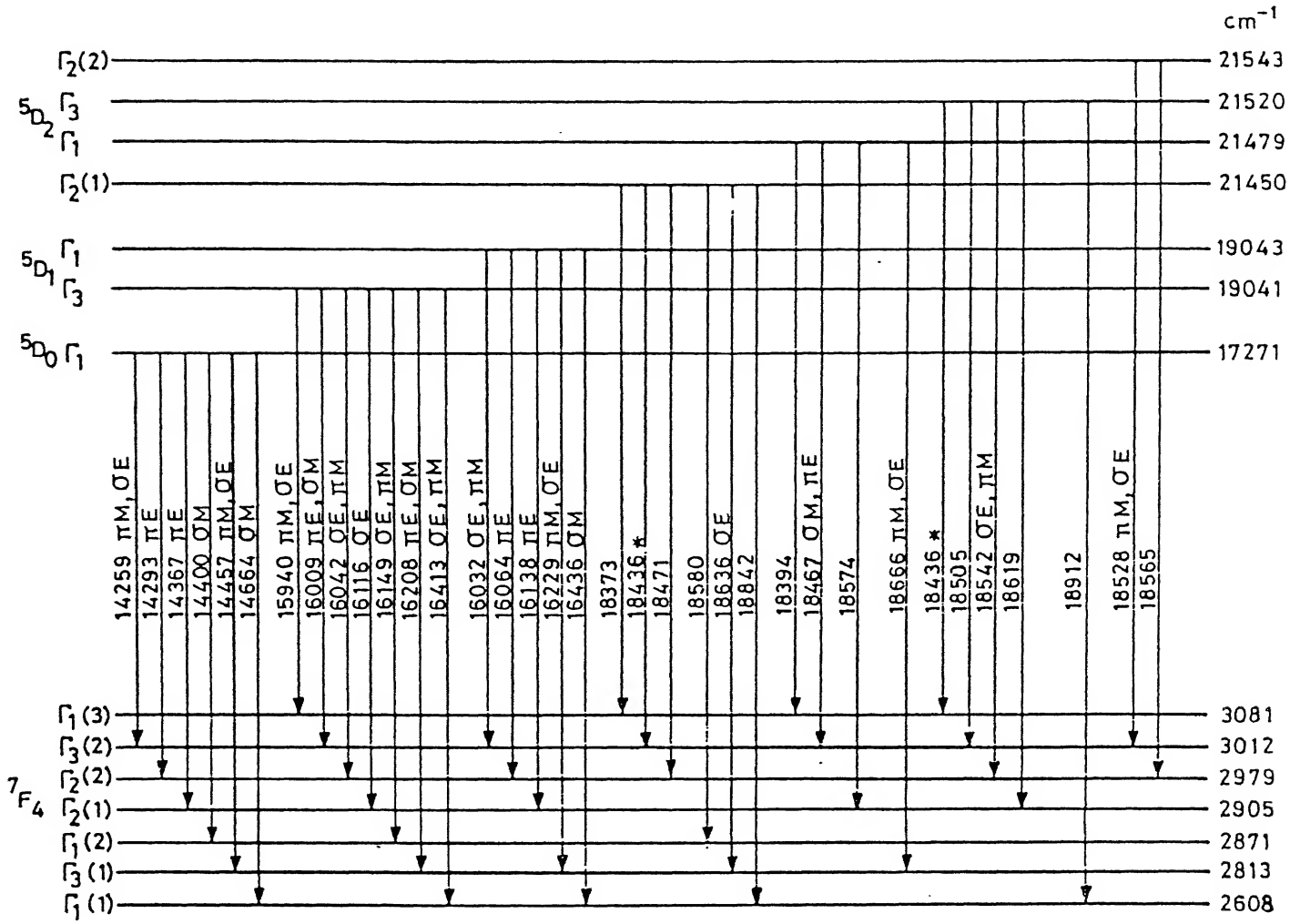

FIG.4.6 : FLUORESCENCE TRANSITIONS TERMINATING ON THE $^7F_4$ MULTIPLET.

(*Indicates wavenumbers corresponding to two transitions)

difference consideration alone. All the assignments in this group support the assignments made for the ^5D_o-$^7F_4$ and $^5D_1$-$^7F_4$ groups. Fig 4.6 shows observed fluorescence transition terminating on the $^7F_4$ multiplet.

^5D_o-$^7F_5$ FLUORESCENCE

The $^7F_5$ multiplet splits into 8 Stark components in S_4 symmetry ($3\Gamma_1+2\Gamma_2+3\Gamma_{3,4}$). We have observed only four lines in the spectral range 13200 cm^{-1} - 13500 cm^{-1} (Fig 3.28 , Table 3.7). These lines could be observed only with R-6G dye laser excitation at 16938 cm^{-1}. The line at 13485 cm^{-1} is dominantly π-E.D. type and is attributed to the $\Gamma_1 - \Gamma_2(1)$ transition. The two lines at 13472 cm^{-1} and 13271 cm^{-1} are σ-E.D. types and are assigned to the $\Gamma_1 - \Gamma_3(1)$ and $\Gamma_1 - \Gamma_3(2)$ transitions respectively. The line at 13219 cm^{-1} seen in σ-polarization only but extremely weak can be assigned to the $\Gamma_1 - \Gamma_3(3)$ transition. These four transitions give the 4 Stark levels, $\Gamma_2(1)$, $\Gamma_3(1)$, $\Gamma_3(2)$ and $\Gamma_3(3)$ of the $^7F_5$ multiplet at 3786 cm^{-1}, 3799 cm^{-1}, 4000 cm^{-1} and 4052 cm^{-1} respectively.

$^5D_1$-$^7F_5$ FLUORESCENCE

We have observed 15 lines in the spectral range 14900 cm^{-1} - 15300 cm^{-1} (Fig 3.23 and Table 3.5). This group could be recorded only with 457.9 nm excitation. The line at 15283 cm^{-1} could not be identified. The line at 15245 cm^{-1}

is σ-E.D. (dominant)+π-M.D. type and is attributed to the $\Gamma_1 - \Gamma_3(1)$ transition with the $\Gamma_3(1)$ level predicted at 3798 cm^{-1}. The 15236 cm^{-1} line appears to be unpolarized and energy wise can correspond to the $\Gamma_1 - \Gamma_2(2)$ transition belonging to $^5D_0 - ^7F_3$ group or the $\Gamma_3 - \Gamma_2(1)$ transition belonging to $^5D_1 - ^7F_5$ group. The line at 15223 cm^{-1} is π-E.D. type and is assigned to the $\Gamma_3 - \Gamma_3(1)$ transition. The lines at 15214, 15203 and 15054 cm^{-1} are extremely weak and could not be assigned to Eu^{3+} transitions. The line at 15191 cm^{-1} predicts a Γ_3 level of $^7F_5$ at 3852 cm^{-1} or a Γ_1 level at 3830 cm^{-1}, both are not supported by any other evidence and consequently this line is left unassigned. The 15177 cm^{-1} line is σ-E.D. and corresponds to the $\Gamma_3 - \Gamma_1(1)$ transition. This assigns the $\Gamma_1(1)$ level of the $^5F_7$ multiplet at 3844 cm^{-1}. The extremely weak, σ-E.D. type line at 15044 cm^{-1} is assigned to the $\Gamma_1 - \Gamma_3(2)$ transition and gives the $\Gamma_3(2)$ line of $^7F_5$, a position of 4000 cm^{-1}. The relatively strong line at 15022 cm^{-1} (σ-E.D.+σ-M.D.) is attributed to the $\Gamma_3 - \Gamma_3(2)$ transition. The lines at 15014 cm^{-1} and 14994 cm^{-1} are σ-E.D. transitions assigned to the $\Gamma_3 - \Gamma_1(2)$ and $\Gamma_1 - \Gamma_3(3)$ transitions respectively. The assignments predict the positions of the $\Gamma_1(2)$ and $\Gamma_3(3)$ levels of $^7F_5$ at 4007 cm^{-1} and 4050 cm^{-1} respectively. The 14971 cm^{-1} line is dominant π-E.D. type with some contribution from σ-M.D. and corresponds to the $\Gamma_3 - \Gamma_3(3)$ transition.

$^5D_2$-$^7F_5$ FLUORESCENCE

This group of fluorescence lines is observed in the spectral range of 17370 cm^{-1} - 17750 cm^{-1} (Fig 3.17 , Table 3.5). The Following lines are identified as belonging to this group. The lines at 17745 and 17719 cm^{-1} are (π-M.D.+σ-E.D.) and (σ-M.D.+π-E.D.) types corresponding to the $\Gamma_2(2) - \Gamma_3(1)$ and $\Gamma_3 - \Gamma_3(1)$ transitions respectively. The 17691 cm^{-1} line is a π-E.D. type and can correspond to the $\Gamma_1 - \Gamma_2(1)$ and $\Gamma_2(2) - \Gamma_1(1)$ transitions. It is not possible to make a more definite assignment for this line. The line at 17678 cm^{-1} is (π-M.D.+σ-E.D.) and is assigned to the $\Gamma_1 - \Gamma_3(1)$ transition. The three lines at 17605 cm^{-1}, 17533 cm^{-1} and 17443 cm^{-1} are π-E.D. type and are assigned to the $\Gamma_2(1) - \Gamma_1(1)$, $\Gamma_2(2) - \Gamma_1(2)$, $\Gamma_2(1) - \Gamma_1(2)$ transitions respectively. Further from σ-E.D. transitions lines at 17480 cm^{-1} 17451 cm^{-1}, 17428 cm^{-1} and 17400 cm^{-1}, are attributed to the $\Gamma_1 - \Gamma_3(2)$, $\Gamma_2(1) - \Gamma_3(2)$, $\Gamma_1 - \Gamma_3(3)$ and $\Gamma_2(1) - \Gamma_3(3)$ transitions. Thus out of the eight Stark components of $^7F_5$ we are able to give tentative assignments to six. The observed fluorescence transitions to the $^7F_5$ multiplet are shown in Fig 4.7.

$^5D_2$-$^7F_6$ FLUORESCENCE

We could not observe any fluorescence from ^5D_o and $^5D_1$ to the $^7F_6$ multiplet. The $^5D_2$-$^7F_6$ fluorescence has been

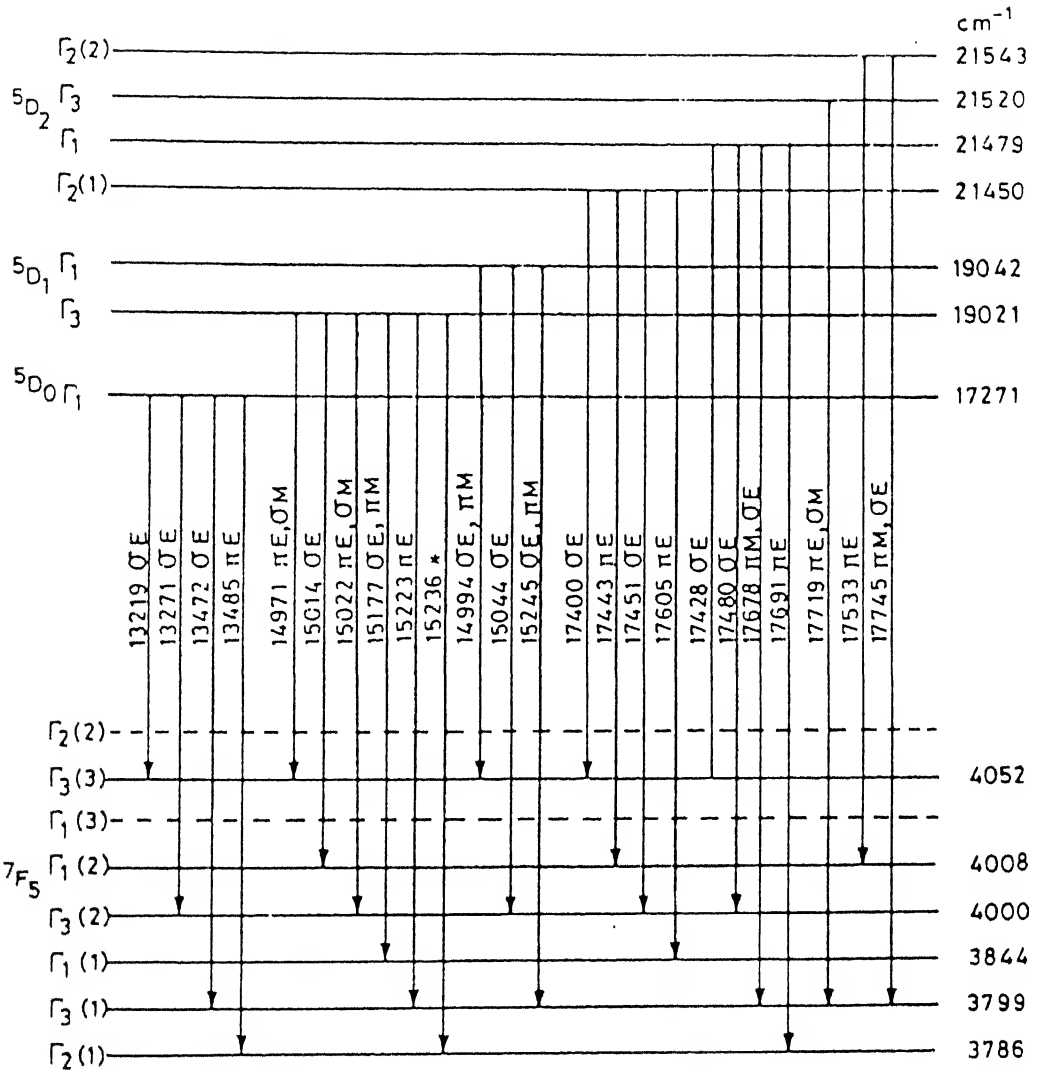

FIG.4.7 : FLUORESCENCE TRANSITIONS TERMINATING ON THE $^7F_5$ MULTIPLET.

(*Indicates wavenumber corresponding to two transitions)

observed (Fig 3.18), but could not be analyzed. These lines are closely spaced, broad and not well resolved.

Table 4.1 lists the mean positions of the energy levels, the tentative symmetry assignments and the CG's of the multiplets as obtained from experimental results. The procedure employed for obtaining these results is outlined in appendix III.

EXTRA-LINES

The fluorescence spectra recorded from our sample have many lines which apparently do not belong to Eu^{3+}. These lines are marked a, b or c in Figures 3.13 to 3.28 and Tables 3.5 to 3.7. The lines marked 'b' are Hg-lines due to the room light while those marked 'c' correspond to Ar^{+} lines. There is a very strong line at 20866 cm^{-1} and a weak line at 20788 cm^{-1}, which may correspond to the $^3P_o(\Gamma_1') - {}^3H_4(\Gamma_2')$ and $^3P_o(\Gamma_1') - {}^3H_4(\Gamma_3')$ transitions of Pr^{3+}. This indicates the presence of small Pr^{3+} impurity in the crystal under study. Other extra lines which may originate from Pr^{3+} impurity are 20706 cm^{-1} (vibronic), 20671 cm^{-1} vibronic and 18580 cm^{-1} ($^3P_o - {}^3H_5$). The remaining extra lines marked 'a' have not been accounted for in this work.

3. CALCULATION OF ENERGY LEVELS

As mentioned earlier, $H'_{cry} < H'_{s-o} + H'_{Coul}$ but H'_{cry} is not so small to be confidently treated within the framework of

TABLE 4.1

OBSERVED POSITIONS OF ENERGY LEVELS OF $LiYF_4:Eu^{3+}$

S.No.	Multiplet	Symmetry Assignment (tentative)	Energy (cm^{-1})	C.G. (cm^{-1})
1.	^7F_o	Γ_1	0	0
2.	$^7F_1$	Γ_1	429	365
		$\Gamma_{3,4}$	333	
3.	$^7F_2$	Γ_1	1175	1033.6
		Γ_2	1152	
		$\Gamma_{3,4}$	976	
		Γ_2	889	
4.	$^7F_3$	Γ_2	2038	1921.9
		$\Gamma_{3,4}$	1954	
		Γ_1	1902	
		$\Gamma_{3,4}$	1873	
		Γ_2	1859	
5.	$^7F_4$	Γ_1	3081	2899.3
		$\Gamma_{3,4}$	3012	
		Γ_2	2979	
		Γ_2	2905	
		Γ_1	2871	

		$\Gamma_{3,4}$	2813	
		Γ_1	2608	
6.	$^7F_5$	Γ_2	-	3948
		$\Gamma_{3,4}$	4052	
		Γ_1	-	
		Γ_1	4008	
		$\Gamma_{3,4}$	4000	
		Γ_1	3844	
		$\Gamma_{3,4}$	3799	
		Γ_2	3786	
7.	^5D_o	Γ_1	17271	17271
8.	$^5D_1$	Γ_1	19043	19028.3
		$\Gamma_{3,4}$	19021	
9.	$^5D_2$	Γ_2	21543	21502.4
		$\Gamma_{3,4}$	21520	
		Γ_1	21479	
		Γ_2	21450	
10.	$^5L_6$	Γ_2	25418	*
		$\Gamma_{3,4}$	25415	
		$\Gamma_{3,4}$	25241	
		Γ_2	25027	
		$\Gamma_{3,4}$	24953	

*Two Γ_2 and three Γ_1 levels of $^5L_6$ could not be obtained.

the first order perturbation. However the exact calculation requiring simultaneous treatment of these interactions is not only cumbersome but has its own shortcomings; for example the simultaneous parametrization of the crystal field and free ion interactions tends to accommodate the inadequacies of each other. Although such an approach has been used in some cases but the usual procedure is to carry out such calculations in two steps. In first step the spin-orbit and the residual Coulomb interactions are considered and the wave functions so generated are used to obtain the crystal field splittings.

3.1 FREE ION CALCULATIONS

The following procedure was adopted to calculate the positions of the free ion energy levels. The free ion energy matrices for the Eu^{3+} ($4f^6$ configuration) were constructed in the intermediate coupling scheme following the procedure outlined in appendix III. The free ion Hamiltonian included the Coulomb, the spin-orbit and the configuration interactions. The angular parts of the Coulomb interaction were directly taken from Ref.[8] of Chapter II, while angular parts of the spin-orbit and the configuration interactions were calculated using the expressions discussed in Chapter II. We have no experimental data for multiplets with J more than six; consequently the programs were written for multiplets with J = 0 to 6 only. These programs use the subroutine 'EIGEN' obtained

from 'IBM 360 Scientific Subroutine Package' to diagonalize the energy matrices and to arrange the eigen values in the ascending order. The free ion matrices were constructed one for each J value. Since the sizes of the free ion energy matrices were large requiring a huge amount of data to be fed to the computer to build up these matrices, it was desirable to check the correctness of the programming process. This was done by comparing some of our calculations with those applicable to Eu^{3+} in aqueous solutions [1]. There was almost complete agreement in general, however, a few discrepancies exist. Our calculated positions of $^5D_4$, $^5F_4$ and $^5I_4$ levels are 27672, 33672 and 33893 cm^{-1} whereas they are placed at 27670, 33651 and 33914 cm^{-1} respectively in Ref.[1]. We checked our programs and energy matrices several times, but could not find any reason for this discrepancy.

Experimentally, the free ion energy levels are obtained from the centres of gravity (CG's) of the observed positions of the Stark components of a given multiplet. Usually some components are missing in the spectra either because the relevant transition may be forbidden or only weakly allowed. In such cases the approximate positions of the missing levels can be estimated on the basis of their calculated positions. The approximate CG's so obtained can be further improved with each refinement in the crystal field calculations. The results presented in this section are obtained by considering

only those multiplets (except $^7F_5$) for which all the Stark components could be identified. The free ion level positions of ^7F_o, $^7F_1$, $^7F_2$, $^7F_3$, $^7F_4$, ^5D_o, $^5D_1$ and $^5D_2$ are well established from our experimental results. The missing two levels of $^7F_5$($\Gamma_1^7(3)$ and $\Gamma_2^7(2)$) were taken at their calculated positions in reference[2]. A program for free ion parameterization can be written using the minimization subroutine 'MINFUN'(described in appendix III). The large size of the free ion matrices, however, makes any minimization exercise impractical (and expensive) for Eu^{3+}, as it requires enormously large CPU time. We adopted the following approximate procedure to reduce the discrepancy between the observed and calculated energies of free ion levels. We started with the free ion parameters given in reference [2]. The starting parameters gave an r.m.s. deviation of nearly 55 cm^{-1}. The free ion parameters were changed one at a time in small steps and the r.m.s. deviation calculated at each step. Thus for each parameter, the minimum r.m.s. deviation and the corresponding values of the parameters were obtained, while rest of the parameters were kept at their starting values. When these new parameters were used for free ion energy calculations, the r.m.s. deviation first went-up to 96 cm^{-1}. However, slightly modified procedure of varying the parameters brought the r.m.s. deviation down to 24 cm^{-1}. Somewhat different procedures gave slightly different r.m.s.

deviation. All these trials indicate that we do not have a unique set of parameters but the parameters obtained in this manner (Table 4.2) are not too far off the mark. These parameters were used to obtain the zero-order wavefunctions needed to carry out the crystal field calculations. Table 4.3 gives the free ion parameters, free ion energies and eigenfunctions.

3.2 CRYSTAL FIELD CALCULATIONS

(A) CALCULATIONS WITHOUT J-J MIXING

In order to obtain crystal field split energy levels, the crystal field energy matrices were constructed for the three representations $\Gamma_1, \Gamma_2, \Gamma_{3,4}$ for each multiplet separately. This procedure neglects J-J mixing effects. The zero-order wavefunctions obtained in the previous section were used for this purpose. The angular parts of the crystal field matrix elements were calculated using the expressions given in Chapter II. A general program was written to calculate these angular parts by defining two quantities

$$ATOM(k) = (-1)^{S+L'+J+k}\sqrt{[(2J+1)(2J'+1)]}\begin{Bmatrix} J & J' & k \\ L' & L & S \end{Bmatrix} \times \langle f^6\ UWSL||U^{(k)}||f^6\ U'W'\ SL'\rangle \quad .....1$$

and

$$F(k,q) = (-1)^{J-J_z}\begin{pmatrix} J & k & J' \\ -J_z & q & J'_z \end{pmatrix}\langle f||C^{(k)}||f\rangle \quad .....2$$

TABLE 4.2

EXPERIMENTAL AND CALCULATED FREE ION LEVEL-POSITIONS

S.No.	Multiplet	Observed position (cm^{-1})	Calculated[a] position (cm^{-1})	Calculated[b] position (cm^{-1})
1.	^7F_o	0	0	0
2.	$^7F_1$	365	369	379
3.	$^7F_2$	1034	1071	1043
4.	$^7F_3$	1922	1854	1899
5.	$^7F_4$	2899	2816	2876
6.	$^7F_5$	3948	3846	3922
7.	^5D_o	17271	17234	17229
8.	$^5D_1$	19028	19001	19041
9.	$^5D_2$	21502	21446	21535
		r.m.s. deviation	56 cm^{-1}	24 cm^{-1}

a Calculated using parameters of reference [2].

$E^1 = 5544\ cm^{-1}$ $E^2 = 24.83\ cm^{-1}$ $E^3 = 585\ cm^{-1}$

$\zeta = 1285\ cm^{-1}$ $\alpha = 20\ cm^{-1}$ $\beta = -640\ cm^{-1}$ $\gamma = 1750\ cm^{-1}$

b Calculated using our values.

$E' = 5549.2\ cm^{-1}$ $E^2 = 24.8\ cm^{-1}$ $E^3 = 585.2\ cm^{-1}$

$\zeta = 1307\ cm^{-1}$ $\alpha = 17.1\ cm^{-1}$ $\beta = -639.4\ cm^{-1}$

$\gamma = 1749.8\ cm^{-1}$

INTERMEDIATE COUPLING WAVEFUNCTIONS

FREE ION PARAMETERS (IN cm^{-1})

E^1= 5549.2 E^2= 24.8 E^3 = 585.2 ζ = 1307.0 α= 17.1 β=-639.4 γ= 1749.8

J	EIGEN VALUE cm^{-1}	EIGEN VECTORS							
0		7F 3P5	5D1 3P6	5D2 1S1	5D3 1S2	3P1 1S3	3P2 1S4	3P3	3P4
	17229.	-.245E+00 .260E-01	-.561E+00 .268E+00	-.137E+00 -.320E-01	.659E+00 -.708E-01	-.189E+00 .241E-02	.160E-01 .583E-01	.234E+00	.123E-01
	0.	.966E+00 .371E-02	-.190E+00 .349E-01	.101E-01 -.286E-02	.167E+00 -.603E-02	-.266E-01 .775E-04	.448E-03 .468E-02	.282E-01	-.276E-04
1		7F 3P2 3D4	5P 3P3 3D5	5D1 3P4 1P	5D2 3P5	5D3 3P6	5F1 3D1	5F2 3D2	3P1 3D3
	19043.	.218E+00 -.115E-01 -.220E-02	.223E-02 -.169E+00 .430E-02	.593E+00 -.718E-02 -.592E-04	.145E+00 -.219E-01	-.699E+00 -.196E+00	.358E-01 .160E-02	.511E-01 -.220E-02	.138E+00 -.439E-02
	379.	.973E+00 -.134E-04 -.119E-02	-.306E-02 .184E-01 -.498E-02	-.172E+00 -.460E-03 -.438E-04	.130E-01 .309E-02	.148E+00 .238E-01	.168E-01 -.133E-02	.260E-01 .387E-02	-.185E-01 .171E-02
2		7F 5G1 3P6 3F3 1D2	5S 5G2 3D1 3F4 1D3	5P 5G3 3D2 3F5 1D4	5D1 3P1 3D3 3F6 1D5	5D2 3P2 3D4 3F7 1D6	5D3 3P3 3D5 3F8	5F1 3P4 3F1 3F9	5F2 3P5 3F2 1D1
	21535.	.172E+00 -.185E-02 -.111E+00 .197E-01 .539E-02	-.500E-02 .138E-01 .716E-02 -.110E-01 .615E-02	.153E-01 .331E-02 -.153E-01 -.234E-02 -.110E-01	.618E+00 .809E-01 -.159E-01 -.276E-03 -.293E-02	.140E+00 -.382E-02 -.157E-02 -.151E-01 .108E-01	-.725E+00 -.877E-01 .241E-01 .322E-01	.608E-01 .264E-02 .140E-01 .104E-01	.875E-01 -.212E-01 .115E-01 -.475E-02
	1043.	.981E+00 .163E-01 .114E-01 -.398E-02 -.505E-03	.577E-03 -.448E-02 -.212E-02 .280E-02 -.534E-03	-.477E-02 -.150E-01 .596E-02 -.335E-03 .120E-02	-.142E+00 -.923E-02 .258E-02 -.184E-02 .228E-03	.168E-01 -.412E-03 -.194E-02 .167E-02 -.122E-02	.117E+00 .759E-02 -.761E-02 -.562E-02	.292E-01 -.842E-03 -.359E-02 -.574E-03	.456E-01 .233E-02 -.110E-02 .587E-03

3

	7F	5P	5D1	5D2	5D3	5F1	5F2	5G1
	5G2	5G3	5H1	5H2	3D1	3D2	3D3	3D4
	3D5	3F1	3F2	3F3	3F4	3F5	3F6	3F7
	3F8	3F9	3G1	3G2	3G3	3G4	3G5	3G6
	3G7	1F1	1F2	1F3	1F4			
24378.	.119E+00	.303E-01	.634E+00	.113E+00	-.730E+00	.778E-01	.118E+00	-.187E-01
	.382E-01	.223E-01	-.108E-01	-.618E-02	.140E-01	-.293E-01	-.267E-01	.229E-02
	.436E-01	.336E-01	.279E-01	.452E-01	-.244E-01	-.563E-02	.159E-02	-.328E-01
	.748E-01	.244E-01	.696E-02	-.277E-02	.811E-02	-.471E-02	.186E-02	-.558E-02
	.278E-02	.232E-02	.715E-03	.248E-02	-.163E-02			
1899.	.987E+00	-.443E-02	-.105E+00	.186E-01	.809E-01	.395E-01	.629E-01	.362E-01
	-.107E-01	-.335E-01	.136E-02	.241E-02	-.212E-02	.551E-02	.225E-02	-.205E-02
	-.688E-02	-.582E-02	-.159E-02	-.630E-02	.469E-02	-.824E-03	-.319E-02	.232E-02
	-.887E-02	-.326E-03	.839E-04	.859E-03	.164E-02	-.489E-03	.146E-02	.977E-03
	.141E-02	-.506E-03	.330E-04	-.332E-03	.246E-03			

4

	7F	5D1	5D2	5D3	5F1	5F2	5G1	5G2
	5G3	5H1	5H2	5I1	5I2	3F1	3F2	3F3
	3F4	3F5	3F6	3F7	3F8	3F9	3G1	3G2
	3G3	3G4	3G5	3G6	3G7	3H1	3H2	3H3
	3H4	4H5	3H6	3H7	3H8	3H9	1G1	1G2
	1G3	1G4	1G5	1G6	1G7	1G8		
26577.	.922E-01	.686E-01	-.589E-02	-.725E-01	-.247E-02	-.281E-01	-.561E+00	.394E+00
	.590E+00	-.253E+00	-.244E+00	.274E-01	.865E-01	.338E-01	.322E-01	.408E-01
	-.323E-01	.864E-02	-.432E-02	-.291E-01	.791E-01	-.614E-03	-.177E-02	-.189E-01
	-.313E-01	-.166E-02	-.395E-01	-.213E-01	-.854E-01	.373E-01	.179E-01	-.648E-01
	-.400E-01	-.181E-03	.172E-01	-.674E-02	-.321E-01	-.639E-01	-.955E-02	-.162E-02
	-.145E-01	.212E-02	.539E-02	.343E-02	-.186E-01	.795E-02		
2876.	.989E+00	-.627E-01	.153E-01	.439E-01	.447E-01	.742E-01	.619E-01	-.208E-01
	-.578E-01	.335E-02	.558E-02	-.288E-03	-.482E-03	-.570E-02	-.138E-02	-.620E-02
	.516E-02	-.138E-02	-.317E-02	.205E-02	-.865E-02	.836E-03	.109E-02	.136E-02
	.444E-02	-.127E-02	.340E-02	.137E-02	.352E-02	-.158E-02	-.276E-03	.194E-02
	.155E-02	-.436E-04	-.176E-03	.438E-03	.115E-02	.244E-02	.513E-03	.199E-03
	.766E-03	-.110E-03	-.147E-03	-.397E-03	.885E-03	-.388E-03		

5

	7F	5F1	5F2	5G1	5G2	5G3	5H1	5H2
	5I1	5I2	5K	3G1	3G2	3G3	3G4	3G5
	3G6	3G7	3G8	3H2	3H3	3H4	3H5	3H6
	3H7	3H8	3H9	3I1	3I2	3I2	3I4	3I5
	3I6	1H1	1H2	1H3	1H4			
26719.	.123E+00	.576E-02	-.176E-01	-.620E+00	.425E+00	.558E+00	-.291E+00	-.253E+00
	.376E-01	.127E+00	-.363E-01	-.172E-01	-.857E-02	-.372E-01	.218E-02	-.333E-01
	-.260E-02	-.349E-01	.663E-01	.431E-01	-.114E+00	-.748E-01	.211E-02	-.329E-01
	.409E-02	-.549E-01	-.124E+00	-.190E-01	-.437E-01	-.593E-02	.342E-01	-.440E-01
	.157E-01	-.930E-03	-.675E-02	.633E-02	.884E-02			
3922.	.988E+00	.402E-01	.713E-01	.926E-01	-.374E-01	-.878E-01	.625E-02	.909E-02
	-.610E-03	-.111E-02	.187E-03	.275E-02	.104E-02	.744E-02	-.185E-02	.505E-02
	.963E-03	.581E-02	-.447E-02	-.128E-02	.673E-02	.461E-02	-.285E-03	-.737E-03
	.701E-03	.313E-02	.743E-02	.135E-03	.888E-03	.373E-04	-.471E-03	.866E-03
	-.276E-03	.308E-04	.443E-03	-.395E-03	-.612E-03			

6	7F 5K 3H7 3I6 1I2	5G1 5L 3H8 3K1 1I3	5G2 3H1 3H9 3K2 1I4	5G3 3H2 3I1 3K3 1I5	5H1 3H3 3I2 3K4 1I6	5H2 3H4 3I3 3K5 1I7	5I1 3H5 3I4 3K6	5I2 3H6 3I5 1I1
25157.	.228E-01 -.108E+00 .838E-03 .194E-01 .635E-02	-.583E-01 .936E+00 -.124E-01 .154E+00 -.315E-01	.545E-01 -.184E-01 -.387E-01 .141E+00 -.136E-02	.645E-01 .121E-01 -.189E-01 .301E-01 .779E-02	-.478E-01 -.355E-01 -.457E-01 .583E-01 .373E-01	-.376E-01 -.224E-01 -.654E-02 .173E+00 .225E-01	.158E-01 .273E-02 .362E-01 -.419E-01	.541E-01 .128E-01 -.468E-01 -.315E-01
4998.	.982E+00 .330E-03 .101E-02 -.868E-03 -.287E-03	.128E+00 -.164E-03 .547E-02 -.368E-03 .145E-02	-.636E-01 -.904E-02 .170E-01 -.342E-03 .107E-03	-.124E+00 -.337E-02 .483E-03 -.359E-04 -.169E-03	.919E-02 .138E-01 .204E-02 -.132E-03 -.158E-02	.110E-01 .102E-01 .145E-03 -.432E-03 -.105E-02	-.743E-03 -.138E-02 -.131E-02 .937E-04	-.172E-02 -.313E-02 .206E-02 .135E-02

* For LS bases notation of Nielson & Koster is used

The quantities $\langle||U^{(k)}||\rangle$ were obtained from the tables of Nielson and Koster, while 3-J and 6-J symbols were calculated using appropriate subroutines. Some matrix elements were calculated manually in order to check the computer programs written for this purpose. The energy matrices obtained in this manner were diagonalized using the 'EIGEN' subroutine. The optimization subroutine 'MINFUN' was used to obtain the best set of parameters. A brief note on the 'MINFUN' subroutine and programming is given in appendix III.

Out of the seven parameters (B_q^k's) appropriate to S_4 symmetry group, the axial parameters (q=0) are independent of the choice of x and y axes of coordinates. The values of the remaining four parameters (with $q \neq 0$) are dependent on the choice of x and y axes. Although the choice of the z-axis is dictated by the crystal symmetry axis ($\bar{c}$-axis), no unique choice exists for the x and y axes. A rotation of the coordinate system through an angle ϕ about the z-axis leaves the axial parameters unchanged, but the non axial parameters transform as [3].

$$[B_q^k] = \text{Cos}(q,\phi) \left\{B_q^k\right\} + \text{Sin}\,(q\,\phi) \left\{B_{-q}^k\right\} \qquad \ldots\ldots 3$$

Where $[B_q^k]$ are the parameters in the new coordinate system and $\left\{B_q^k\right\}$ are those in the old coordinate system. A proper choice of angle ϕ can make one of the $[B_q^k]$ parameters zero, so that we need to determine only six parameters. In our

calculations presented here, we have set $B^4_{-4}(= B'^4_4)$ to zero. At one stage we tried to consider all the seven parameters and also the six parameters with $B'^6_4 = 0$, but the results were unchanged.

The experimental values of the crystal field splittings were obtained by taking differences of the Stark components of a given multiplet with respect to its lowest Stark component. In this manner, a total of 23 such energy differences were obtained, 19 belonging to the ^7F_J(J=0 to 5) and 4 to the ^5D_J(J=0 to 2) multiplets.

The multiplets with J=0 are non-degenerate and do not play any role in the crystal field parameterization as far as calculations without J-J mixing are concerned. We did not consider the $^5L_6$ multiplet for lack of sufficient experimental data.

Görller et al [2], have reported results of crystal field parameterization for the Stark levels of the ^7F_J(J=0 to 5) multiplets and obtained an r.m.s. deviation of about 3 cm^{-1} considering J-J mixing within the ^7F_J multiplets. However when we used their parameters to calculate the crystal field splittings without J-J mixing effects, the resulting r.m.s. deviation was approximately 23 cm^{-1} and when $^5D_1$ and $^5D_2$ multiplets were also included the r.m.s. deviation went up to about 25 cm^{-1}. We carried out a least squares fitting to

the six crystal field parameters ($B_4^{'4}$ was arbitrarily set to zero) in an attempt to bring better agreement in our calculations and experimental results. The subroutine 'MINFUN' was initialized for the 'search mode' with parameters of ref [2]. This gave a large number of approximate minima and the corresponding parameters. When these sets of parameters, were used as starting parameters in the 'convergence mode' of the 'MINFUN', they all converged to values given in Table 4.4. The r.m.s. deviations$ obtained from our least square fittings to 19 energy differences (corresponding to ^7F_J, J=0 to 5) and 23 energy differences (including ^5D_J, J=0 to 2) were 17.5 and 20.1 cm^{-1} respectively. The calculated energy splittings along with the experimental values and the crystal field wave-vectors are

$ The r.m.s. deviation has been defined as

$$\sigma = \sqrt{(\sum_i \Delta_i^2)/n}$$

Where Δ_i is the differences between calculated and experimentally observed splittings; n is the number of energy differences used in the least squares fit. Here a point is worth noting that if we take n as the number of levels involved the r.m.s. deviation will get reduced because the lowest components of multiplets taken as reference to calculate splittings will not contribute anything to the numerator while denominator will have a higher value.

TABLE 4.4

CRYSTAL FIELD PARAMETERS (in cm^{-1})-WITHOUT J-J MIXING

	Set A Fit with 19 energy differences	Set B Fit with 23 energy differences
B_o^2	380.60±(2.29)	370.54±(2.23)
B_o^4	-818.25±(3.79)	-821.25±(3.78)
B_o^6	- 81.618±(3.79)	- 81.452±(3.79)
B_4^4	-972.95±(2.98)	-1001.0±(2.92)
B_4^6	-825.72±(2.66)	-816.02±(2.56)
$B_4'^4$	0.0	0.0
$B_4'^6$	300.73±(7.54)	272.46±(8.41)
r.m.s. deviation	17.5 cm^{-1}	20.1 cm^{-1}

. In set A only ^7F_J multiplets are considered whereas parameters of set B are obtained when ^5D_J multiplets are also included.

. Calculated splittings using parameters of set A and set B differ to an extent of±2 or 3 cm^{-1} for some of the levels.

given in Table 4.5. To check reliability of our minimization procedure we repeated the above calculations with a totally random set of starting parameters. The final values of B_o^2, B_o^4 and B_o^6 remained the same, but some of the non-axial parameters changed sign. The change in the sign of the non-axial parameters (B_q^k, $q \neq 0$) did not modify the r.m.s. deviation at all. The theoretically calculated order of energy levels is in agreement with the experimental results. The relatively large r.m.s. deviation here is due to the neglect of J-J mixing effects and partly due to the fact that we have more data to account for. To estimate contribution from J-J mixing effects we have attempted a limited J-J mixing calculation.

B. CALCULATIONS WITH J-J MIXING

A detailed consideration of J-J mixing effects in $LiYF_4:Eu^{3+}$ needs to solve the energy matrices of order upto 761x761, even if the matrices are broken into the three submatrices for each representation. This is a rather difficult job. We have carried out a limited J-J mixing calculation involving only two lowest multiplets for each J from J=0 to J=6. Thus six crystal field energy matrices corresponding to three irreducible representations and two multiplets were constructed considering matrix elements between $|JJ_z\rangle$ and $|J', J_z'\rangle$ bases with $J' \neq J$ as well. The procedure for calculating matrix elements is outlined briefly in appendix III.

TABLE 4.5

OBSERVED AND CALCULATED CRYSTAL FIELD SPLITTINGS AND WAVEFUNCTIONS (WITHOUT J-J MIXING)

CRYSTAL FIELD PARAMETERS (IN cm^{-1})

B20= 370.64 B40=-821.25 B60= -81.45 B44=-1001.00 B64=-816.02 B44I= 0.00 B64I= 272.46

MULT.	IRR REP	OBS. SPL. cm^{-1}	CALC. SPL. cm^{-1}	BASES [J, Jz>
7F0	1	0.	0.	[0 0> (.100E+01 .000E+00)
5D0	1	0.	0.	[0 0> (.100E+01 .000E+00)
7F1	1	96.	109.	[1 0> (.100E+01 .000E+00)
	3	0.	0.	[1 1> (.100E+01 .000E+00)
5D1	1	22.	35.	[1 0> (.100E+01 .000E+00)
	3	0.	0.	[1 1> (.100E+01 .000E+00)
7F2	1	286.	272.	[2 0> (.100E+01 .000E+00)
	2	263.	263.	[2 2> (.707E+00 .000E+00) [2 -2> (.707E+00 .000E+00)
		0.	0.	(.707E+00 .000E+00) (-.707E+00 .000E+00)
	3	87.	124.	[2 1> (.100E+01 .000E+00)
5D2	1	29.	20.	[2 0> (.100E+01 .000E+00)
	2	93.	46.	[2 2> (-.707E+00 .000E+00) [2 -2> (.707E+00 .000E+00)
		0.	0.	(.707E+00 .000E+00) (.707E+00 .000E+00)
	3	70.	40.	[2 1> (.100E+01 .000E+00)
7F3	1	43.	40.	[3 0> (.100E+01 .000E+00)
	2	179.	155.	[3 2> (.705E+00 -.546E-01) [3 -2> (-.705E+00 -.546E-01)
		0.	0.	(.705E+00 -.546E-01) (.705E+00 .546E-01)

	3			[3 1>	[3 -3>	
		95.	64.	(.970E+00 .799E-03)	(-.180E+00 .163E+00)	
		14.	15.	(.180E+00 .163E+00)	(.970E+00 -.799E-03)	
5D3	1			[3 0>		
		--	0.	(.100E+01 .000E+00)		
	2			[3 2>	[3 -2>	
		--	20.	(.691E+00 -.150E+00)	(-.691E+00 -.150E+00)	
		--	1.	(.691E+00 -.150E+00)	(.691E+00 .150E+00)	
	3			[3 1>	[3 -3>	
		--	35.	(.311E+00 -.704E-01)	(.948E+00 .231E-01)	
		--	0.	(.948E+00 -.231E-01)	(-.311E+00 -.704E-01)	
7F4	1			[4 0>	[4 4>	[4 -4>
		473.	481.	(-.686E+00 .249E-02)	(.503E+00 -.107E+00)	(.504E+00 .103E+00)
		263.	255.	(-.539E-08 .246E-09)	(-.691E+00 .152E+00)	(.694E+00 .136E+00)
		0.	0.	(.727E+00 .111E-01)	(.477E+00 -.916E-01)	(.474E+00 .106E+00)
	2			[4 2>	[4 -2>	
		371.	362.	(.704E+00 .713E-01)	(-.521E+00 .478E+00)	
		297.	284.	(-.478E+00 .521E+00)	(.713E-01 .704E+00)	
	3			[4 1>	[4 -3>	
		404.	422.	(-.440E+00 -.234E-01)	(.898E+00 -.115E-01)	
		205.	212.	(.898E+00 .115E-01)	(.440E+00 -.234E-01)	
5G4	1			[4 0>	[4 4>	[4 -4>
		--	67.	(.822E-01 -.402E+00)	(.444E-01 .643E+00)	(-.294E+00 .574E+00)
		--	56.	(.349E-10 -.483E-08)	(-.629E+00 .323E+00)	(.706E+00 .472E-01)
		--	0.	(.912E+00 .189E-02)	(.279E+00 -.770E-01)	(.279E+00 .781E-01)
	2			[4 2>	[4 -2>	
		--	33.	(.682E+00 -.186E+00)	(.682E+00 .186E+00)	
		--	17.	(-.682E+00 .186E+00)	(.682E+00 .186E+00)	
	3			[4 1>	[4 -3>	
		--	43.	(-.797E-01 -.258E-01)	(.996E+00 -.207E-02)	
		--	14.	(.996E+00 .207E-02)	(.797E-01 -.258E-01)	
7F5	1			[5 0>	[5 4>	[5 -4>
		--	240.	(-.136E+00 .136E+00)	(.686E+00 -.104E+00)	(.108E+00 -.685E+00)
		222.	233.	(.233E-07 -.212E-07)	(.698E+00 -.110E+00)	(-.106E+00 .699E+00)
		58.	63.	(.609E-05 .981E+00)	(-.803E-01 .110E+00)	(.803E-01 .110E+00)
	2			[5 2>	[5 -2>	
		--	312.	(-.705E+00 .529E-01)	(.705E+00 .529E-01)	
		0.	0.	(.705E+00 -.529E-01)	(.705E+00 .529E-01)	
	3			[5 1>	[5 -3>	[5 5>
		266.	285.	(-.512E+00 .388E-01)	(.858E+00 .232E-01)	(.000E+00 .000E+00)
		214.	180.	(.000E+00 .000E+00)	(.000E+00 .000E+00)	(.100E+01 .000E+00)
		13.	27.	(.858E+00 -.232E-01)	(.512E+00 .388E-01)	(.000E+00 .000E+00)
5G5	1			[5 0>	[5 4>	[5 -4>
		--	45.	(.817E-01 -.266E+00)	(.715E-01 .675E+00)	(-.439E+00 .519E+00)
		--	43.	(-.447E-07 .896E-08)	(-.539E+00 .457E+00)	(.703E+00 .738E-01)
		--	9.	(.961E+00 .956E-03)	(.181E+00 -.771E-01)	(.181E+00 .774E-01)
	2			[5 2>	[5 -2>	
		--	33.	(.700E+00 -.970E-01)	(.700E+00 .970E-01)	
		--	0.	(.700E+00 -.970E-01)	(-.700E+00 -.970E-01)	

	3		[5 1>	[5 -3>	[5 5>		
	--	62.	(.000E+00 .000E+00)	(.000E+00 .000E+00)	(.100E+01 .000E+00)		
	--	31.	(.454E+00 -.889E-01)	(.886E+00 .455E-01)	(.000E+00 .000E+00)		
	--	8.	(.886E+00 -.455E-01)	(-.454E+00 -.889E-01)	(.000E+00 .000E+00)		
7F6	1		[6 0>	[6 4>	[6 -4>		
	--	255.	(.774E+00 -.311E-07)	(.448E+00 .610E-02)	(.448E+00 -.610E-02)		
	--	113.	(.147E-08 .125E-08)	(-.707E+00 -.956E-02)	(.707E+00 -.970E-02)		
	--	19.	(.619E-04 -.633E+00)	(-.751E-02 .547E+00)	(.740E-02 .547E+00)		
	2		[5 2>	[6 -2>	[6 6>		
			[6 -6>				
	--	370.	(.708E-01 -.303E-01)	(.722E-01 -.267E-01)	(.685E+00 .157E+00)		
			(.389E+00 -.585E+00)				
	--	369.	(-.236E-01 -.872E-02)	(.231E-01 .989E-02)	(-.391E+00 -.589E+00)		
			(.689E+00 -.158E+00)				
	--	249.	(.176E-01 .703E+00)	(-.176E-01 .703E+00)	(.438E-01 -.633E-01)		
			(-.438E-01 -.633E-01)				
	--	0.	(-.706E+00 .177E-01)	(.706E+00 .177E-01)	(.207E-01 .143E-01)		
			(-.207E-01 .143E-01)				
	3		[6 1>	[6 -3>	[6 5>		
	--	259.	(.724E+00 -.274E-01)	(.529E+00 -.763E-03)	(.439E+00 .485E-01)		
	--	176.	(-.249E+00 .306E-01)	(-.393E+00 .339E-01)	(.884E+00 .225E-01)		
	--	7.	(-.642E+00 .154E-01)	(.751E+00 .934E-02)	(.152E+00 .189E-01)		
5L6	1		[6 0>	[6 4>	[6 -4>		
	--	416.	(-.496E+00 .183E-05)	(.614E+00 .138E-01)	(.614E+00 -.138E-01)		
	--	317.	(-.153E-08 .123E-09)	(-.707E+00 -.159E-01)	(.707E+00 -.158E-01)		
	--	12.	(.868E+00 -.590E-04)	(.351E+00 .783E-02)	(.351E+00 -.788E-02)		
	2		[6 2>	[6 -2>	[6 6>		
			[6 -6>				
	465.	412.	(.705E+00 -.259E-01)	(-.705E+00 -.259E-01)	(.982E-02 -.419E-01)		
			(-.982E-02 -.419E-01)				
	--	91.	(.497E-02 .135E+00)	(-.499E-02 .135E+00)	(.676E+00 .158E+00)		
			(-.676E+00 .158E+00)				
	74.	85.	(-.158E-02 -.430E-01)	(-.159E-02 .430E-01)	(.687E+00 .161E+00)		
			(.687E+00 -.161E+00)				
	--	-15.	(.694E+00 -.256E-01)	(.694E+00 .254E-01)	(-.309E-01 .132E+00)		
			(-.309E-01 -.132E+00)				
	3		[6 1>	[6 -3>	[6 5>		
	462.	410.	(-.575E+00 .274E-01)	(.790E+00 .556E-02)	(.203E+00 .559E-01)		
	288.	272.	(-.293E-02 .928E-03)	(-.251E+00 .646E-01)	(.956E+00 .978E-02)		
	0.	0.	(.818E+00 -.140E-01)	(.554E+00 .209E-01)	(.145E+00 .448E-01)		

r.m.s. deviatin=20.1

The splittings are given with respect to the lowest Stark level (observed) of a given multiplet.

The 5L6 multiplet is not included in the crystal field least squares analysis

The numbers in the parenthesis"()" represent respectively the real and imaginary parts of a coefficient.

The expressions and general procedure outlined where J-J mixing effects are neglected are applicable here as well. The resulting sizes of matrices did not exceed 13x13, but the size of intermediate computations increased immensely. Therefore the programs were written to calculate and use the ATOM(k) and F(k,q) in the program itself and to obtain angular parts of the matrix elements only in the final stage, decreasing storage requirements. The matrices were diagonalized in a similar fashion as described in the previous section. To take account of free ion splittings the calculated free ion eigen values were added to the diagonal matrix elements appropriately. For least squares fitting the comparison between observed and calculated crystal field splittings was made taking lowest Stark component of each multiplet as reference.

When the parameters of ref [2] were used for these calculations, resulting r.m.s. deviation was approximately 5 cm^{-1} for 19 energy differences corresponding to ^7F_J(J=0 to 5) and when ^5D_J(J=0 to 2) were also included it went up to about 14 cm^{-1} for 23 energy differences. The six parameter least squares fits were attempted for 19 energy differences and then for 23 energy differences. We could achieve an r.m.s. deviation as low as about 2.9 cm^{-1} and 13.1 cm^{-1} for 19 and 23 energy differences respectively. Table 4.6 gives the crystal field parameters obtained from

TABLE 4.6

CRYSTAL FIELD PARAMETERS (in cm^{-1}) (WITH J-J MIXING)

	Set C Fit with 19 energy differences	Set D Fit with 23 energy differences
B_o^2	367.40±(2.31)	360.51±(.23)
B_o^4	-721.79±(3.71)	-723.18±(.49)
B_o^6	-43.919±(4.60)	-42.617±(.43)
B_4^4	-927.66±(2.74)	-929.66±(.12)
B_4^6	-809.77±(2.59)	-808.83±(.13)
$B_4'^4$	0.0	0.0
$B_4'^6$	237.84±(9.00)	238.39±(.45)
r.m.s. deviation	2.9 cm^{-1}	13.1 cm^{-1}

In set C only ^7F_J multiplets are considered whereas parameters of set D are obtained when ^5D_J multiplets are also included.

Calculated splittings using parameters of sets C and D differ at most by ± 2 or 3 cm^{-1}.

these fits and Table 4.7 gives the experimental splittings, the calculated splittings and the crystal field wavefunctions (with J-J mixing effects). We notice considerably improved agreement for the low lying levels (i.e. ^7F_J multiplets), thus establishing a significant contribution of J-J mixing effects for these closely spaced multiplets. The neglect of higher multiplets in these calculations is justified by relatively pure character of ^7F wavefunctions (96% to 99%). Other workers [4,5] have also used somewhat similar approach to calculate energy levels of Eu^{3+} in other hosts. The agreement for higher levels (^5D_J multiplets) is not so good even when J-J mixing effects are considered. A similar situation is encountered elsewhere [5] where somewhat different truncation procedure was used. The mixing of the ^3P states was suggested as a possible cause for this disagreement. This however may not be so as we have used intermediate wavefunctions which take care of these effects to a certain extent. Though we do not have any satisfactory explanation for this poor agreement, we nevertheless feel that a more exact J-J mixing calculations involving other nearby multiplets should improve the situation but computational complexities have prevented us from performing such calculations. It should be pointed out that we accounted for the free ion contributions in the J-J mixing calculations by adding to the diagonal matrix elements, the calculated

TABLE 4.7

OBSERVED AND CALCULATED CRYSTAL FIELD SPLITTINGS AND WAVEFUNCTIONS (WITH J-J MIXING)

CRYSTAL FIELD PARAMETERS (IN cm^{-1})

B20= 360.61 B40=-723.18 B60= -42.62 B44= -929.66 B64=-808.83 B44I= 0.0 B64I= 238.39

IRR REP	MULT.	OBS. SPL. cm^{-1}	CALC. SPL. cm^{-1}	B A S E S [J, Jz>		
1				[0 0> [3 0> [4 -4> [5 -4> [6 -4>	[1 0> [4 0> [5 0> [6 0>	[2 0> [4 4> [5 4> [6 4>
	7F6	--	221.	(-.204E-01 .508E-03) (.189E-03 .759E-02) (.557E-02 -.714E-02) (.471E-01 -.111E-01) (.508E+00 -.378E-01)	(-.181E-03 -.727E-02) (.687E-01 -.171E-02) (.239E-03 .956E-02) (.687E+00 -.171E-01)	(.763E-02 -.190E-03) (.592E-02 .686E-02) (-.476E-01 -.975E-02) (.509E+00 .125E-01)
		--	146.	(-.250E-03 .975E-02) (-.545E-01 -.140E-02) (.219E-01 -.226E-02) (.584E-01 -.250E-02) (.691E+00 -.139E-01)	(.274E-01 .704E-03) (.418E-03 -.163E-01) (-.179E+00 -.459E-02) (.175E-03 -.668E-02)	(-.134E-04 .720E-03) (-.218E-01 -.338E-02) (.582E-01 .549E-02) (-.590E+00 -.494E-01)
		--	22.	(.165E-01 -.122E-04) (-.593E-05 -.808E-02) (-.335E-01 -.619E-02) (-.336E-01 -.937E-02) (-.479E+00 .196E-01)	(.561E-05 .760E-02) (-.987E-01 .734E-04) (-.726E-05 -.101E-01) (.725E+00 -.539E-03)	(.579E-02 -.424E-05) (-.335E-01 .624E-02) (.336E-01 -.942E-02) (-.479E+00 -.189E-01)
	7F5	--	225.	(-.551E-02 .453E-03) (-.704E-03 -.857E-02) (-.556E-01 .271E-01) (-.668E+00 .195E+00) (.545E-01 .811E-03)	(-.297E-03 -.362E-02) (.381E-01 -.313E-02) (.107E-01 .130E+00) (.136E-01 -.112E-02)	(.163E-01 -.134E-02) (-.593E-01 -.177E-01) (.690E+00 .833E-01) (.536E-01 -.969E-02)
		222.	222.	(-.702E-03 -.209E-02) (.314E-01 -.105E-01) (.487E-01 -.260E-01) (.606E+00 -.354E+00) (-.477E-01 .304E-01)	(.207E-03 -.693E-04) (.242E-02 .720E-02) (.274E-01 -.918E-02) (-.551E-02 -.164E-01)	(-.299E-02 -.890E-02) (-.516E-01 .862E-02) (.697E+00 -.930E-01) (.554E-01 -.450E-02)

	58.	60.	(.871E-06 .322E-02) (-.480E-02 .130E-05) (.119E+00 .242E-01) (-.382E-01 -.901E-01) (.123E+00 .102E-01)	(.163E-01 -.441E-05) (.534E-07 .178E-03) (.960E+00 -.260E-03) (-.914E-07 -.341E-03)	(.971E-06 .359E-02) (-.119E+00 .243E-01) (-.332E-01 .901E-01) (-.123E+00 .103E-01)
7F4	473.	471.	(.191E-01 -.486E-04) (.115E-04 .452E-02) (.517E+00 .108E+00) (-.560E-01 -.576E-02) (.404E-01 .283E-02)	(-.300E-04 -.118E-01) (-.657E+00 .167E-02) (.235E-04 .925E-02) (.779E-02 -.198E-04)	(-.105E-01 .266E-04) (.516E+00 -.111E+00) (.559E-01 -.704E-02) (.403E-01 -.304E-02)
	263.	269.	(-.116E-01 .854E-04) (.128E-02 .174E+00) (-.129E+00 .669E+00) (.503E-02 -.553E-01) (.250E-02 -.298E-01)	(-.514E-03 -.700E-01) (.117E-01 -.858E-04) (-.123E-02 -.168E+00) (.553E-02 -.406E-04)	(-.605E-02 .444E-04) (-.139E+00 -.667E+00) (-.584E-02 -.552E-01) (.294E-02 .297E-01)
	0.	0.	(-.843E-03 .830E-01) (-.263E-02 -.267E-04) (-.899E-01 .454E+00) (.763E-02 -.215E-01) (.826E-02 -.772E-01)	(.884E-02 .897E-04) (-.752E-02 .741E+00) (-.636E-02 -.646E-04) (-.392E-03 .386E-01)	(-.305E-03 .300E-01) (.806E-01 .456E+00) (.719E-02 .217E-01) (-.669E-02 -.774E-01)
7F3	43.	40.	(.874E-07 -.177E-02) (.976E+00 .484E-04) (-.113E+00 -.191E-01) (-.946E-02 .117E-01) (.435E-01 .487E-02)	(.124E+00 .617E-05) (-.432E-07 .856E-03) (.219E-01 .108E-05) (-.270E-07 .542E-03)	(.738E-07 -.147E-02) (.113E+00 -.191E-01) (-.946E-02 -.117E-01) (-.435E-01 .487E-02)
7F2	286.	290.	(.679E-06 .648E-01) (.639E-03 -.756E-08) (-.238E-02 -.115E-01) (.887E-02 .101E-01) (-.192E-02 .250E-02)	(.651E-03 -.704E-08) (-.341E-06 -.326E-01) (.258E-03 -.268E-08) (-.114E-06 -.109E-01)	(.104E-04 .997E+00) (.238E-02 -.115E-01) (.887E-02 -.101E-01) (.192E-02 .250E-02)
7F1	96.	95.	(-.182E-04 .463E-09) (-.131E-06 -.109E+00) (-.128E-02 .611E-01) (-.252E-02 -.351E-02) (.750E-02 -.291E-01)	(.119E-05 .989E+00) (.644E-03 -.822E-09) (-.297E-07 -.247E-01) (.223E-03 -.338E-09)	(.347E-03 -.444E-09) (-.128E-02 -.611E-01) (.252E-02 -.351E-02) (.750E-02 .291E-01)
7F0	0.	0.	(.994E+00 -.936E-06) (-.236E-09 -.343E-03) (-.486E-01 -.795E-03) (.617E-04 .351E-03) (.245E-01 .651E-02)	(-.371E-09 .115E-04) (-.435E-01 .410E-07) (-.196E-09 -.312E-03) (-.398E-03 .441E-09)	(-.673E-01 .633E-07) (-.486E-01 .795E-03) (-.617E-04 .351E-03) (.245E-01 -.651E-02)

2

[2 2>
[3 -2>
[5 2>

[2 -2>
[4 2>
[5 -2>

[3 2>
[4 -2>
[6 2>

7F6	--	317.	(.137E-02 -.201E-02) (-.419E-02 .646E-02) (.408E-02 -.797E-02) (.313E-01 -.565E-01)	(.906E-03 -.225E-02) (.603E-02 -.113E-01) (-.435E-02 .782E-02) (.644E+00 -.285E+00)	(.304E-02 -.707E-02) (.608E-02 -.113E-01) (.295E-01 -.574E-01) (-.121E+00 -.693E+00)
	--	317.	(.190E-02 -.331E-02) (.382E-02 -.582E-02) (.858E-02 -.136E-01) (-.155E-01 .230E-01)	(-.226E-02 .307E-02) (.562E-02 -.930E-02) (.898E-02 -.134E-01) (.658E+00 -.229E+00)	(.378E-02 -.585E-02) (-.624E-02 .890E-02) (.148E-01 -.234E-01) (.610E-01 .704E+00)
	--	215.	(-.149E-01 .495E-02) (-.233E-02 -.561E-02) (-.724E-01 .321E-02) (.700E+00 .109E-02)	(-.151E-01 -.448E-02) (.237E-01 .208E-02) (.725E-01 .927E-03) (-.508E-01 -.384E-01)	(.215E-02 -.568E-02) (.235E-01 -.282E-02) (.699E+00 -.231E-01) (-.496E-01 .400E-01)
	--	0.	(.445E-02 -.122E-01) (.642E-02 -.254E-01) (.719E-03 .104E+00) (.115E-01 -.698E+00)	(.445E-02 -.122E-01) (.417E-02 -.625E-02) (-.718E-03 .104E+00) (.181E-01 -.233E-01)	(-.642E-02 -.254E-01) (.417E-02 .625E-02) (.115E-01 .698E+00) (.181E-01 .233E-01)
7F5	--	287.	(-.190E-02 -.521E-02) (-.719E-03 -.166E-01) (-.468E-01 -.700E+00) (-.523E-02 -.728E-01)	(.190E-02 -.522E-02) (.101E-01 .380E-01) (-.458E-01 .700E+00) (-.871E-02 .119E-01)	(-.717E-03 .166E-01) (-.101E-01 .380E-01) (.522E-02 -.728E-01) (.871E-02 .119E-01)
	0.	0.	(-.523E-01 .789E-02) (.641E-01 .577E-02) (.693E+00 -.476E-01) (.101E+00 -.163E-02)	(.523E-01 .790E-02) (-.260E-01 -.596E-02) (.693E+00 .477E-01) (-.979E-02 -.662E-02)	(.641E-01 -.576E-02) (.260E-01 -.595E-02) (-.101E+00 -.165E-02) (.979E-02 -.661E-02)
7F4	371.	369.	(.152E-01 .129E-02) (-.739E-01 .275E-01) (.367E-01 .187E-01) (.979E-03 -.374E-02)	(-.150E-01 .293E-02) (.656E+00 .221E+00) (.345E-01 -.226E-01) (-.574E-02 -.926E-02)	(-.754E-01 -.193E-01) (-.538E+00 .292E+00) (-.138E-02 -.361E-02) (.470E-02 -.983E-02)
	297.	295.	(.110E-01 .136E-01) (.474E-01 -.123E-01) (.305E-01 .134E-01) (-.207E-01 -.189E-02)	(.164E-01 -.598E-02) (.562E+00 .423E+00) (-.330E-01 -.432E-02) (-.272E-02 .106E-01)	(-.343E-01 -.351E-01) (.700E+00 -.717E-01) (-.187E-01 -.909E-02) (-.779E-02 .763E-02)
7F3	179.	178.	(.313E-02 -.874E-01) (.439E-01 -.698E+00) (.430E-02 .199E-01) (.576E-02 -.460E-02)	(-.316E-02 -.874E-01) (.104E-01 .483E-01) (.430E-02 -.199E-01) (.460E-02 -.662E-02)	(.441E-01 .698E+00) (-.104E-01 .483E-01) (-.576E-02 -.460E-02) (-.451E-02 -.662E-02)
	0.	0.	(-.363E-02 .893E-01) (-.445E-01 .693E+00) (-.330E-02 -.501E-01) (.491E-02 -.319E-01)	(-.363E-02 -.893E-01) (-.217E-02 .779E-01) (.330E-02 -.501E-01) (.515E-02 -.691E-02)	(.445E-01 .693E+00) (-.217E-02 -.779E-01) (.491E-02 .319E-01) (.515E-02 .691E-02)

7F2	263.	262.	(.701E+00 -.719E-02) (-.885E-01 -.915E-04) (-.458E-02 .623E-02) (.141E-01 .470E-02)	(.701E+00 .718E-02) (-.724E-02 -.414E-02) (.458E-02 .623E-02) (-.348E-02 -.282E-02)	(.885E-01 -.923E-04) (-.724E-02 .414E-02) (.141E-01 -.470E-02) (-.348E-02 .282E-02)
	0.	0.	(-.699E+00 .657E-02) (.815E-01 .104E-02) (-.553E-01 .637E-02) (-.238E-01 -.491E-02)	(.699E+00 .655E-02) (.298E-01 -.346E-02) (-.553E-01 -.637E-02) (.220E-02 .180E-02)	(.815E-01 -.105E-02) (-.298E-01 -.346E-02) (.238E-01 -.491E-02) (-.220E-02 .180E-02)
			[1 1> [3 -3> [5 1> [6 1>	[2 1> [4 1> [5 -3> [6 -3>	[3 1> [4 -3> [5 5> [6 5>
7F6	--	229.	(-.339E-02 .200E-01) (.461E-02 -.701E-02) (-.790E-02 -.595E-02) (-.217E-01 .590E+00)	(-.133E-01 .122E-01) (-.896E-02 .603E-01) (-.879E-03 .447E-01) (-.226E-01 .453E+00)	(-.101E-01 .204E-01) (.491E-02 .930E-02) (.255E-01 -.697E-01) (-.152E+00 .637E+00)
	--	187.	(-.973E-02 -.170E-02) (-.329E-02 .457E-02) (.384E-02 .123E+00) (-.231E-01 -.386E+00)	(-.517E-02 .316E-01) (-.113E-01 .116E-01) (-.343E-02 -.408E-01) (-.182E-01 -.552E+00)	(-.116E-01 .408E-01) (-.457E-02 -.132E-01) (.123E-01 -.914E-01) (-.117E+00 .709E+00)
	--	10.	(-.129E-01 .283E-02) (-.190E-01 -.499E-02) (.115E+00 -.687E-02) (.704E+00 -.546E-02)	(.154E-01 -.840E-02) (-.614E-01 .762E-04) (.327E-01 -.605E-02) (-.677E+00 -.650E-02)	(-.130E-01 -.656E-03) (-.315E-01 -.757E-02) (.364E-01 -.731E-02) (-.153E+00 -.302E-01)
7F5	266.	272.	(-.884E-02 -.249E-02) (.381E-02 -.156E-02) (-.374E+00 -.330E+00) (-.132E-01 -.197E-01)	(-.287E-01 -.164E-01) (-.373E-03 -.663E-02) (.513E+00 .535E+00) (-.690E-01 -.670E-01)	(-.338E-01 -.619E-02) (.461E-02 .165E-03) (-.407E+00 -.153E+00) (-.217E-01 .117E-01)
	214.	209.	(.354E-01 .322E-02) (.198E-01 .122E-01) (.393E-01 .181E-01) (-.430E-01 -.291E-01)	(.424E-01 -.823E-03) (.124E+00 .254E-01) (.455E+00 .236E+00) (-.752E-02 -.824E-03)	(.777E-01 .192E-01) (.239E-01 .161E-01) (.830E+00 .139E-01) (.989E-01 -.573E-03)
	-13.	12.	(.941E-02 .177E-03) (.844E-01 .188E-01) (.839E+00 .695E-02) (-.430E-01 -.541E-02)	(-.529E-01 .616E-02) (-.468E-01 -.628E-02) (.403E+00 .383E-01) (.116E+00 .790E-02)	(-.220E-01 .112E-01) (.115E+00 .234E-01) (-.266E+00 .107E+00) (-.841E-01 .705E-02)
7F4	404.	403.	(-.103E-01 .152E-02) (.460E-01 .111E-01) (-.102E+00 .195E-01) (.112E-01 -.105E-01)	(.265E-01 -.838E-02) (-.448E+00 -.198E-01) (-.422E-01 .147E-01) (-.149E-01 .541E-02)	(.575E-01 .154E-01) (.880E+00 -.920E-02) (.548E-01 -.160E-01) (.361E-01 -.145E-02)

	205.	208.	(-.476E-01 .278E-02) (-.963E-01 -.251E-01) (.340E-03 .850E-02) (.180E-01 -.323E-02)	(.303E-01 -.594E-02) (.866E+00 .116E-01) (-.591E-01 -.167E-01) (-.686E-01 -.144E-02)	(-.950E-01 .893E-02) (.455E+00 -.217E-01) (-.854E-01 .202E-01) (-.589E-01 .125E-02)
7F3	95.	92.	(.918E-02 .508E-01) (-.722E-01 -.605E+00) (.148E-01 .346E-01) (-.710E-02 -.915E-03)	(-.149E-01 -.201E+00) (-.246E-01 .175E-01) (-.104E-02 .139E-01) (.815E-02 .566E-02)	(.224E-02 .760E+00) (-.152E-01 .823E-02) (-.752E-02 -.583E-01) (-.345E-02 -.410E-01)
	14.	13.	(-.800E-01 .838E-03) (.761E+00 .952E-02) (-.477E-01 .111E-01) (.300E-01 -.424E-02)	(.323E-01 -.131E-01) (-.140E+00 -.793E-02) (-.471E-01 .319E-02) (-.158E-01 -.890E-03)	(.613E+00 .809E-01) (-.151E-01 .763E-02) (-.528E-01 .364E-02) (-.439E-01 .115E-02)
7F2	87.	89.	(-.255E-01 .331E-03) (-.149E+00 -.330E-02) (.342E-01 -.106E-02) (-.101E-01 .745E-03)	(.973E+00 -.360E-04) (-.264E-01 .139E-02) (.343E-01 .314E-02) (.313E-01 .805E-02)	(.131E+00 -.363E-03) (-.313E-01 -.465E-02) (-.696E-01 .549E-02) (-.459E-01 .938E-02)
7F1	0.	0.	(.178E-03 .993E+00) (-.133E-02 .834E-01) (-.562E-03 -.177E-01) (.282E-03 .147E-02)	(-.185E-03 .384E-01) (.363E-03 .406E-01) (.457E-02 -.227E-01) (.651E-02 -.250E-01)	(-.236E-03 .612E-02) (-.205E-03 .261E-01) (-.133E-02 -.366E-01) (-.604E-02 -.228E-01)

[0 0>
[3 0>
[4 -4>
[5 -4>
[6 -4>

[1 0>
[4 0>
[5 0>
[6 0>

[2 0>
[4 4>
[5 4>
[6 4>

535	--	101.	(.181E-02 -.127E-04) (-.311E-04 -.436E-02) (-.261E+00 -.452E-02) (-.607E+00 -.163E-02) (-.211E-01 -.121E-02)	(-.238E-04 -.336E-02) (.349E+00 -.246E-02) (-.529E-03 -.746E-01) (.248E-02 -.175E-04)	(-.115E-01 .811E-04) (-.251E+00 .929E-02) (.606E+00 -.102E-01) (-.211E-01 .151E-02)
	--	71.	(.238E-03 .185E-05) (.183E-03 -.230E-01) (-.111E-01 .285E+00) (-.196E-02 .626E+00) (.516E-03 .954E-02)	(.561E-04 -.706E-02) (-.193E-01 -.162E-03) (.180E-02 -.227E+00) (-.146E-02 -.116E-04)	(.698E-02 .558E-04) (-.556E-02 -.286E+00) (-.800E-02 .626E+00) (.658E-03 -.953E-02)
	--	0.	(.192E-04 .730E-03) (.440E-02 -.108E-03) (.281E-01 -.314E-01) (.165E+00 .567E-01) (-.299E-01 .141E-02)	(.280E-02 -.690E-04) (-.117E-02 -.473E-01) (.965E+00 -.238E-01) (-.628E-04 -.255E-02)	(.235E-04 .952E-03) (-.296E-01 -.300E-01) (.152E+00 -.647E-01) (.299E-01 -.630E-04)

500	0.	0.	(.100E+01 .147E-06) (-.101E-10 .559E-04) (.770E-02 .102E-04) (-.951E-04 -.226E-04) (-.254E-02 -.755E-03)	(.201E-11 .141E-05) (.591E-02 .863E-09) (.579E-11 -.194E-04) (-.337E-03 .358E-10)	(.597E-02 .102E-08) (.770E-02 -.102E-04) (.951E-04 -.226E-04) (-.254E-02 .755E-03)
			[2 2> [3 -2> [5 2> [6 -2>	[2 -2> [4 2> [5 -2> [6 4>	[3 2> [4 -2> [6 2> [6 -4>
535	--	47.	(-.164E-01 .153E-01) (.569E-02 -.287E-02) (.499E+00 -.448E+00) (-.223E-01 .129E-01)	(.208E-01 -.840E-02) (-.204E+00 .881E-01) (.617E+00 -.263E+00) (-.642E-02 .115E-01)	(.501E-02 -.395E-02) (.155E+00 -.147E+00) (.211E-01 -.148E-01) (.131E-01 -.946E-03)
	--	25.	(-.405E-02 .551E-02) (-.788E-02 .610E-02) (-.239E+00 .592E+00) (.680E-03 -.881E-02)	(-.320E-02 .604E-02) (-.179E+00 .245E+00) (.430E+00 -.472E+00) (-.237E-02 .921E-03)	(.208E-02 -.974E-02) (-.143E+00 .267E+00) (.755E-02 -.443E-02) (.414E-03 .299E-02)
534	--	24.	(-.125E-01 -.145E-01) (.110E-01 .776E-03) (-.691E-01 -.271E+00) (-.290E-03 .126E-01)	(-.116E-01 -.152E-01) (.632E+00 .145E+00) (.251E+00 .122E+00) (.220E-01 -.173E-02)	(.146E-02 -.109E-01) (.139E-01 .649E+00) (.124E-01 .226E-02) (-.614E-02 .212E-01)
	--	17.	(-.485E-02 .128E-01) (.854E-02 .122E-01) (-.217E-01 .250E+00) (-.511E-04 -.655E-02)	(-.136E-01 .113E-02) (.629E+00 .203E+00) (.246E+00 .482E-01) (.187E-01 -.522E-02)	(.932E-02 .116E-01) (-.212E-01 -.660E+00) (.638E-02 .188E-02) (.102E-01 -.165E-01)
506	465.	384.	(.295E-02 -.611E-03) (-.533E-02 -.163E-02) (-.270E-01 .126E-02) (-.705E+00 -.241E-01)	(-.295E-02 -.611E-03) (-.146E-02 -.244E-02) (-.270E-01 -.126E-02) (.199E-01 -.415E-01)	(-.533E-02 .163E-02) (.146E-02 -.244E-02) (.705E+00 -.241E-01) (-.199E-01 -.415E-01)
	--	87.	(-.237E-02 .155E-02) (-.483E-03 -.485E-02) (-.101E-01 .192E-02) (-.120E+00 -.361E-01)	(-.124E-02 -.254E-02) (.202E-01 -.928E-02) (.774E-02 .682E-02) (-.442E+00 .537E+00)	(.289E-02 -.393E-02) (.126E-01 .183E-01) (-.121E+00 -.300E-01) (-.106E+00 -.687E+00)
	74.	83.	(.279E-02 -.827E-03) (.277E-02 -.481E-02) (.703E-02 .597E-02) (.105E-01 .445E-01)	(.281E-02 -.781E-03) (-.180E-01 -.112E-01) (-.279E-02 .879E-02) (.698E+00 .993E-01)	(-.490E-02 -.261E-02) (-.933E-02 .191E-01) (-.147E-01 -.433E-01) (.539E+00 -.455E+00)
	-15.	-16.	(-.690E-03 -.513E-04) (.254E-02 -.789E-02) (.773E-04 .980E-02) (-.198E-01 .696E+00)	(.689E-03 -.596E-04) (-.444E-03 -.282E-02) (-.408E-04 -.980E-02) (-.115E+00 -.500E-01)	(.263E-02 .786E-02) (.410E-03 -.282E-02) (.282E-01 .695E+00) (.114E+00 -.514E-01)

503	--	35.	(-.527E-02 .123E-02)	(-.409E-02 -.355E-02)	(.706E+00 .334E-01)
			(-.540E+00 -.300E+00)	(.958E-02 .945E-03)	(.892E-02 .363E-02)
			(.637E-02 .235E-03)	(-.575E-02 -.277E-02)	(-.755E-02 -.131E-02)
			(-.729E-02 -.236E-02)	(.522E-02 -.126E-02)	(.403E-02 .355E-02)
	--	16.	(-.345E-02 -.119E-01)	(.159E-02 .122E-01)	(.279E+00 .649E+00)
			(.105E-01 .707E+00)	(-.503E-02 -.138E-01)	(.103E-02 .145E-01)
			(-.467E-02 -.108E-01)	(-.154E-03 -.118E-01)	(.149E-02 .460E-02)
			(-.522E-03 -.481E-02)	(.371E-02 .497E-02)	(.135E-02 -.605E-02)
502	93.	42.	(.576E-04 .707E+00)	(.576E-04 -.707E+00)	(-.597E-05 .125E-01)
			(.597E-05 .125E-01)	(-.360E-02 -.123E-01)	(-.359E-02 .123E-01)
			(.488E-02 .138E-01)	(-.488E-02 .188E-01)	(-.377E-03 -.209E-02)
			(-.377E-03 .209E-02)	(.386E-03 -.241E-02)	(.386E-03 .241E-02)
	0.	0.	(.502E-04 .707E+00)	(-.502E-04 .707E+00)	(.200E-04 .483E-02)
			(.200E-04 -.483E-02)	(.342E-02 .175E-01)	(-.342E-02 .175E-01)
			(-.478E-02 -.150E-01)	(-.478E-02 .150E-01)	(.349E-03 .656E-04)
			(-.349E-03 .656E-04)	(-.157E-04 -.283E-02)	(.157E-04 -.283E-02)

			[1 1>	[2 1>	[3 1>
			[3 -3>	[4 1>	[4 -3>
			[5 1>	[5 -3>	[5 5>
			[6 1>	[6 -3>	[6 5>
535	--	67.	(.427E-02 -.418E-02)	(-.127E-01 -.291E-02)	(-.325E-01 .453E-03)
			(.205E-01 .632E-02)	(-.314E+00 .539E-01)	(.150E+00 -.179E-02)
			(.227E+00 .705E-01)	(.680E+00 -.193E-01)	(-.534E+00 -.116E+00)
			(-.383E-03 -.335E-02)	(-.630E-03 -.317E-02)	(.227E-01 .943E-03)
	--	53.	(.357E-02 .157E-01)	(-.349E-02 .643E-02)	(-.134E-01 -.682E-02)
			(.333E-02 .607E-02)	(-.273E-01 -.222E+00)	(.318E-01 .885E-01)
			(.123E+00 -.153E+00)	(.101E+00 .580E+00)	(-.178E-01 .745E+00)
			(-.121E-02 .116E-01)	(-.593E-02 .846E-02)	(.358E-02 -.101E-01)
	--	6.	(.615E-02 -.131E-02)	(.595E-02 -.211E-02)	(.149E-01 .359E-02)
			(.222E-01 .868E-02)	(.139E+00 -.170E-01)	(.145E+00 -.490E-01)
			(.930E+00 -.127E-01)	(-.702E-01 -.295E-01)	(.255E+00 -.117E+00)
			(.196E-01 -.382E-02)	(-.423E-01 -.350E-02)	(-.699E-03 .522E-02)
534	--	59.	(.195E-03 -.303E-02)	(.533E-02 .111E-01)	(-.973E-02 -.360E-01)
			(.437E-02 -.290E-01)	(.490E-01 .230E+00)	(-.192E-01 .949E+00)
			(.400E-01 -.180E+00)	(.150E-01 -.671E-01)	(.777E-02 -.355E-01)
			(.124E-01 .337E-01)	(-.422E-02 -.128E-01)	(-.185E-02 -.974E-02)
	--	0.	(.489E-02 -.156E-02)	(-.371E-03 .301E-03)	(-.333E-02 .467E-04)
			(-.489E-01 -.122E-01)	(.876E+00 -.242E-01)	(-.198E+00 -.450E-01)
			(-.593E-01 .933E-02)	(.422E+00 .296E-01)	(-.510E-01 -.307E-01)
			(.127E-01 .768E-03)	(-.334E-01 -.477E-02)	(-.303E-01 .483E-02)

5G6	462.	375.	(.209E-02 -.153E-02)	(-.910E-03 .205E-03)	(.556E-03 .125E-02)
			(-.713E-03 -.125E-02)	(.352E-01 .333E-01)	(.148E-01 .254E-01)
			(.266E-01 .205E-01)	(.822E-02 .649E-02)	(.106E-01 .683E-02)
			(-.426E+00 -.400E+00)	(.546E+00 .564E+00)	(.847E-01 .174E+00)
	288.	250.	(-.952E-03 .162E-02)	(-.535E-03 .545E-02)	(-.259E-02 .551E-02)
			(.208E-02 -.432E-02)	(-.790E-02 .243E-01)	(-.613E-03 -.132E-02)
			(-.582E-02 -.179E-01)	(-.934E-03 .337E-03)	(.751E-04 .190E-01)
			(.405E-02 -.214E-02)	(-.703E-01 -.229E+00)	(.111E-02 .970E+00)
	0.	0.	(.129E-02 -.113E-02)	(.328E-03 .131E-02)	(.446E-02 .458E-02)
			(-.374E-02 -.628E-02)	(.807E-02 .717E-02)	(-.918E-02 -.201E-01)
			(.991E-02 .747E-02)	(-.306E-02 -.856E-03)	(-.831E-02 -.187E-02)
			(.586E+00 .550E+00)	(.390E+00 .413E+00)	(.651E-01 .125E+00)
503	--	39.	(.243E-03 .438E-02)	(.798E-04 -.638E-02)	(.630E-01 .300E+00)
			(.650E-02 .949E+00)	(.148E-01 .505E-01)	(-.109E-02 .223E-01)
			(-.109E-01 -.353E-01)	(.476E-03 .116E-01)	(-.357E-02 -.567E-02)
			(.147E-02 .474E-02)	(.308E-03 .183E-02)	(.146E-03 .192E-02)
	--	9.	(.266E-04 .354E-02)	(-.412E-03 -.450E-03)	(-.283E-01 .950E+00)
			(.700E-01 -.298E+00)	(-.774E-03 -.197E-01)	(-.118E-01 .320E-01)
			(.130E-02 -.922E-03)	(-.629E-02 .252E-01)	(-.719E-02 -.182E-01)
			(.421E-04 -.503E-02)	(.902E-03 -.434E-02)	(-.188E-02 -.723E-02)
502	70.	41.	(-.774E-02 .755E-04)	(.100E+01 -.144E-04)	(.227E-02 -.787E-05)
			(.644E-02 -.119E-03)	(-.565E-02 -.604E-04)	(-.984E-02 -.526E-02)
			(.623E-03 .569E-04)	(.658E-02 .147E-02)	(-.141E-01 .312E-02)
			(-.184E-02 .780E-04)	(.126E-02 .571E-03)	(-.492E-02 .667E-03)
501	0.	0.	(.100E+01 -.487E-04)	(.770E-02 .503E-04)	(-.458E-02 .239E-04)
			(-.320E-02 .218E-04)	(.246E-03 -.288E-04)	(.353E-03 -.323E-04)
			(-.462E-02 -.206E-04)	(-.144E-01 -.383E-02)	(-.114E-01 .577E-03)
			(-.173E-03 .213E-04)	(-.239E-02 -.697E-03)	(-.207E-02 .598E-03)

r.m.s deviatin=13.1 cm

The splittings are given with respect to the lowest Stark level (observed) of a given multiplet

The 5G6 multiplet has not been used for least squars analysis

The numbers in the parenthesis"()" represent respectively the real and imaginary parts of a coefficient.

free ion positions but in principle one should diagonalize the free ion and crystal field energy matrices simultaneously. A comparative look of Tables 4.5 and 4.7 shows clearly that the effect of J-mixing is prominent on the ^7F_J multiplets while the ^5D_J multiplets are somewhat unaffected by this. This is rather strange.

In conclusion we can say that our limited J-J mixing calculations using intermediate wavefunctions seem to adequately account for the observed splittings of the ^7F_J multiplets but not quite so for the ^5D_J and other multiplets. Perhaps more detailed free ion and J-J mixing calculations are needed to simulate upper levels satisfactorily.

-xx-

REFERENCES

[1] W T Carnall, P R Fields and K Rajnak; J Chem Phys 49 10 4450 (1968).

[2] C Görller-Walrand et al; Inorganica Chimica Acta 109 83 (1985).

[3] C Rudowicz; Chemical Physics 97 43 (1985).

[4] J Huang and J Loriers et al; J Chem Phys 80 12 6204 (1984).

[5] J Hölsa and P Porcher; J Chem Phys 75 5 2108 (1981).

-xx-

CHAPTER-V

SUMMARY

In this thesis we have attempted an in-depth spectroscopic study of Eu^{3+} doped in $LiYF_4$ single crystal. When we undertook this investigation, no published work on the analysis of the spectroscopic data existed for this system. Subsequently Görller et al [1] have reported an analysis of the fluorescence originating from the ^5D_o and $^5D_1$ multiplets of Eu^{3+}. Our analysis of the $LiYF_4:Eu^{3+}$ data represents a somewhat different approach as compared to the one used by the authors of reference [1]. Further we have considered several additional multiplets, not analysed so far. Görller et al have analysed ^7F_o, $^7F_1$, $^7F_2$, $^7F_3$, $^7F_4$ and $^7F_5$ multiplets whereas our analysis extends to ^5D_o, $^5D_1$, $^5D_2$ and $^5L_6$ multiplets as well. Moreover, unlike their work, we have recorded polarized spectra and the polarization information was extremely useful in the symmetry assignment of levels.

The absorption spectrum was obtained by using a 1000W tungsten-halogen lamp and the fluorescence was excited by the 457.9 nm and 514.5 nm lines of the Ar^+ laser and by a R-6G ring dye laser. The 457.9 nm line of Ar^+ laser non-resonantly excites the $^5D_2$ multiplet of Eu^{3+} and produces fluorescence from the $^5D_2$, $^5D_1$ and ^5D_o multiplets. The 514.5 nm line produces fluorescence from the $^5D_1$ and ^5D_o

multiplets. The ^5D_o level can be excited selectively by tuning the R 6G dye laser to the $^7F_1(\Gamma_3^-)$-$^5D_o(\Gamma_1^+)$ transition. It can also be excited by a phonon assisted process when the dye laser is tuned to 17630 cm^{-1}. The excitation spectrum was recorded by monitoring the $^5D_o(\Gamma_1^+)$-$^7F_1(\Gamma_1^+)$ transition at 16840 cm^{-1} and scanning the dye laser from 16900 to 17800 cm^{-1}.Th excitation spectrum confirms the position of the ^5D_o level at 17270 cm^{-1} and has been useful in identifying Raman and vibronic lines in the fluorescence spectra. We have not attempted a serious analysis of the excitation spectrum because of the limited precision of these measurements (expected error in locating peaks is about 5-6 cm^{-1}). The complete structure of the $^5D_1$ and $^5D_2$ multiplets and partial structure of the $^5L_6$ multiplet could be established from the absorption data. The $^7F_o \rightarrow {}^5D_o$ and $^5D_3$ absorption could not be observed due to the forbidden nature of these transitions. $^5D_2$- ^7F_J(J=0 to 6), $^5D_1$- ^7F_J(J=0 to 5) and ^5D_o - ^7F_J(J=0 to 5)fluorescence has been recorded in π, σ and axial modes. All spectra were recorded at liquid nitrogen temperature. The Stark structures of the $^7F_1$, $^7F_2$, $^7F_3$ and $^7F_4$ have been established completely and the structure of the $^7F_5$ could be established only partially. The analysis of the $^5D_2$ - $^7F_6$ fluorescence has not been attempted because the lines belonging to this group are rather closely spaced, weak and broad. For better understanding of $^5D_2$ - $^7F_6$ fluorescence, it would

be necessary to use a sample with higher Eu^{3+} concentration. Our experimentally inferred positions of the Stark levels belonging to the ^7F_J(J=0 to 4) and $^5D_{0,1}$ multiplets are in agreement (within ± 3 cm^{-1}) with those reported by Görller et al. However, some disagreement exists for the structure of the $^7F_5$ multiplet. For example, our analysis of the experimental data would place the Γ_2 and Γ_3 levels of the $^7F_5$ multiplet at 3786 cm^{-1} and 3799 cm^{-1} as compared to 3795 cm^{-1} and 3807 cm^{-1} reported by these authors. They have not observed the $^7F_5(\Gamma_1)$ levels at 3844 cm^{-1} and 4008 cm^{-1} which we have been able to establish.

The CG's of the Stark components and hence the positions of the free ion levels of the $^7F_0$, $^7F_1$, $^7F_2$, $^7F_3$, $^7F_4$, $^7F_5$, $^5D_0$, $^5D_1$ and $^5D_2$ have been found to lie at 0 cm^{-1}, 365 cm^{-1}, 1034 cm^{-1}, 1921 cm^{-1}, 2899 cm^{-1}, 3948 cm^{-1}, 17271 cm^{-1}, 19028 cm^{-1} and 21502 cm^{-1} respectively. The free ion Hamiltonian consisting of the spin-orbit, the residual Coulomb and the configuration interactions was solved numerically by treating the radial quantities as adjustable parameters in an effort to bring the calculated free ion energies of the nine multiplets in agreement with their experimentally inferred values. A systematic least squares analysis could not be carried out due to the large size of the free ion matrices. We had to resort to an approximate approach to perform this task. Only one parameter was varied at a time

till the minimum in the r.m.s. deviation was obtained for that parameter. This procedure was repeated for the remaining parameters. In this manner we could obtain an r.m.s. deviation of 24 cm^{-1} between the calculated free ion levels and the experimental CG's.

The experimental crystal field splittings were obtained by taking differences of the observed Stark level positions with respect to the lowest Stark level of a given multiplet. Thus 23 such energy differences were obtained; 19 belonging to the ^7F_J(J=0 to 5) and 4 to the ^5D_J(J=0 to 2) multiplets. The $^5L_6$ multiplet was excluded from this analysis due to insufficient experimental data.

The crystal field Hamiltonian was treated as a perturbation over the free ion Hamiltonian taking intermediate coupling wavefunctions as zeroth-order wavefunctions. Initially crystal field calculations were performed neglecting J-J mixing effects i.e. crystal field matrix elements with $J \neq J'$ were neglected. The least squares analysis was carried out for 19 energy differences and then for 23 energy differences, which gave r.m.s. deviations of 17.5 and 20.1 cm^{-1} respectively. These deviations are considerably larger than the 3 cm^{-1} r.m.s. deviation reported by Görller et al, who considered J-J mixing effects within ^7F_J manifold. If, however, we use crystal field parameters reported by these

authors, the r.m.s. deviations for 19 and 23 energy differences go up to about 23.2 and 24.8 cm^{-1} respectively. It was felt that large r.m.s. deviation may be due to our neglecting of J-J mixing effects. To estimate the contribution of J-J mixing, we have carried out a limited J-J mixing calculation. Exact J-J mixing calculations are difficult to perform for $LiYF_4:Eu^{3+}$, because this needs large size matrices to be diagonalized. We have considered only two lowest multiplets for each J (from J=0 to 6), and thus 6 energy matrices (corresponding to two multiplets and three irreducible representations) were constructed including matrix elements for $J \neq J'$ as well. These calculations gave very good agreement for ^7F_J multiplet but for upper levels agreement was poor. The least squares fit to the 19 energy differences gave a low r.m.s. deviation of 2.9 cm^{-1} while that for 23 levels (including the ^5D_J multiplets) was 13.1 cm^{-1}. In fact the neglect of higher multiplets in case of the ^7F_J manifold may be justified due to relatively pure nature of the ^7F wavefunctions (96% to 99%), but the same is not true for the higher levels. Other authors have encountered similar situation for Eu^{3+} in other hosts. The authors of ref [2] suggested the mixing of ^3P states as a possible cause for the poor agreement for the ^5D_J multiplets. This conjecture does not seem to hold, as we have used intermediate

coupling wavefunctions where contribution of ^3P states are included. Though we do not have any satisfactory explanation for this poor agreement, we nevertheless feel that a more exact J-J mixing calculation involving other nearby multiplets should improve the situation but computational complexities have prevented us from performing such calculations. It should be pointed out that we accounted for the free ion contributions in the J-J mixing calculations by adding to the diagonal matrix elements, the calculated free ion positions but in principle one should diagonalize the free ion and crystal field energy matrices simultaneously.

We find that the order of calculated energy levels is in agreement with the experimental assignment based on polarization information in both the calculations (i.e. with and without J-J mixing effects). It may be mentioned that we always got the same values of the crystal field parameters irrespective of whatever values were used to initialize the minimization subroutine.

We may conclude by saying that the $LiYF_4:Eu^{3+}$ is a rather complex system and our effort to interpret the somewhat incomplete data can be considered only a preliminary effort in that direction. Our description of the system is an improvement over the only other effort made so far. More detailed experimental and theoretical analysis especially for upper multiplets is needed for a better understanding

of this system. The role of phonons and other lattice effects vis-a-vis the observed temperature dependence of the positions of the spectral lines and the existence of efficient phonon assisted excitation effects are some of the other areas for future investigations.

-xx-

REFERENCES

[1] C Görller-Walrand et al; Inorganica Chimica Acta 109 83 (1985).

[2] J Hölsa and P Porcher; J Chem Phys 75 5 2108 (1981).

-xx-

APPENDIX-I

TABLE AI-1

LS TERMS OF $4f^6$ CONFIGURATION

S.No.	S	L	$(\omega_1\ \omega_2\ \omega_3)$	$(U_1\ U_2)$	Nielson and Koster Notation $(2S+1)_{Lr}$	Seniority Quantum Number(v)
1.	3	3	(100)	(10)	7F	6
2.	2	0	(111)	(00)	5S	4
3.	2	1	(210)	(11)	5P	6
4.	2	2	(111)	(20)	5D1	4
5.	2	2	(210)	(20)	5D2	6
6.	2	2	(210)	(21)	5D3	6
7.	2	3	(111)	(10)	5F1	4
8.	2	3	(210)	(21)	5F2	6
9.	2	4	(111)	(20)	5G1	4
10.	2	4	(210)	(20)	5G2	6
11.	2	4	(210)	(21)	5G3	6
12.	2	5	(210)	(11)	5H1	6
13.	2	5	(210)	(21)	5H2	6
14.	2	6	(111)	(20)	5I1	4
15.	2	6	(210)	(20)	5I2	6
16.	2	7	(210)	(21)	5K	6
17.	2	8	(210)	(21)	5L	6
18.	1	1	(110)	(11)	3P1	2
19.	1	1	(211)	(11)	3P2	4

20.	1	1	(211)	(30)	3P3	4
21.	1	1	(221)	(11)	3P4	6
22.	1	1	(221)	(30)	3P5	6
23.	1	1	(221)	(31)	3P6	6
24.	1	2	(211)	(20)	3D1	4
25.	1	2	(211)	(21)	3D2	4
26.	1	2	(221)	(20)	3D3	6
27.	1	2	(221)	(21)	3D4	6
28.	1	2	(221)	(31)	3D5	6
29.	1	3	(110)	(10)	3F1	2
30.	1	3	(211)	(10)	3F2	4
31.	1	3	(211)	(21)	3F3	4
32.	1	3	(211)	(30)	3F4	4
33.	1	3	(221)	(10)	3F5	6
34.	1	3	(221)	(21)	3F6	6
35.	1	3	(221)	(30)	3F7	6
36.	1	3	(221)	(31) A	3F8	6
37.	1	3	(221)	(31) B	3F9	6
38.	1	4	(211)	(20)	3G1	4
39.	1	4	(211)	(21)	3G2	4
40.	1	4	(211)	(30)	3G3	4
41.	1	4	(221)	(20)	3G4	6
42.	1	4	(221)	(21)	3G5	6
43.	1	4	(221)	(30)	3G6	6
44.	1	4	(221)	(31)	3G7	6

45.	1	5	(110)	(11)	3H1	2
46.	1	5	(211)	(11)	3H2	4
47.	1	5	(211)	(21)	3H3	4
48.	1	5	(211)	(30)	3H4	4
49.	1	5	(221)	(11)	3H5	6
50.	1	5	(221)	(21)	3H6	6
51.	1	5	(221)	(30)	3H7	6
52.	1	5	(221)	(31) A	3H8	6
53.	1	5	(221)	(31) B	3H9	6
54.	1	6	(211)	(20)	3I1	4
55.	1	6	(211)	(30)	3I2	4
56.	1	6	(221)	(20)	3I3	6
57.	1	6	(221)	(30)	3I4	6
58.	1	6	(221)	(31) A	3I5	6
59.	1	6	(221)	(31) B	3I6	6
60.	1	7	(211)	(21)	3K1	4
61.	1	7	(211)	(30)	3K2	4
62.	1	7	(221)	(21)	3K3	6
63.	1	7	(221)	(30)	3K4	6
64.	1	7	(221)	(31) A	3K5	6
65.	1	7	(221)	(31) B	3K6	6
66.	1	8	(211)	(21)	3L1	4
67.	1	8	(221)	(21)	3L2	6
68.	1	8	(221)	(31)	3L3	6
69.	1	9	(211)	(30)	3M1	4

70.	1	9	(221)	(30)	3M2	6
71.	1	9	(221)	(31)	3M3	6
72.	1	10	(221)	(31)	3N	6
73.	1	11	(221)	(31)	3O	6
74.	0	0	(000)	(00)	1S1	0
75.	0	0	(220)	(22)	1S2	4
76.	0	0	(222)	(00)	1S3	6
77.	0	0	(222)	(40)	1S4	6
78.	0	1	(222)	(30)	1P	6
79.	0	2	(200)	(20)	1D1	2
80.	0	2	(220)	(20)	1D2	4
81.	0	2	(220)	(21)	1D3	4
82.	0	2	(220)	(22)	1D4	4
83.	0	2	(222)	(20)	1D5	6
84.	0	2	(222)	(40)	1D6	6
85.	0	3	(220)	(21)	1F1	4
86.	0	3	(222)	(10)	1F2	6
87.	0	3	(222)	(30)	1F3	6
88.	0	3	(222)	(40)	1F4	6
89.	0	4	(200)	(20)	1G1	2
90.	0	4	(220)	(20)	1G2	4
91.	0	4	(220)	(21)	1G3	4
92.	0	4	(220)	(22)	1G4	4
93.	0	4	(222)	(20)	1G5	6
94.	0	4	(222)	(30)	1G6	6

95.	0	4	(222)	(40) A	1G7	6
96.	0	4	(222)	(40) B	1G8	6
97.	0	5	(220)	(21)	1H1	4
98.	0	5	(220)	(22)	1H2	4
99.	0	5	(222)	(30)	1H3	6
100.	0	5	(222)	(40)	1H4	6
101.	0	6	(200)	(20)	1I1	2
102.	0	6	(220)	(20)	1I2	4
103.	0	6	(220)	(22)	1I3	4
104.	0	6	(222)	(20)	1I4	6
105.	0	6	(222)	(30)	1I5	6
106.	0	6	(222)	(40) A	1I6	6
107.	0	6	(222)	(40) B	1I7	6
108.	0	7	(220)	(21)	1K1	4
109.	0	7	(222)	(30)	1K2	6
110.	0	7	(222)	(40)	1K3	6
111.	0	8	(220)	(21)	1L1	4
112.	0	8	(220)	(22)	1L2	4
113.	0	8	(222)	(40) A	1L3	6
114.	0	8	(222)	(40) B	1L4	6
115.	0	9	(222)	(30)	1M1	6
116.	0	9	(222)	(40)	1M2	6
117.	0	10	(220)	(22)	1N1	4
118.	0	10	(222)	(40)	1N2	6
119.	0	12	(222)	(40)	1Q	6

APPENDIX-II

DOUBLE MONOCHROMATOR GDM 1000

The GDM-1000 double monochromator has two autocollimated monochromators, each with a concave mirror and a grating (651 lines/mm) in Littrow arrangement, placed one behind the other so that the dispersion of the gratings are added and coma aberration of mirrors annulled. This gives a sharp image of the entrance slit in the plane of the outlet slit and is free from coma. Other image aberrations are negligible due to the chosen focal length of the mirrors (f=1100 mm, aperture ratio 1:10.4) and the small angle of incidence of rays on the concave mirrors. A field flattening lens in front of the outlet slit is used to compensate for the curvature of the field arising from the concave mirrors and wavenumber dependence of the line curvature. The monochromator incorporates a built-in 25 Hz chopper and an automarking generator.

TABLE AII-1

CALIBRATION CHART

Source used for calibration : Ne discharge tube
Spectral region 23000-17000 cm^{-1} (IInd order)

Standard Wave No. (cm^{-1})	Observed on GDM 1000 (cm^{-1})
22737.9	22738
22580.8	22580
22281.2	22279
22037.3	22036
21475.7	21475
21256.7	21256
21236.6	21236
21231.1	21231
21222.1	21221
21207.4	21207
20881.5	20881
20715.3	20714
20471.2	20469
20173.4	20172
19850.1	19849
19436.6	19435
18759.0	18759
18722.8	18721
18715.1	18714
18516.6	18515
17396.5	17395
17347.8	17347
17086.8	17084
17001.3	17000

TABLE AII-2

CALIBRATION CHART

Source used for calibration : Ne discharge tube

Spectral region 17350-11300 cm^{-1} (Ist order)

Standard Wave No. (cm^{-1})	Observed on GDM 1000 (cm^{-1})
17347.8	17344
17086.8	17083
17001.3	16998
16734.9	16732
16583.8	16581
16462.7	16460
16278.5	16276
16224.3	16222
16084.2	16082
15957.9	15955
15786.8	15784
15666.6	15664
15619.5	15617
15153.9	15152
14973.9	14972
14431.1	14429
14219.9	14218
13939.4	13938
13802.3	13801
12047.7	12046
11936.6	11935
11771.1	11767
11521.4	11520
11518.2	11516
11384.7	11383

TABLE AII-3

POLARIZATION RESPONSE OF GDM-1000 MONOCHROMATOR

Source used: 1000-W Tungsten-Halogen Lamp

Spectral region: 25600 cm^{-1} - 17500 cm^{-1} (IInd Order)

Wavenumber (cm^{-1})	(Arb.units) E|| Slit (I_σ)	E ⊥ Slit (I_π)	I_σ/I_π
25578	1.4	0.7	2.0
25178	2.7	1.5	1.8
24778	4.6	2.5	1.84
24378	6.8	4.7	1.7
23978	8.7	6.2	1.4
23578	10.8	8.6	1.26
23178	12.5	11.0	1.14
22778	13.7	13.2	1.04
22578	14.1	14.1	1.0
22378	14.2	14.9	0.95
21978	14.7	16.4	0.90
21578	14.8	17.3	0.86
21178	14.1	17.5	0.81
20778	13.2	17.0	0.78
20378	11.8	16.0	0.74
19978	10.1	14.5	0.70
19578	8.3	12.6	0.66
19178	6.6	9.3	0.71
18778	5.1	8.2	0.62
18378	3.9	8.3	0.47
17978	3.1	7.9	0.39
17578	2.2	6.6	0.33

TABLE AII-4

POLARIZATION RESPONSE OF GDM-1000 MONOCHROMATOR

Source used: 1000-W Tungsten-Halogen Lamp

Spectral region: 17500-13000 cm^{-1} (Ist Order)

Wavenumber (cm^{-1})	(arb.units) E|| Slit (I_σ)	E ⊥ Slit (I_π)	I_σ/I_π
17488	17.3	2.7	6.41
17288	17.9	2.8	6.39
17088	18.3	3.1	5.90
16888	18.6	3.5	5.31
16688	18.8	3.8	4.95
16488	18.8	4.3	4.37
16288	18.8	5.0	3.76
16188	18.6	5.3	3.51
16088	18.4	6.4	2.88
15988	17.8	6.1	2.92
15888	17.2	5.5	3.13
15688	15.8	3.6	4.39
15488	13.9	1.9	7.32
15388	13.0	1.4	9.29
15288	12.3	1.2	10.25
15188	11.4	1.2	9.5
15088	10.5	1.2	8.75
14888	8.8	1.2	7.33
14688	7.0	1.2	5.83
14488	5.5	1.2	4.58
14288	4.4	1.2	3.33
14088	2.7	1.0	2.70
13888	1.8	0.7	2.57
13688*	8.4	5.4	1.56
13488*	4.8	3.3	1.45
13288*	4.2	2.9	1.45

*Recording parameters such as sensitivity and slit width were different.

APPENDIX-III

A. PROCEDURE FOR THE LEVEL ASSIGNMENT

The assignment of transitions involving multiplets with J=0 (as one of the states) is straightforward and the positions and symmetry (irreducible representations) of these states could be assigned easily using the polarization selection rules described in Chapters II and IV. All transitions in the absorption spectrum, the fluorescence transitions terminating on $^7F_0$ and those originating from $^5D_0$ fall in this category. The level assignment for fluorescence transitions originating from and terminating on multiplets with $J \neq 0$ require more careful handling of the experimental data. The multiplets studied in this work are relatively well separated and in most cases it was possible to unambiguously associate a given group of fluorescence lines to transitions between a pair of multiplets. We will illustrate the procedure adopted in such cases by taking the example of $^5D_1$-$^7F_3$ fluorescence.

The multiplets $^5D_1$ and $^7F_3$ have two ($\Gamma_1+\Gamma_{3,4}$) and five ($\Gamma_1+2\Gamma_2+2\Gamma_{3,4}$) components respectively. Thus a maximum of 10 transitions are expected ignoring selection rules. There are 9 observed lines from 17185 cm^{-1} to 16984 cm^{-1} which may belong to this group. Since we know the positions of both the components of $^5D_1$ from the analysis of other groups, we can construct the following table where the first column lists all the observed fluorescence lines and the second and third

columns give the difference of these from the positions of $^5D_1$ Stark components.

Observed transition wavenumber (cm^{-1})	$^5D_1(\Gamma_{3,4})$ 19021 cm^{-1}	$^5D_1(\Gamma_1)$ 19043 cm^{-1}
17185	1836	<u>1858</u>
17171	1850	1872
17162	<u>1859</u>	1881
17149	1872	1894
17119	1902	1924
17091	1930	<u>1952</u>
17069	<u>1952</u>	1974
17006	2015	<u>2037</u>
16984	<u>2037</u>	2059

From this table we notice that the lines at 17185 and 17162 cm^{-1} terminate on the same final level (1859$\pm$1 cm^{-1}) and their polarization behavior suggest them to be ($\Gamma_{3,4}-\Gamma_2$) and ($\Gamma_1-\Gamma_2$) transitions respectively (C.f. table 3.5 and 3.6) of Chapter III). Thus one of the Γ_2 levels of $^7F_3$ can be placed at 1859 cm^{-1}. Similarly other Γ_2 and both $\Gamma_{3,4}$ levels of the $^7F_3$ can be placed at 2037 cm^{-1}, 1872 cm^{-1} and 1952 cm^{-1} respectively. The remaining one transition at 17119 cm^{-1} may be assigned to a level at 1902 or 1924 cm^{-1}, but its polarization behavior suggests it to be $\Gamma_1 \longleftrightarrow \Gamma_{3,4}$ transition. Since both $\Gamma_{3,4}$ levels of $^7F_3$ are already fixed, the only possibility left is to assign Γ_1 at 1902 cm^{-1}. This assignment could be further confirmed by similar analysis of the $^5D_2$-$^7F_3$ group. In this manner all the components of $^7F_3$ could be identified.

B. PROGRAMMING DETAILS

1. FREE ION CALCULATIONS

For the free ion calculations the energy matrices of the combined electrostatic, spin-orbit and configuration interactions are constructed. A typical matrix element is of the form

$$E(I) = AE1(I) * E^1 + AE2(I) * E^2 + AE3(I) * E^3 + ASO(I) * \zeta_{4f} + AAL(I) * \alpha + ABE(I) * \beta + AGA(I) * \gamma \quad \ldots.1$$

Where, the radial parts are denoted by their usual notations and the quantities multiplying them are the corresponding angular parts. Since the energy matrix is real and symmetric, only one half of the matrix elements need to be calculated. For the $Eu^{3+}(4f^6)$ configuration, a total of 4228 matrix elements have to be calculated if the calculations are restricted to J values lying between 0 to 6 only. The angular parts of all the matrix elements were stored sequentially and were then broken into submatrices, one for each J. The order of the matrices corresponding to J = 0,1,2,3,4,5 and 6 were 14,19,37,37,46,37 and 38 respectively. The angular parts of the Coulomb and configuration interactions were taken directly from the tables, whereas the angular parts of the spin-orbit interaction were calculated with the help of a

---

Computations were done on DEC 1090 system at Computer Centre, IIT Kanpur.

separate program using subroutines for calculating 3-J and 6-J symbols. The reduced matrix elements of $V^{(11)}$ were taken from tables. All these matrices were diagonalized using the 'EIGEN' subroutine taken from the 'IBM360 Scientific Subroutine Package'. The eigen values were printed out taking the energy eigen value of the lowest level as the zero of the energy scale. The eigen vector could be printed out whenever needed.

2. CRYSTAL FIELD CALCULATIONS

The crystal field Hamiltonian in terms of the tensor operators is written as

$$H'_{cry}(S_4) = \sum_{k=2,4,6} B_o^k C_o^k + \sum_{k=4,6} [B_4^k (C_4^{(k)} + C_{-4}^{(k)}) + iB_4'^k (C_4^{(k)} - C_{-4}^{(k)})] \quad \ldots 2$$

A typical matrix elements of this Hamiltonian can be expressed as

$$\langle f^N\, SLJJ_z | \Sigma\, B_q^k\, C_q^{(k)} | f^N\, S'L'J'J_z' \rangle = \delta_{ss'} \sum_{k,q} F(k,q) \cdot ATOM(k) \cdot B_q^k \quad \ldots 3$$

Where

$$F(k,q) = (-1)^{J-J_z} \begin{pmatrix} J & k & J' \\ -J_z & q & J_z' \end{pmatrix} \langle f || C^{(k)} || f \rangle \quad \ldots 4$$

$$ATOM(k) = (-1)^{S+L'+J+k} \cdot \sqrt{[(2J+1)(2J'+1)]} \cdot \begin{Bmatrix} J & J' & k \\ L' & L & S \end{Bmatrix} \cdot \langle f^N\, SL || U^{(k)} || f^N\, SL' \rangle \quad \ldots 5$$

The non-zero reduced matrix elements of $U^{(k)}$ were taken from

the tables of Nielson and Koster were stored as such along with their SL values. The J,S and L values of the connecting states of the matrix elements were generated from the stored data within the computer program for all the matrices and were arranged in the sequential order compatible with the free ion wavefunction. The quantities F(k,q) and ATOM(k) were then calculated in that sequence and stored in a three dimensional array specifying the irreducible representation Γ_i, the (k,q) values and the sequence (Ni) of the matrix elements for a given J, as the three dimensions. Even zeros were included at this stage.

The free ion wavefunctions were generated in a separate program by diagonalizing the free ion matrices and the products of the coefficients of the connecting |LSJ> states were combined with the corresponding $U^{(k)}$ and summed over appropriately. They were subsequently multiplied by F(k,q)'s and then by the crystal field parameters to obtain the final crystal field matrix elements.

2.1 CALCULATIONS WITHOUT J-J MIXING

The crystal field energy matrices were constructed for each representation of a given J multiplet (i.e. the matrix elements between J and J' with $J \neq J'$ were neglected). The resulting matrices were not more than 4 x 4 dimension but each matrix element was obtained summing over, all LS basis states

because of the intermediate coupling used for these calculations. For example, the calculation of a single matrix element of a J with N |LS> basis states needs 7 N^2 ATOM(k)'s to be evaluated. The total number of $U^{(k)}$ were more than $14x10^3$. The crystal field matrices were complex and hence were converted into real matrices of double the dimensionality by a program written for this purpose and then diagonalized using the subroutine 'EIGEN'.

2.2 CALCULATIONS WITH J-J MIXING

To include J-J mixing effects, the energy matrices were constructed for each representation for all ^7F_J multiplets (J=0 to 6) and all $^5D_{o,1,2,3}$, $^5G_{4,5}$ and $^5L_6$ multiplets separate by now including the matrix elements with $J \neq J'$ as well. This made calculations of the matrix elements more complicated and lengthy because now a given |JLS> basis of the wavefunction of a given J-multiplet were to be combined with all the |JLS> basis of the wavefunctions of other interfering multiplets. Though the resulting matrices did not exceed 13x13, the intermediate storage requirements increased immensely. For example, now the total number of ATOM(k) for the ^7F_J multiplets alone was more than 10^5. The program were modified not to store ATOM(k) and F(k,q) separately, but to be evaluated and used in the program itself. The calculated free ion eigen values were added to the diagonal

matrix elements of the crystal field energy matrices. These matrices were diagonalized in a similar fashion as for without J-J mixing. Several internal checks were made to ensure that no computational mistakes remain.

3. MINFUN

This program to minimize a function of several variables was written by W E Humphrey at Lawrence Radiation Laboratory [1]. This program was modified for some of its input requirements [2].

Theory

This program uses the Ravine stepping method for finding the minimum of a function defined in the parameter space. A brief description of this program is given here. The variable names used here appear as a symbol in the MINFUN.

Operation 1: The search procedure begins by computing the gradient $\overline{GB}$ of the function at the initial point $\overline{XB}$ in the parameter space. The starting direction of search $\overline{EXVEC}$ is taken apposite to $\overline{GB}$ i.e. - $\overline{GB}$.

Operation 2: A step is taken to point c such that

$$\overline{XC} = \overline{XB} + (STEP.WT)\ \overline{EXVEC} \qquad ....6$$

Where STEP is the step size and WT is the relative weight of the parameter. The value of the function FC and gradient $\overline{GC}$ at this point are evaluated and a hyper-plane is defined

as to include $\overrightarrow{GC}$ and $\overline{EXVEC}$. A unit vector $\overline{PERP}$ perpendicular to $\overline{EXVEC}$ and parallel to $-\overline{GC} + (\overline{GC}.\overline{EXVEC})\,\overline{EXVEC}$ is defined.

Operation 3: A step is taken along $\overline{PERP}$ from $\overline{XC}$ to another point $\overline{XT} = \overline{XC} + (ALPHM.WT)\,\overline{PERP}$ where ALPHM is determined in the programme and is of the order of twice the step size. Assuming the quadratic relation between function and ALPH, a point $\overline{XA}$ can be determined such that function FA is less than FC and FT where

$$\overline{XA} = \overline{XC} + (ALPH.WT)\,\overline{PERP} \qquad .....7$$

Operation 4: If function FA is truly a minimum (i.e. less than FC and FT) then the vectors $\overline{EXVEC}$ and $\overline{XB}$ are redefined as

$$\overline{EXVEC} = \frac{\overline{XA} - \overline{XB}}{|\overline{XA} - \overline{XB}|} \qquad .....8$$

and

$$\overline{XB} = \overline{XB} + (STEP.WT)\,\overline{EXVEC} \qquad .....9$$

This completes a full step and control returns to operation 2 to begin the next step. If FA is not a new minimum, the control is returned to operation 3 with ALPHM half of its previous value. In the case that ALPH becomes more than twice the step size STEP, the previous parts of this step is skipped and the new step is taken along $\overline{GC}$ from $\overline{XC}$.

INPUT PARAMETERS

1. ISWS (1-6): Each element of this array controls the corresponding sense switch and can have values 0 or 1. For details see Table (A III-1)

2. NPAR: Number of variable parameters n in the function.

3. NSTEP: The maximum number of steps for the run.

4. STEP: Magnitude of the step. If it is positive the search mode is used. If step is negative, convergence mode is used. If step is zero, it is set to +1.0 by the program.

5. EPST: The tolerance. Normally it is zero. In the convergence mode if the function does not change by this much amount for each of the eleven consecutive steps, the run is terminated.

6. X: Starting values of the parameters.

7. WT: The weight factors corresponding to the changes in the parameters. These must be non-zero.

8. DIRIN: The initial direction for the first step. The individual elements of this vector may be of any size, as they are normalized by MINFUN. However, their signs are taken into account. These may be put as zeros, if no special direction is required.

TABLE A-III-1

SENSE SWITCHES

Value of i option No.	Comment
1	= 0 for maximum likelihood function = 1 for chi-squared function This affects only the error analysis.
2	not referenced-may be set to zero
3	Different minimizing procedures will be used by MINFUN, subject to certain tests, in order to give quicker convergence.
4	Error analysis is carried out at termination of run, including the error matrix and estimates of standard deviations of parameters. This option must <u>not</u> be used in the searching mode, as the error analysis is then carried out for the last point reached and not at the minimum.
5	Additional intermediate print-out is produced, describing each new maximum and minimum as it is discovered; and giving summary tables with graphs of the function and each parameter over each group of 50 steps.
6	= 0 for end of run = 1 if data follows Thus a blank card following <u>all</u> data ends the run.

9. FCNDATA: Data for the input to FCN subroutine, if any.

3.1 MODIFICATIONS [2]

Since no rigid criterion was available for the choice of WT'S in help of MINFUN the program was modified so as to generate the WT'S internally and vector DIRIN was set to zero in the program. Thus no input data for WT and DIRIN was required by the modified version of the program.

REFERENCES

[1] W E Humphrey; A general minimizing routine-MINFUN, Programmer's notes P-6, 9.7.62 UCRL Berkley.

[2] B P Singh; Spectroscopic properties of $PbMoO_4$ and $PbWO_4$ single crystals doped with Pr^{3+} and Nd^{3+}, A PhD Thesis (Unpublished), Department of Physics, IIT Kanpur (1983).

-x-